MULTIPLE SCATTERING SUPPRESSION FOR

CROSS-CORRELATION OF A FLOWING

FLUID TO DETERMINE

PARTICLE SIZE

By

RYAN MATTHEW CAMBERN

Bachelor of Science

Oklahoma State University

Stillwater, Oklahoma

1997

Submitted to the Faculty of the
Graduate College of the
Oklahoma State University
in partial fulfillment of
the requirements for
the Degree of
MASTER OF SCIENCE
July, 1999

MULTIPLE SCATTERING SUPPRESSION FOR

CROSS-CORRELATION OF A FLOWING

FLUID TO DETERMINE

PARTICLE SIZE

Thesis Approved:

Ronald L. Dougherty

Thesis Adviser

A. J. Ghajar

B

Wayne B. Powell

Dean of the Graduate College

ACKNOWLEDGEMENTS

I would like to begin by expressing my deepest gratitude to Dr. Ronald L. Dougherty. His guidance throughout my college career and especially during my time as a graduate has been immeasurable. I would also like to thank Dr. Bruce J. Ackerson for his help in completing the research for this project. Without his thoughts and "magic touch", my work on the project never would have been a success.

I would also like to thank the faculty and staff of the Mechanical Engineering Department. Special thanks go to Dr. Afshin J. Ghajar for sitting on my thesis committee. He is a man that I truly admire and respect. A heartfelt thank you to Ms. Janet Smith she has been like my Stillwater mom. I would also like to thank Mike Lucas and his staff in the Chemistry/Physics Machine shop for all their help in producing the setup used for the flow experiments.

To my colleagues, Farhad Dorri-Nowkoorani, Kiley Benes, and Sanjay Sundaresan, I want to express my deepest thanks. Especially to Sanjay, my partner on this project over the last two years. He showed me the benefits of dedication and hard work in the academic world, but moreover he has been a friend. I hope I have been as big an influence on him.

Throughout my years at OSU, I have developed many friendships. A few of those people deserve mention here: Bret Collier, Brent Foster, Jack Nichols, and Amy Nichol. They all have had the pleasure of enduring my company during this last year of my master's thesis work. They have all been great listeners and supporters. I especially would like to thank Amy; our friendship began before OSU, it grew during our time at OSU and hopefully it will last long beyond. She truly is my best friend in the world.

The biggest thanks go to my family. My parents have always been there when I needed them the most. I especially want to thank my mom for helping me get through all

of those stressful 'events'. She has always been there with an encouraging reminder to "Take one day at a time!".

TABLE OF CONTENTS

LIST OF TABLES

LIST OF FIGURES

Figure | Page

Figure		Page

NOMENCLATURE

a	radius of a particle (nm)
A	cross-sectional area (m^2)
A_m	amount of multiple scattering
2b	height of test cell (mm)
B_m	amount of single scattering
2c	width of test cell (mm)
d	'waist' diameter of the laser beam (μm)
D	incident laser beam diameter (mm)
D_h	hydraulic diameter of the flowing fluid test cell (mm or m)
D_o	diffusion constant of particles (m^2/s)
E	magnitude of the electric field (N/C)
E_s	magnitude of the scattered electric field (N/C)
E*	complex conjugate of the electric field (N/C)
f	focal length of the lens (mm)
g^1	normalized electric field correlation function
G^1	electric field correlation function (V/m)
g^2	normalized intensity correlation function
i	complex number $\sqrt{-1}$
I_s	scattered intensity (kHz)
j	count variable used in summations
k_B	Boltzmann constant (1.380658 x 10^{-23} J/K)
$\bar{k}_i$	incident beam wave vector (m^{-1})
$\bar{k}_s$	scattered wave vector (m^{-1})
l*	effective transport mean free path in DWS theory (μm)
L	length a particle travels through the incident laser beam
L_e	length necessary to obtain fully developed flow (mm)
n	index of refraction
np	number of particles with which the viewed particle interacts
N	number of particles in the detection volume
P	wetted perimeter (m)
$\hat{p}$	pressure (Pa)
q	magnitude of the scattering wave vector (m^{-1})
$\bar{q}$	scattering wave vector (m^{-1})
Q	flow rate (ml/min)

r	magnitude of a spatial position vector (m)
$\bar{r}$	spatial position vector (m)
Re	Reynolds number
t	correlation time (msec)
T	absolute temperature (K)
u	constant used for a two cumulant fit
$\bar{v}$	fluid velocity vector (mm/s)
v	fluid velocity (mm/s)
v_x	fluid velocity in x-direction (m/s)
w	constant used for a two cumulant fit
X	denotes translation of the top fiber mount in the x-direction
Y	denotes translation of the top fiber mount in the y-direction

Greek

α	angle through which the laser and detector may travel (degrees)
α_m	detection width (mm)
$\beta_{1,2}$	angle used in calculation of θ for the flowing fluid setup (degrees)
β_m	scattering volume created by a focused beam in a sample (cm^3)
γ^2	signal-to-noise ratio
δ	rotation angle of flowing test cell (degrees)
δ_m	sample volume (cm^3)
$\varepsilon_{o,\, i}$	amplitude of the incident wave vector (V)
η	viscosity of the sample solvent (Pa s)
θ	scattering angle (degrees)
κ	experimental proportionality constant
λ	wavelength of the incident laser beam (nm)
μ	dynamic viscosity (Pa s)
π	numerical constant = 3.14159265
ρ	fluid density (kg/m^3)
τ	correlation delay time (s)
$\tau_{diffusion}$	time it takes a particle to move one unit length under Brownian motion (sec)
$\tau_{Doppler}$	time between fluctuations of two particles moving at different velocities (sec)
$\tau_{transit}$	time it takes a particle to move through the focused laser beam (sec)
ϕ	tilt angle (degrees)

Abbreviations

Ar-Ion	argon ion
BM	denotes back micrometer for top fiber mount
CT	correlation transfer theory
DWS	diffusing-wave spectroscopy

FM	denotes front micrometer for top fiber mount
GRIN	graded-index lenses
HCN	hydrogen-cyanide
He-Ne	helium neon
LDV	laser doppler velocimetry
MSS	multiple scattering suppression
Nd: YAG	neodymium-yttrium-aluminum-garnet
PMMA	polymethylmethacrylate
PMT	photomultiplier tube
PSL	polystyrene latex
RT	radiative transfer theory
VIDE	visible infrared double extinction

Subscripts

A, B	denoted different wavelength lasers and detectors
L	laser arm
D	detector arm

Superscripts

1	denotes electric field correlation function
2	denotes intensity field correlation function

CHAPTER I

INTRODUCTION

1.1 Background

In a wide variety of industrial applications, a reliable and accurate method of determining small particle characteristics in suspensions is essential. Companies such as those that design and produce filtering systems are looking for more accurate and faster methods to measure particle size and density. These measurements will enable those companies to test the efficiency of their products. There are four main types of particle testing procedures performed today, off-line testing, on-line testing, in-line testing, and in-situ testing [Dorri-Nowkoorani (1995)].

The first three of these procedures require alteration of the original particle suspension to successfully make measurements. Alterations may include either diluting the sample for in-line testing or static sampling (removing a sample from the flow) for both off- and on-line testing. These alterations have raised questions as to the accuracy of the results as well as their representation of actual flow field behavior. Of these procedures, in-situ testing is the least intrusive method used to measure particle properties in a section of the process. Because of the nature of this procedure, many companies are interested in developing it into an accurate method of testing.

The use of in-situ measuring techniques many times employs the theory of dynamic light scattering (DLS) or photon correlation spectroscopy (PCS). The use of DLS to determine particle characteristics is based on single scattering data. Single scattering occurs within dilute solutions. In single scattering, photons are scattered only once from a colloidal particle prior to detection. When single scattering occurs, an autocorrelation of the light can be used to determine particle characteristics [Berne and Pecora (1976)]. However, single scattering rarely occurs in industrial processes. Multiple scattering is much more common and occurs when dealing with turbid fluids such as oil and gasoline. Photons that have been scattered by a particle in the solution once and are scattered by at least one more particle before being detected are said to be multiply scattered. Multiple scattering affects the time dependence of the autocorrelation function [Lock (1997a)], which can lead to DLS measurements that are inaccurate and difficult to process.

Several techniques have been developed over the last two decades to deal with particle suspensions that are neither single scattering nor completely opaque. Ideally, these techniques look to eliminate the effects of multiple scattering, but this has proven to be a difficult task that requires expensive equipment. One of these techniques incorporates a two-color system that is complex to align, can handle only moderately dense solutions, and still can not be relied upon to deliver high quality single scattering data [Lock (1997a)]. Recently several techniques have been developed that employ various methods of cross-correlation to suppress the effects of multiple scattering instead of trying to eliminate those effects. In 1997, Meyer *et al.* developed a different approach to the problem of multiple scattering suppression. The method uses a single focused beam and two slightly separated detectors to suppress multiple scattering effects by cross-correlation of the single scattering signals. This method was then to be proven highly effective on static fluid samples by Nobbmann *et al.* [1997].

1.2 Objective

The research discussed in this thesis has two goals. The first goal is to continue the work done by Nobbmann et al. (1997) on static fluid samples. The second and most important goal is to prove that the theory of multiple scattering suppression could be adapted to flowing fluid solutions.

To help in the accomplishment of these goals, a foundation of theory will first be presented briefly discussing dynamic light scattering and multiple scattering suppression (MSS). The major equations and some discussion of these theories are given, while a list of published resources will be used to fill in any gaps and to further explain the derivation of those theories. A detailed explanation of the flow suppression theory will then follow.

With a foundation of theory laid, Chapters IV and V will discuss the experimental setups used in implementing those theories. Chapter IV will discuss the static fluid setup, the procedure used to make samples, the computer correlation package, and the procedure used to collect data. Included in the procedure will be a detailed description of the alignment procedure used for each experiment. The experiments included work done to determine the effects of different scattering angles, different concentrations of particles and different particle sizes on the accuracy of the data collected.

Chapter V deals with applying the method used in the static fluid setup to a setup where the particle suspension is flowing. As with the static setup, the physical setup and procedure will be discussed. The first flowing fluid experiments dealt with single scattering samples to show how flow rate, particle sizes, and sample alignment affected the accuracy of the data collected. The next experiments performed dealt with the scattering angle, particle concentration, and flow rates. The results of these experiments as well as the results from Chapter IV will be discussed in Chapter VI. The remaining sections of this thesis contain a literature review of work in related areas and some recommendations on how to further advance this project.

CHAPTER II

LITERATURE REVIEW

2.1 Introduction

The research covered by this thesis is a combination of two relatively new theories. The first theory deals with multiple scattering suppression for a dynamic light scattering analysis of a solution in order to accurately characterize particles, specifically determining their size. The second theory deals with suppression of flow effects in a shearing system to accurately characterize particles. The following literature review is divided into three sections. Section 2.2 deals with the many aspects of light scattering experimentation. The publications presented in this section will give a time line perspective of how light scattering experiments have evolved into the setup used in the research described by this thesis. These publications are not directly related to the current research described within this thesis, but do give the reader background into light scattering as well as knowledge of other techniques used to analyze light scattering data. Section 2.3 of the literature review will discuss the experiments that directly relate to the research described in this thesis, namely single-beam, two-detector multiple scattering suppression. Publications describing a technique used to suppress flow effects in light scattering experiments are discussed in section 2.4 of the literature review.

2.2 Light Scattering Techniques

Studies involving light scattering by small particles have been performed for over a century. Experiments by Tyndall, Rayleigh, Gans, Debye, Mie and others laid the foundation for the light scattering experiments of today. With the invention of the laser, the field of light scattering experimentation has seen great improvements in the accuracy of results as well as an increase in experimental and industrial applications [Berne and Pecora (1976)]. The following review will give some insight into the recent developments in light scattering research. The review is not a complete listing of all of the work done in the field of light scattering, but it does highlight the work that lead to the research covered in this thesis.

George Phillies (1981a) gave a theoretical discussion on quasielastic light scattering spectroscopy. He described how a two-beam, two-detector cross-correlation setup could be more effective in the suppression of multiple scattering effects than a single-beam, single-detector autocorrelation setup. The discussion began with the single-beam, single detector setup and the intensity equations for one single scattering and one double scattering event as well as the time dependent versions of these equations. These same equations were then developed for the two-beam, two-detector setup. A comparison of the single scattering equations given for both of these setups revealed that they are equivalent as long as the scattering angle remains 90°, while the double scattering equations are not. Double scattering effects were smaller by a factor of $(np/N)^2$ in the two-beam, two-detector setup than in the single-beam, single-detector setup, where np is the number of particles with which a viewed particle interacts, N is the number of particles in the detection volume, and $np \ll N$. Phillies also noted that several conditions must be set for successful data collection. Those conditions are as follows:

1. The wavelength of each laser used must be equal to within one-tenth of the wavelength inside the sample. This means the beams must be aligned within 0.5 mrad of each other.

2. Focusing of any lenses used must be exact, to maintain the planar aspect of the incident and scattered waves.

3. Light scattering by this geometry would be seen by both detectors. At a scattering angle of 90°, this effect was irrelevant; but at other scattering angles, this effect would be cumulative and would make data analysis more difficult.

Phillies presented experimental proof of the theory previously described in a second publication (1981b). The experimental setup consisted of a 25 mW He-Ne laser, an attenuator, a 50 % reflective plate beamsplitter, two focusing lens, two mirrors, three pairs of irises, two RCA 7265 photomultiplier tubes, and a 64 channel Langley-Ford digital correlator. The single laser beam was split into two equal beams that were routed into opposing sides of a 1-cm^2 fluorimeter cell with polished sides. The photomultiplier tubes and irises were then positioned across from each other on the other two sides of the test cell. As described in the first publication, the major problem with this experimental setup was exact alignment of all components. A majority of the publication dealt with the alignment procedure for the split beams and the two photomultipliers. Alignment also dealt with the test cell itself. The test cell was tilted less than 0.5° to eliminate backscattering into the photomultipliers from the opposing walls. Experimental results were presented for two scattering media: 0.091 μm polystyrene latex spheres (PSL) suspended in 0.4 g/l sodium lauryal sulphate at concentrations of 2.1 x 10^{-5} to 1.18 x 10^{-2} percent by volume and bovine serum albumin in 0.15*M* NaCl at a concentration of 20 percent by weight. The data showed that the use of a single-detector setup would overestimate the diffusion coefficient of 0.091 μm PSL particles in concentrations greater than 10^{-3}, while the two-detector setup would be concentration independent. Finally, it was reported that the experiments on serum albumin matched the results of earlier work done by Hall *et al.* (1980).

Like Phillies (1981a,b), Dhont and de Kruif (1983) published work done on the theory followed by a second publication [Mos *et al.* (1986)] that described the experimental work done on that theory. In 1983, Dhont and de Kruif described how Phillies had overlooked a second order term in dealing with the theory of double scattering. They further describe how Phillies used an incomplete form of the Siegert relation in his calculations. This oversight is found to be insignificant, however, since the use of a two-laser beam, two-detector setup causes the double scattering effects to be negligible in the measured intensity correlation function. The paper also describes the difficulties associated with collecting and analyzing data from a scattering angle other than 90°. To help eliminate these difficulties, it was suggested that two different wavelength lasers and two different absorbing filters be used. It was also shown that the two detectors should be placed at scattering angles related to each other and to the wavelength of the two lasers used. This relation was given by the following equation:

$$\frac{\sin\left(\frac{\theta_A}{2}\right)}{\sin\left(\frac{\theta_B}{2}\right)} = \frac{\lambda_A}{\lambda_B}, \qquad (2\text{-}1)$$

where the subscripts A and B represent two different lasers, θ_A and θ_B are the scattering angles for each detector, and λ_A and λ_B are the wavelengths for each laser.

In 1986, Mos *et al.* (including Dhont and de Kruif) described the experimental setup that they used to prove their theory for elimination of multiple scattering effects. The experimental setup described in this paper resembles the one previously described in the review of Phillies' (1981) experiments. Also like the work done by Phillies, this paper describes in detail the alignment procedure involved in collecting reliable data and the difficulties associated with aligning the setup. Experiments were performed on two colloidal systems. The first sample was polystyrene latex spheres (diameter equal to 176 nm) of differing concentrations in distilled water. The second sample was silica spheres dispersed in toluene or xylene. The silica spheres had radii reported in the paper to be 36.7 ± 2 nm. Experimental results showed that the diffusion coefficient could be reliably found with the cross-correlation method for various concentrations, while autocorrelation results were not reliable at higher concentrations.

The need to determine particle characteristics is not limited to just liquid media. Gougeon *et al.* (1987) described a technique called visible infrared double extinction (VIDE) used to characterize a cloud of coal particles (diameters ranged from 20 to 80 μm). These clouds had a high optical thickness, but were still in a range considered to be weakly multiple scattering. Two lasers of different wavelengths were used in the experiments: the visible light source was a He-Ne laser (632.8 nm wavelength) and the infrared light source was a Hydrogen-Cyanide (HCN) laser (337 nm wavelength). A cylinder specially designed for these experiments rotated and vibrated to produce the coal cloud. A photomultiplier tube collected the visible light from the sample, while a moll thermopile collected the infrared light. Outputs from both detectors were then sent to a two-channel recorder. Experimental results overestimated the diameter of the coal particles compared to the value of the sieve diameter used, and the difference was attributed to the use of non-spherical coal particles in the experiments. They concluded that the technique would still be applicable to diagnose dense laden flows.

Pine *et al.* (1988) described the use of a new technique in quasielastic light scattering. The new technique was called diffusing-wave spectroscopy (DWS), and it was meant to extend the use of quasielastic light scattering to densely multiple scattering media. Their theory dealt with backscattering and transmission autocorrelation functions for a diffusive media. For transmission the only parameter remaining as a variable during experiments was the transport mean free path, l^*. Experiments used a laser with a wavelength of 488 nm on an optically thick media of 0.497 μm polystyrene latex particles and were found to match their model if l^* was set at 1.43 μm. For comparison with the transmission model, the backscattering model used the same l^*. For an l^* value of 1.43 μm, the experimental data from the backscattering model fit well when a second variable parameter, κ, was set to 2.0. Further experiments were performed on other particle sizes and fit to the backscattering model if κ was varied by ± 10 %. Finally, experiments were conducted on mixtures of two different interacting and non-interacting particle sizes (0.312 μm and 0.497 μm spheres). It was found that the correlation function for the interacting particles decayed slower in both transmission and backscattering.

Wiese and Horn (1991) described the use of a fiber optic as a different approach to quasielastic light scattering detection. Their experimental setup consisted of a He-Ne laser (632.8 nm wavelength), a single mode fiber optic, a coupler that allowed the fiber optic to illuminate the sample and simultaneously collect the backscattering signal, a photomultiplier, and a correlator. They performed experiments to compute the autocorrelation functions of polymer latex particles (diameters ranging from 41 to 326 nm) at various concentrations (ranging from 1 to 40 percent by weight). The experimental results show that multiple scattering effects have a negligible impact on the autocorrelation function even at the higher concentrations. The claim that negligible multiple scattering effects were seen at such high concentrations was intriguing.

Ackerson *et al.* (1992) and Dorri-Nowkoorani *et al.* (1993) and (1994) discussed an alternative to the multiple scattering suppression method for particle characterization. This method utilized the Correlation Transfer Theory (CT) to determine particle size in media ranging from single to highly multiple scattering. The main focus of these papers was that the CT equation and the Radiative Transfer (RT) equation were similar. Therefore, RT solution techniques could be applied to the CT equation in order to obtain a solution.

Segrè *et al.* (1995) described the use of a two-color dynamic light scattering system for multiple scattering suppression. A detailed description of the theory behind this two-color system is provided in their paper. The system consisted of two lasers of differing wavelengths (488 nm and 514.5 nm) and two photomultipliers with filters designed to detect only one color. A German commercial company called ALV provided this setup. The lasers were generally operated at 100 mW and experiments were performed over a range of scattering angles from 20° to 140°. Experiments were conducted on two suspensions: polystyrene (PS) spheres (56 nm radius) in water and polymethylmethacrylate (PMMA) particles (185 nm radius) in dodecane. The concentrations of the two suspensions tested ranged from 0.05 to 1.00 % volume fraction for polystyrene and from 0.01 to 0.25 % volume fraction for PMMA. Results showed that the two-color system worked effectively to characterize particles in multiple scattering suspensions. Preliminary work using the two-color technique described above can also be seen in Schätzel *et al.* (1990).

In 1998, Aberle *et al.* discussed the use of a 3-D cross-connotation method to suppress multiple scattering effects in turbid media. The experimental setup utilized a single laser beam that had been split into two parallel beams. Those two beams were then directed by a lens to cross in the center of the sample cell. This was done to produce two equal scattering vectors that were detected by two monomode fibers. Like the setups described by Phillies (1981a,b) and Mos *et al.* (1986), the alignment of the laser beams and the detection fibers were critical to the collection of reliable data. Experiments were performed over a range of scattering angles from 10° to 135° on 69, 107 ± 10.5, 236 ± 6.58, 453 ± 9.0, and 481 ± 1.8 nm diameter latex spheres in deionized water. The concentrations of the samples were based on optical transmission and ranged from 0.7 to 99.3 %. Experimental results showed that the technique was excellent at suppressing multiple scattering effects for a wide range of particle sizes, a wide range of concentrations and was easy to use over a wide range of scattering angles. Experimental results also showed that this technique was useful in both static and dynamic light scattering applications.

2.3 Multiple Scattering Suppression: Single Beam – Two Detector Setups

Previous to 1997, the majority of work done in the area of multiple scattering had involved two beam, two detector setups for suppression. These setups were effective in suppressing the multiple scattering effects only in semidilute samples. A major complication in dealing with these two-beam, two-detector systems was alignment. Due to this complication, the desire to find a simpler scattering geometry that would allow multiple scattering suppression even in very turbid solutions has been growing. This desire has lead to the design of a system that utilizes a single laser beam and two closely configured detectors to suppress multiple scattering effects. The following articles describe the development and use of this system.

Meyer *et al.* (1997a) developed an experimental setup incorporating a single laser beam (514.5 nm wavelength) and two fiber optic cables with polished ends. The setup was capable of running experiments with the fibers separated at three different vertical distances of 0.25, 0.50, and 0.75 mm. Experiments were performed at scattering angles of 60°, 90°, 120°, and 135° on 0.107 and 0.204 μm diameter particles of polystyrene latex spheres for concentrations ranging from 0.0017 to 5.0 percent by weight. It was found in their experiments that decay time had little dependence on the three separation lengths listed above. Therefore results were given for only a fiber separation of 0.25 mm (1.5 mrad) and involved mostly 0.107 μm particles. Normalized autocorrelation and cross-correlation functions were plotted for various concentrations against delay time so the effect of concentration on each could be seen. As the concentrations increased, the linearity (a measure of data reliability) of the autocorrelation functions became markedly less while the cross-correlation functions remained steady. They also gave results showing how the calculation of diameter was correct using cross-correlation data for all concentrations while calculations using the autocorrelation data dropped by more than an order of magnitude. A second publication by Meyer *et al.* describing the same experiment is also listed in the references of this thesis under (1997b).

Theoretical work done by Lock (1997a) accompanied the experimental work done by Meyer *et al.* (1997a,b) on multiple scattering suppression by a single beam/two detector setup. Lock limited the calculations given in his paper to single and double scattering only, but noted that his work could be applied to higher orders of multiple scattering. Lock first gave a mathematical description of the experimental scattering geometry. Then in terms of the electric field equations, he described single and double scattering by non-interacting spherical particles in a liquid solution. Next, he derived the electric-field correlation functions for a single beam cross-correlation system. Lastly, the intensity cross-correlation function was derived, the level of double scattering suppression was given and the time dependence of the autocorrelation and cross-correlation functions was derived. Lock concluded with the fact that a focused laser beam produced smaller far-zone coherence in the direction transverse to the beam for multiple scattering than that produced by single scattering. Like the experimental papers that Meyer *et al.* (1997a,b) published, two papers dealing with this subject were published in 1997 by Lock. Both are listed in the references of this thesis. The difference between Lock's two papers is that the calculations in the (1997a) paper ignore polarization and angular dependence of scattered light, while the (1997b) paper includes those effects in the derivation of the autocorrelation and cross-correlation functions.

The final publication builds on the work covered by the first four publications cited in this section. In 1997, Nobbmann *et al.* furthered the experimental work done by Meyer *et al.* (1997a,b) by developing a setup that allowed examination of how the multiple scattering contribution to the cross-correlation function was reduced with increasing fiber separation. Nobbmann *et al.* utilized the same basic setup as the one described by Meyer *et al.*, with one major difference. The detector housing in Nobbmann's setup used a beam-splitter to divide the scattered beam equally into two single-mode fibers that use GRIN lenses for better detection. This design allowed the two fibers to be physically separated by 90° when they are effectively separated by only milliradians. The separation was accomplished by the use of a micrometer mounted to the top fiber holder. Experimental results were given for polystyrene latex spheres with a diameter of 0.107 μm at volume fractions of 0.15 % and 0.25 %. These experiments were all performed at a scattering angle of 90°. Nobbmann *et al.* were successful in showing the ability of their setup to sweep through a measured amount of separation between fibers and to correctly give the particle diameter when that separation became great enough (~1mrad).

2.4 Flow Effect Suppression

The majority of published articles involving light scattering and flowing fluids deal with laser Doppler velocimetry applications. Laser Doppler velocimetry experiments estimate the velocities of particles within flowing systems. Contrary to LDV experiments, flow effects must be suppressed for experiments where the ability to characterized particles within the flowing fluid is desired. The following review describes two articles where flow effects are suppressed.

Ackerson and Clark (1981) examined the possibility of using dynamic light scattering as a way to study the intensity correlation function for dense solutions of Brownian particles subjected to low shear rates. Both model calculations and experimental results were given and compared. An equation was given for the correlation time-dependent signal-to-background-noise factor. This term was directly related to the measurement of the intensity correlation function. An experimental setup was described which minimized flow effects on the signal-to-background-noise factor, but no experimental data was found using this setup. The experimental setup consisted of an arrangement where the scattered wave vector (the difference of incident and collected light) was perpendicular to the flow velocity vector. Instead of that arrangement, two other experimental setups for flow suppression were described and experiments were performed using those setups. Results from those experiments showed the modest effects of varying stop and pinhole diameters to suppress velocity effect.

In 1998 Hoppenbrouwers and van de Water used a different experimental setup to study dynamic light scattering in fluids subjected to shear flows. Their experimental setup incorporated two beams from either a helium-neon (632.8 nm wavelength) or an Argon-Ion (514.5 nm wavelength) laser that crossed within the flow volume of a Couette device. The scattered signal was collected by using a 1.0 mm diameter pinhole, a lens with a focal length of 100 mm, a multimode fiber optic cable, a photomultiplier, and a real time digital correlator. They claimed that this setup was capable of uncoupling the effects of particle convection due to shear and particle diffusion due to Brownian effects within the correlation function. Doing this would allow the diffusion coefficient to be measured so that particle characterization could be done. They were successful in showing that they could characterize the diameter of 0.204 μm polystyrene spheres in a water-picoline mixture to within 15 % of the known value.

CHAPTER III

THEORY

3.1 Introduction

The primary goal of this thesis is to show experimentally how two independent suppression techniques can be combined to produce usable data from a dense suspension of particles in a flowing setup. To better understand how these experimental suppression techniques work, one must have some general knowledge of the basic light scattering equations, the theory behind multiple scattering suppression, and the concepts that lead to the suppression of flow effects. The purpose of this chapter is merely to give the reader an overview and not a detailed description of the ideas described above. More in-depth coverage can be seen in the cited references and in Sundaresan (1999).

3.2 Basic Dynamic Light Scattering

A light scattering experiment consists of an incident beam, $\vec{k}_i$, entering a sample and being scattered in a new direction towards a detection device. The scattered wave vector, $\vec{k}_s$, defines this new direction. The magnitude of the two wave vectors is given by

$$k_{i,s} = \left|\vec{k}_{i,s}\right| = \frac{2n\pi}{\lambda_{i,s}} \tag{3-1}$$

where n is the index of refraction of the sample, $\lambda_{i,s}$ is the wavelength of the incident and the scattered beams, respectively. The angle between the line of transmission and the position of the detection device is the scattering angle, θ. The scattering wave vector, $\vec{q}$, is the difference between the incident wave vector and the scattered wave vector. Assuming elastic scattering and using the law of sines, the scattering wave vector is defined by the following equation and can be seen in Fig. 1 [Berne and Pecora (1976)]:

$$\vec{q}^{\,2} = \left|\vec{k}_i - \vec{k}_s\right|^2 \Rightarrow \left|\vec{q}\right| = \frac{4\pi n}{\lambda_i}\sin\frac{\theta}{2} \tag{3-2}$$

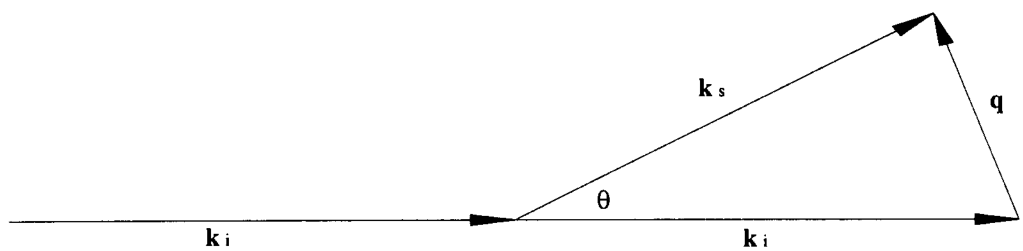

Figure 1: The incident wave vector, $\vec{k}_i$, the scattered wave vector, $\vec{k}_s$, and the scattering angle, θ, used to find the scattering wave vector, $\vec{q}$.

Dynamic light scattering studies the fluctuations of the scattered intensity in a sample over time. For static fluid conditions, the fluctuations are due to Brownian motion of the particles. The motion of the particles changes the scattered electric field, which effects the intensity given by [Berne and Pecora (1976)]

$$I_s(t) \propto |E_s(t)|^2 . \tag{3-3}$$

A measure of the normalized correlation function for the scattered intensity signal is defined by [Nobbmann (1991), (1997)]

$$g^2(\bar{r},\bar{k},\tau) = \frac{\langle I(\bar{r},\bar{k},t) I(\bar{r},\bar{k},t+\tau)\rangle}{\langle I(\bar{r},\bar{k},t)\rangle\langle I(\bar{r},\bar{k},t)\rangle} \tag{3-4}$$

where τ is the delay time and < > is an ensemble average. A second way to define the scattered signal is with the normalized electric field correlation function [Nobbmann (1991), (1997)]

$$g^1(\bar{r},\bar{k},\tau) = \frac{\langle E(\bar{r},\bar{k},t) E^*(\bar{r},\bar{k},t+\tau)\rangle}{\langle E(\bar{r},\bar{k},t)\rangle^2} \tag{3-5}$$

where E* is the complex conjugate of the electric field. If Gaussian statistics dominate in the scattered light, the $g^2(\bar{r},\bar{k},\tau)$ function and the $g^1(\bar{r},\bar{k},\tau)$ function are related by the Siegert relation as follows:

$$g^2(\bar{r},\bar{k},\tau) = 1 + \gamma^2 |g^1(\bar{r},\bar{k},\tau)|^2 \tag{3-6}$$

where γ^2 is the experimental signal-to-noise ratio.

For DLS experiments involving dilute monodisperse samples, the electric field correlation function is found to be [Nobbmann (1991), (1997)]

$$g^1(\bar{q},\tau) = \exp(-D_o q^2 \tau) \tag{3-7}$$

where q is defined by Eq. (3-2), $D_o = \frac{k_B T}{6\pi\eta\ a}$ (the Einstein diffusion constant), k_B is the Boltzmann constant, T is the absolute temperature of the sample, η is the viscosity of the solvent, and a is the radius of the particles.

3.3 Multiple Scattering Suppression

The purpose of this thesis is to show how a dynamic light scattering technique can be applied to a dense suspension of flowing particles to determine size. When dealing with such a system, the first problem encountered is multiple scattering effects. These effects make interpretation of the collected data difficult. The second problem is flow effects, which can add unwanted fluctuations to the light scattering data. This section deals with the theory for a multiple scattering suppression technique. Section 3.4 will discuss the theory on which the technique for flow effect suppression is based.

The concept of using two single-mode fiber optic detectors and a single incident laser beam to suppress multiple scattering was developed by Meyer *et al.* (1997a,b). Theory matching the results from Meyer's experiments for this technique was also presented by Lock (1997a,b). For the system described by Meyer *et al.*, the separation between the two single-mode detectors was not variable during an experiment. Nobbmann *et al.* (1997) described a system that allowed the tilt angle between the two detectors to be adjusted so that a sweep of tilt angles could be mapped (shown clearly in a future figure). That same system was utilized in the research for this thesis.

This system allowed the detectors to remain focused on the same detection area while being separated by small angles (in mrad). According to the van Cittert-Zernike theorem for large angular separations, single scattering will produce larger intensity fluctuations from a laser beam focussed within a multiple scattering sample than the entire multiple scattering from the rest of the sample [Mandel and Wolf (1995)]. This means that as the scattering volume is decreased, the single scattering detection area increases. Proof of this concept can be seen in Meyer *et al.* (1997a,b) and Nobbmann *et al.* (1997).

It is important to note that the area of useful separation between the two detectors was defined by the following two conditions. First, the cross-correlation of singly scattered light was not possible for too large of a separation between the detectors. Second, if the separation was not sufficient, multiple scattering effects dominated. For a cross-correlation function, mapping the signal-to-noise ratio versus the tilt angle showed all three areas. As mentioned above in Eq. (3-6), γ^2 was the signal-to-noise ratio. Through the use of simple approximations and by using the assumptions listed below, the square root of the signal-to-noise ratio was derived by [Nobbmann *et al.* (1997)] as a function of tilt angle between detectors to be:

$$\gamma(\phi) = A_m \frac{\exp\left[\frac{-q^2\phi^2}{8\alpha_m}\right]}{\left[\alpha_m^2\left(\alpha_m\phi^2 4^{-1} + \delta_m\right)\right]^{1/2}} + B_m \frac{\exp\left[\frac{-q^2\phi^2}{4\beta_m}\right]}{\beta_m \sin(\theta)\sqrt{\alpha_m}} \qquad (3\text{-}8)$$

where the ratio of A_m to B_m represents the ratio of multiple-to-single scattering, and the following assumptions were made during the derivation of this equation. The first set of assumptions made was that a small scattering volume created by a focused beam, an intermediate detection width, and a large sample volume, $\beta_m \gg \alpha_m \gg \delta_m$ respectively, were present in the system. Also assumed was that the tilt angle, ϕ (in mrad), was much smaller than the scattering angle, θ (in rad) $\phi \ll \theta$. Therefore, the $\sin(\phi) \cong \phi$ and the $\cos(\phi) \cong 1$. Finally, it was assumed that $\beta_m \sin(\theta^2) \gg \delta_m$. Equation (3-8) is used in

Sundaresan (1999) to illustrate theoretical fits to data taken from three different concentrations of 0.107 mm PSL particles in a rectangular cell at a 90° scattering angle.

As mentioned above on page 22, three areas can be seen in a signal-to-noise ratio versus tilt angle mapping (see Fig. 2). The first area is the 'peak' of the graph and corresponds to the tilt angle for which multiple scattering dominates. No separation between the two detectors gives the maximum of the 'peak' and corresponds to the highest signal-to-noise ratio. Both detectors are focused on the same detection area from within the multiple scattering threshold. The multiple scattering threshold is defined as a spherical volume around the incident beam in the sample where multiple scattering dominates. Data collected from this region generally undersize the diameters of the particles in the suspension. As the tilt angle increases, the signal-to-noise ratio decreases. At approximately ± 1.5 mrad, the 'peak' region turns into the 'shoulder' region for the mapping of Fig. 2. This region corresponds to a region where the bulk of the multiple scattering is suppressed. Evaluation of data collected from within this region generally give correct particle sizes. The final region begins where the signal-to-noise ratio becomes very low. In this region, the separation between the two detectors becomes too large and their signals are not correlated well. For Fig. 2, this region starts at approximately ± 5 mrad and continues for the remainder of the mapping.

The experiments described in this thesis utilized a correlation software package to analyze the data collected for both the static fluid and flowing fluid setups (see Appendix I). Particle sizes were determined by combining Eqs. (3-6) and (3-7) with a two-cumulant expansion as follows [Nobbmann *et al.* (1997)]:

$$g^2(\tau) = 1 + \gamma^2 \exp\left(-2u\tau + 2w\tau^2\right) \qquad (3\text{-}9)$$

where u and w were two constants used for the cumulant fit. The first cumulant u was used to determine the diameter of the particles within the suspension and was defined as

$$u = D_o q^2 \tag{3-10}$$

where D_o is defined after Eq. (3-7) and q is given in Eq. (3-2). The second cumulant was normalized by w/u^2 and was used to determine the exponentiality of the correlation function. For single scattering suspensions, the normalized second cumulant should ideally vanish, but is generally found to be less than 0.04. For multiple scattering samples, a typical normalized second cumulant less than 0.10 indicates suppression of multiple scattering effect.

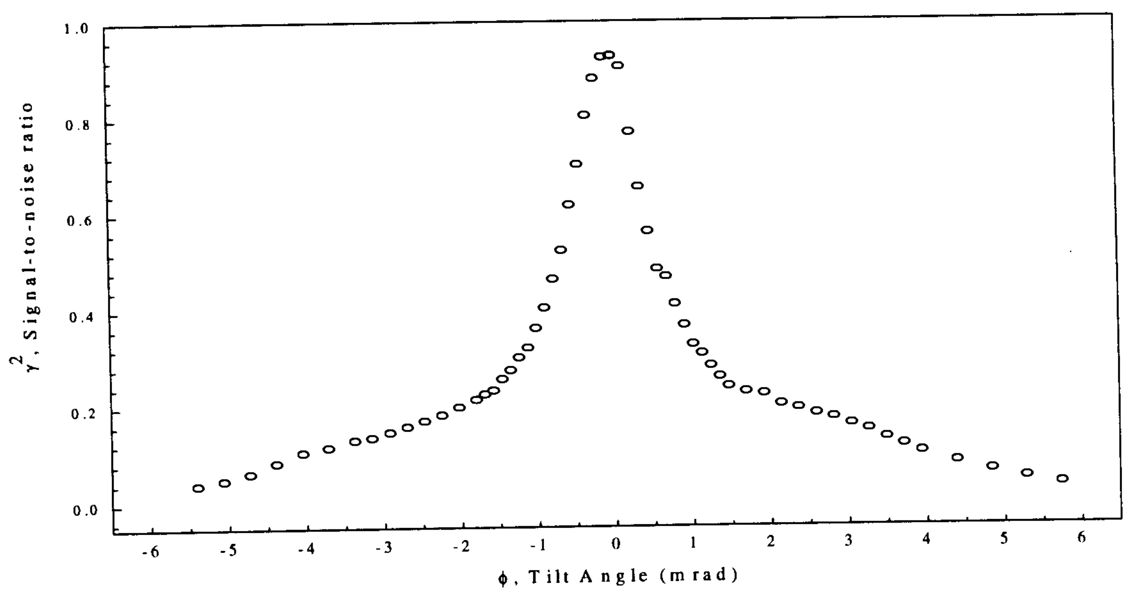

Figure 2: Signal-to-noise ratio versus tilt angle for a cross-correlation measurement taken at a scattering angle of $\theta = 90°$. A sample of 0.107 μm PSL particles at a volume fraction of 0.1330 percent by weight was used.

3.4 Flow Effect Suppression

As mentioned in Section 3.2, the purpose of this thesis is to show how two separate suppression techniques can be used together to determine particle size in a dense flowing suspension of particles. Section 3.3 gave a brief view of the theory behind multiple scattering suppression. The focus of this section will be to describe the theory behind flow effect suppression in systems where flow is present.

Dynamic light scattering experiments focus on fluctuating signals from particles undergoing Brownian motion. As previously stated in Eq. (3-3), this motion affects the electric field correlation, which in turn affects the intensity correlation. A well-defined solution exists for static fluid setups that utilize the fluctuations caused by Brownian motion to determine particle size. In a flowing system, a second source of fluctuations occurs due to the motion of the particles flowing through the scattering volume. The following derivation shows how flow effects influence the electric field correlation function. The unnormalized version of the electric correlation function is

$$G^1(\tau) = \langle E(\bar{q},\tau)E^*(\bar{q},0)\rangle \propto N|\varepsilon_{oi}|^2 \langle e^{i\bar{q}\cdot(\bar{r}(\tau)-\bar{r}(0))}\rangle \tag{3-11}$$

where N is the number of particles in the scattering volume, ε_{oi} is the amplitude of the incident wave, $\bar{r}$ is the spatial coordinate of a particle being correlated, and < > is an ensemble average. Brownian motion and flow change the spatial coordinate of a viewed particle with time. Therefore, the following equation is used to define the motion of the particle through the scattering volume:

$$\bar{r}(\tau) = \delta\,\bar{r}(\tau)_{BM} + \bar{v}(r)\cdot\tau + \bar{r}(0) \tag{3-12}$$

where $\delta\ \bar{r}(\tau)_{BM}$ is the change in the position of the particle due to Brownian motion, $\bar{v}(r)\cdot\tau$ is the change in position of the particle caused by the fluid velocity and r(0) is the initial position of the particle. Substitution of Eq. (3-12) into Eq. (3-11) gives

$$G^1(\tau) \propto N\left|\varepsilon_{oi}\right|^2 \left\langle e^{i\bar{q}\bullet\delta\ \bar{r}(\tau)_{BM} + (i\bar{q}\bullet\bar{v}(r))\tau} \right\rangle \tag{3-13}$$

As with Eq. (3-7), if single scattering of monodisperse particles dominates the system, then the normalized version of Eq. (3-13) is found to be:

$$g^1(\tau) = \exp\left[-D_o q^2\tau + \left[i\bar{q}\bullet\bar{v}(r)\right]\tau\right] \tag{3-14}$$

where normalization occurred by dividing Eq. (3-13) by $N\left|\varepsilon_{oi}\right|^2$.

Equation (3-13) shows how the influence of flow interferes with the analysis of DLS experiments. To accurately size particles in a suspension with a mean flowing velocity, the influence of flow effects must be suppressed. The technique employed here to accomplish this involved the dot product seen in Eq. (3-14). To suppress flow effects, a setup was designed that allowed the scattering wave vector, $\bar{q}$, and the flow vector, $\bar{v}$, to be perpendicular. Discussion of this setup is given in Chapter V of this thesis and in Sundaresan (1999). This geometric setup produced a dot product that was zero and therefore theoretically eliminated the flow effects. A similar setup was explained in Ackerson and Clark (1981) for a system where no mean flow was present.

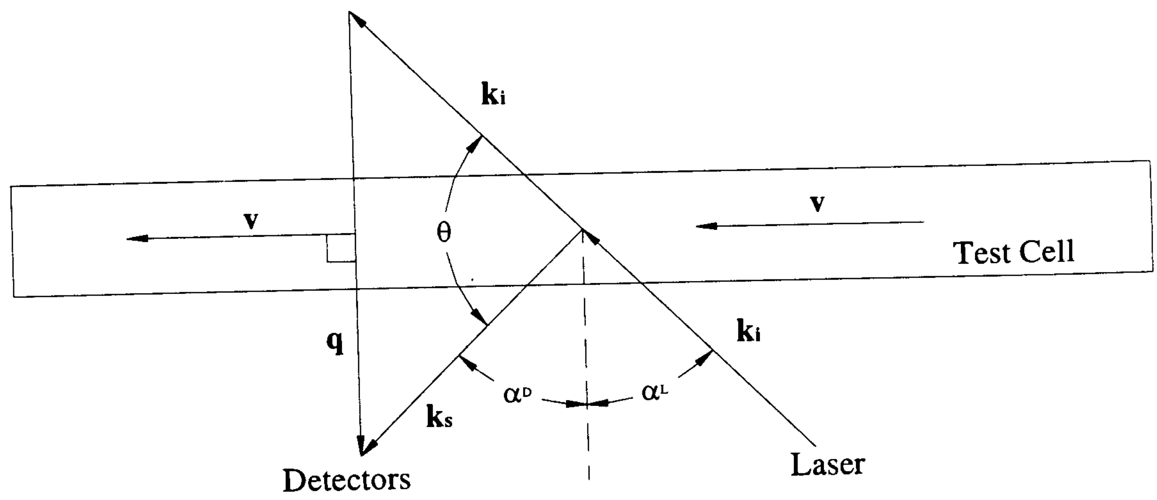

Figure 3: A top view of the geometry that facilitates flow suppression by allowing the scattering wave vector, **q**, and the fluid velocity vector, **v**, to be perpendicular. The incident wave vector, $\mathbf{k}_i$, and the scattered wave vector, $\mathbf{k}_s$, are also shown.

CHAPTER IV

STATIC FLUID CONDITIONS: EXPERIMENTAL SETUP, ALIGNMENT, AND PROCEDURE

4.1 Introduction

The primary goal of this thesis is to demonstrate the feasibility of applying two unrelated suppression techniques together for particle sizing. Those two techniques were multiple scattering suppression and flow effect suppression. The technique described within this chapter involved a setup used for multiple scattering suppression in a non-flowing sample. Although the focus of this thesis deals with a flowing system, a good understanding of multiple scattering suppression was needed. As a means of accomplishing this, experiments were first performed on an existing static fluid setup. This not only allowed for means with which to gain experience with the equipment and data taking process, but also allowed the work previously done by Nobbmann *et al.* (1997) to be expanded. This chapter describes the static fluid suppression setup, the alignment procedure for that setup, the computer program used and its settings, a description of the samples, and the procedure used to collect data with the setup.

4.2 Experimental Setup

A schematic of the experimental setup used for particle sizing in static fluid samples can be seen in Fig. 4. The goniometer was broken up into three main sections: the light source arm, the sample stand, and the detection device arm. The first component necessary to conduct a dynamic light scattering experiment is the light source. In the static fluid experiments, a Helium-Neon (He-Ne) laser (632.8 nm wavelength) was used to provide this light source and was attached to the stationary laser arm of the goniometer. The 20 mW laser was vertically polarized and had an original beam diameter of 0.68 mm. To ensure proper alignment of the laser, a holder capable of small vertical adjustments mounted it to the laser arm.

Also mounted on the laser arm were an adjustable attenuator and a lens holder. The approximate position of these components can be seen in Fig. 4. The attenuator allowed the amount of power coming from the laser to be controlled over a range from 0.08 to 9.54 mW. The range of attenuation was found by direct measurement using a power meter with a wand attachment (see Appendix I). Mounted on the laser arm between the attenuator and the sample stand was a lens holder. The lens holder was designed to allow small adjustments in all planes (x, y, and z). This was valuable during the alignment process, which will be discussed in Section 4.3. A 12.7 mm diameter lens with a focal length of 37 mm was used throughout the experiments. Sundaresan's thesis (1999) contains the heights for and distances between all components used in both the non-flowing and flowing setups.

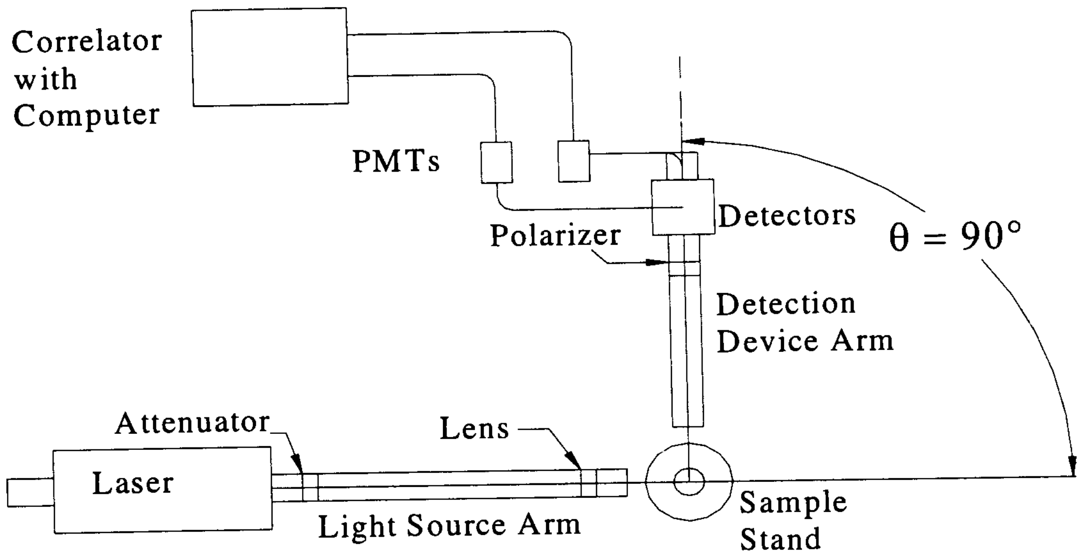

Figure 4: The experimental setup for static fluid samples.

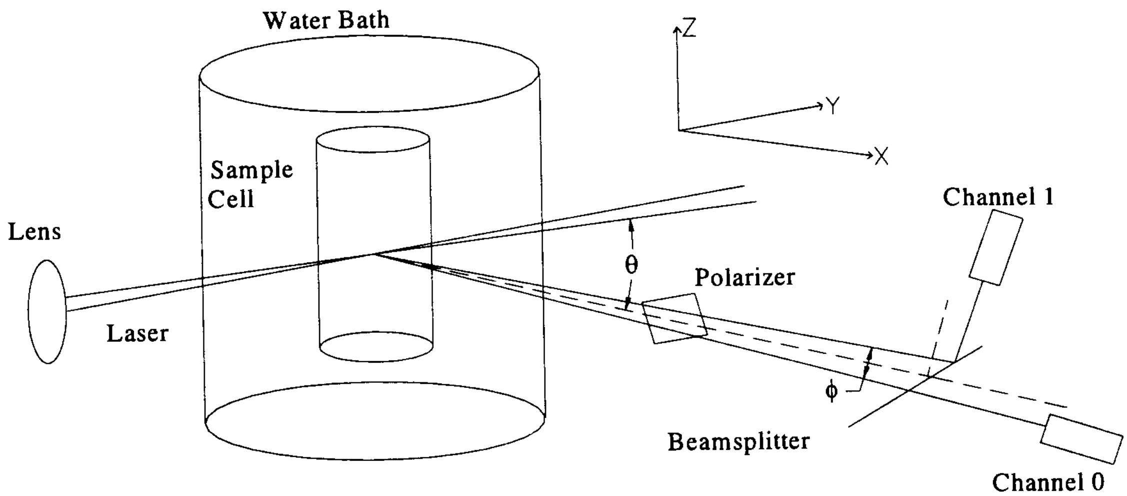

Figure 5: Static fluid setup used for fiber multiple scattering suppression. Shown are the scattering angle, θ, and the tilt angle, φ.

The next essential part for a dynamic light scattering experiment is the sample (Fig. 4). For the static fluid setup, a sample stand was centered along the goniometer's axis of rotation. The stand consisted of a milled aluminum platform sized to hold a water bath. A rod attached the platform to the base of the goniometer allowing only vertical adjustments. A water bath was used in the static fluid setup to accomplish three goals. First, the water bath allowed greater freedom in aligning the laser in the sample. The larger diameter of the water bath meant that slight adjustment had less effect on how the incident beam moved in the sample. Second, the water bath helped to maintain the sample at a constant temperature. Third, the water bath container provided the mechanism used to hold the test tube vertically along the goniometer's axis of rotation. The container was formed in the shape of a small beaker from a section of glass tubing (see Appendix I). To enable proper vertical alignment of the test tube in the water bath, a lid and base were constructed from Teflon tubing. Each piece contained a test tube sized hole (approximately 10 mm in diameter) through the center. The base was designed to sit in the bottom of the container and was used to ensure that the test tube was held vertically. Fisher Scientific test tubes were used throughout the static fluid experiments (see Appendix I). The sample stand, water bath and its parts were all designed to ensure that the samples were held centered along the goniometer's axis of rotation.

The final segment necessary to complete the dynamic light scattering setup is the detection device. The detector housing (Fig. 6) was manufactured from aluminum and was mounted to a plate that in turn could be mounted to the detection device arm of the goniometer (Fig. 4). The detection device consisted of a beamsplitter and two single-mode fiber optic cables (see Appendix I); each connected to a photomultiplier tube.

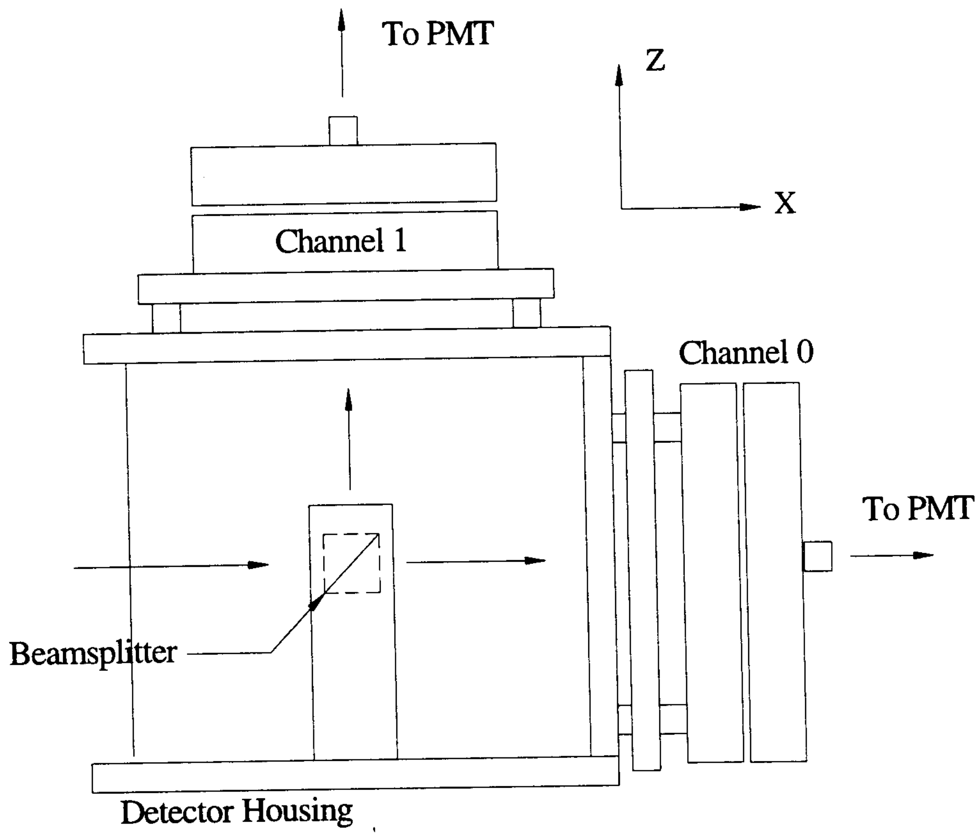

Figure 6: Side view of the detector housing showing where the fiber mounts attach and the location of the beamsplitter.

The detector housing allowed for the mounting of the beamsplitter and the devices used to adjust the fiber optic cables. It was necessary to use a beamsplitter due to the physical constraints of the fiber optic mounts.

As discussed in the theory, each fiber optic detector must look at the same point within the sample, with an angular separation of only a few milliradians. This was physically impossible without the use of the beamsplitter. The nonpolarizing wavelength specific beamsplitter (see Appendix I) divided the scattered signal to each of the fiber optic detectors equally. One fiber optic detector saw direct transmission of the scattered signal and was called channel 0, while the other fiber optic detector, channel 1, was mounted 90° from the line of transmission on top of the detector housing (Figs. 5 and 6). Each fiber optic detector was mounted on a platform capable of small angle tilts as well as two direction translations. The mount for the top fiber was constructed out of two translation stages (see Appendix I) labeled X and Y in Figs. 7 and 8 rotated 90° for translation in both the x- and y-directions. Those two stages were then mounted on an aluminum platform that was capable of tilting through small angles. Two different views of the fiber mount using micrometers are given in Figs. 7 and 8 with approximate dimensions given in Appendix I.

Micrometers were used to tilt and translate the top fiber so that its position could be recorded. Two micrometers were used for tilting the fiber. One micrometer was mounted at a front corner of the tilt plate, while a brass ball was placed under the other front corner to act as a pivot. The second micrometer was mounted at the rear corner of the tilt plate diagonally opposite to the front micrometer and along the same side as the pivot. This setup was mounted to the top of the detector housing by two compression springs and allowed controlled tilting of the top fiber. Two additional micrometers were used to control the translation of the fiber, one in the x-direction the other in the y-direction.

The back fiber mount was similar in its design, but did not utilize micrometers. Instead of micrometers, a series of set screws and springs were used to facilitate the back fiber's movement. Figures 9 and 10 display representations of the mount using set screws. The approximate dimensions of the back fiber mount are given in Appendix I. The lack of micrometers on the back fiber mount was acceptable because, once it was aligned, it remained fixed until realignment was needed for the next experiment. As

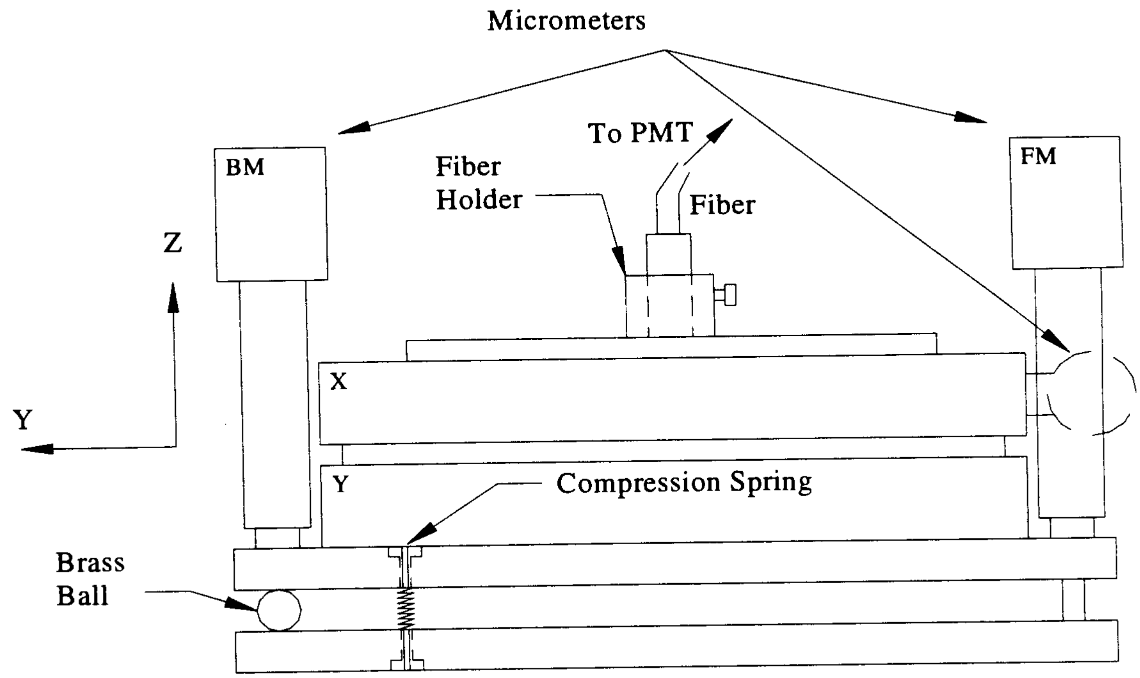

Figure 7: Front view of the top fiber mount. The X and Y denote the direction each translation stage moves, while BM and FM denote the back and front tilt micrometers, respectively.

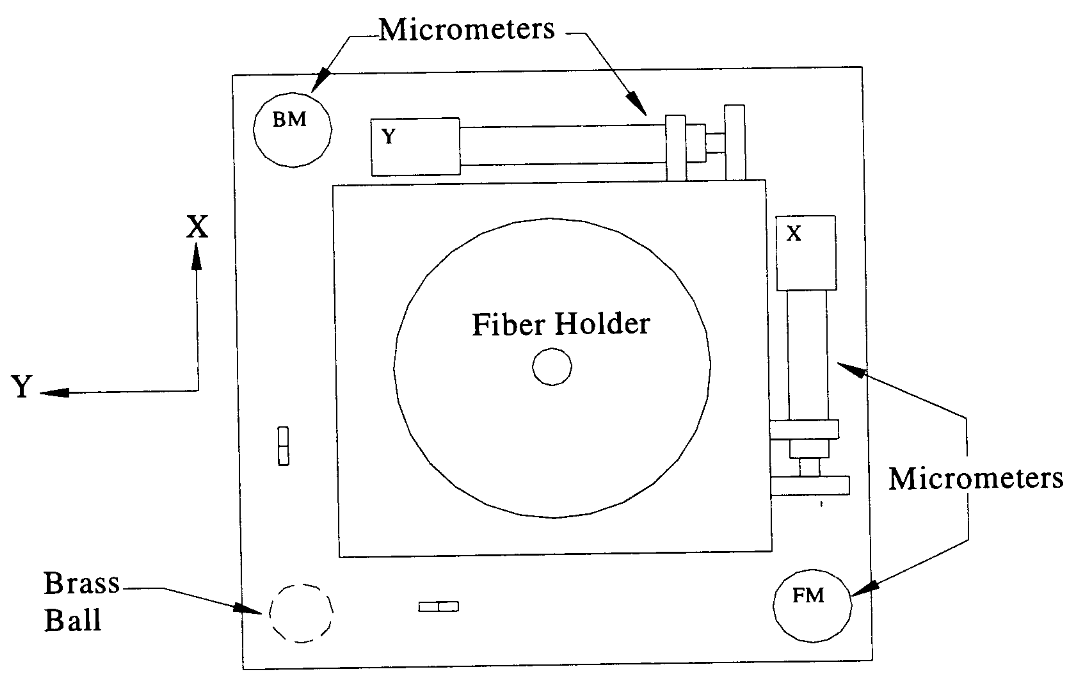

Figure 8: Top view of the top fiber mount. BM, FM, X, and Y are repeated from Fig. 7.

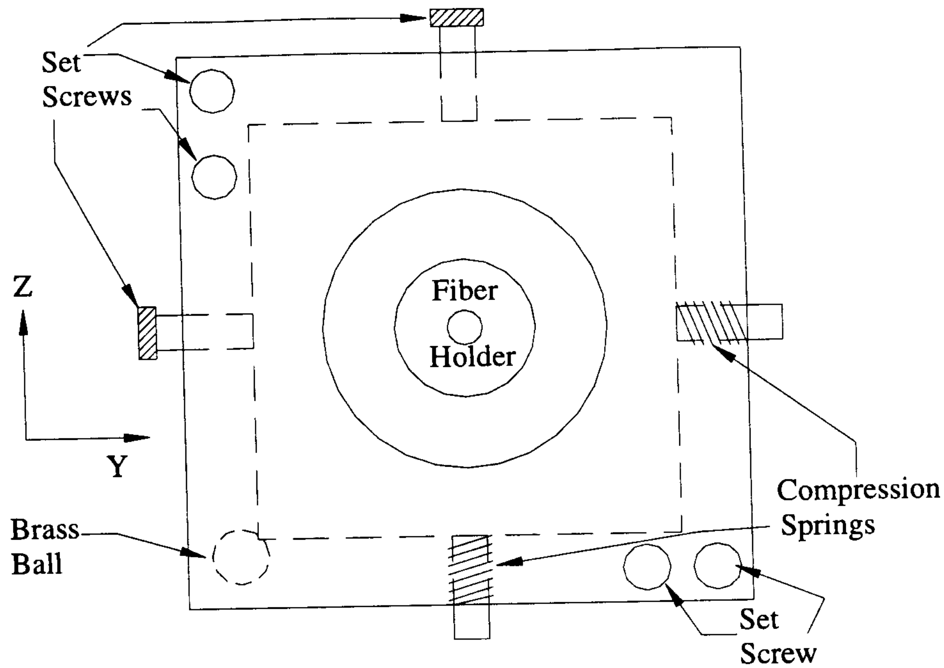

Figure 9: Back view of the rear fiber mount.

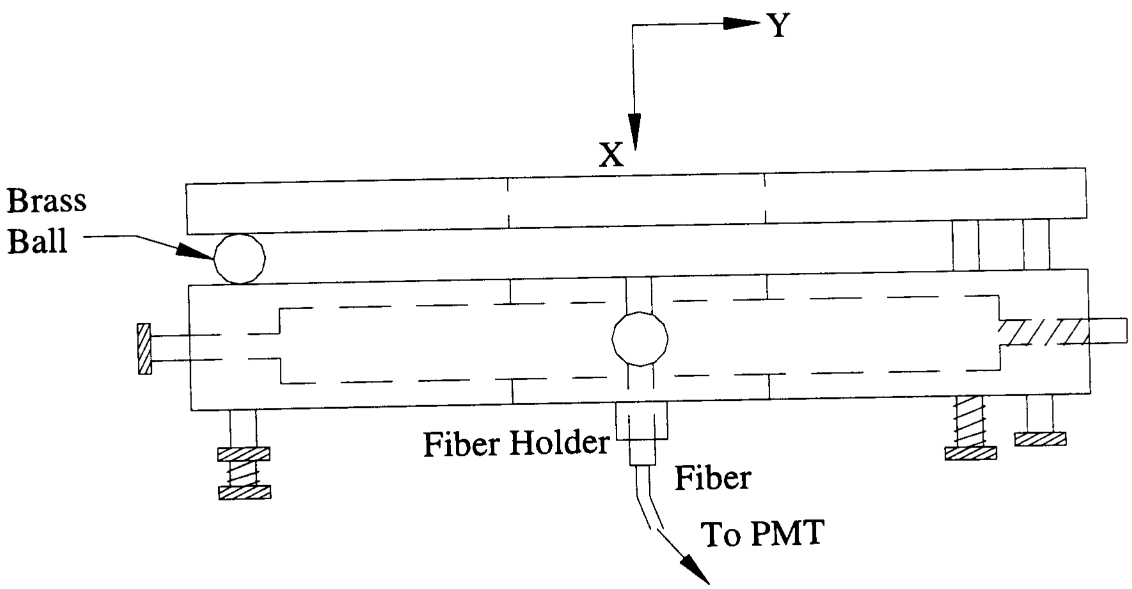

Figure 10: Top view of the rear fiber mount.

described in Section 4.3, the alignment of the setup involved several components including the test cell. Changing the test tube altered the alignment each time. Therefore, the system was realigned after each experiment.

To conduct experiments at several scattering angles, the detector arm railing was mobile and could travel throughout a range of scattering angles from 0° to 130°. No experiments were performed at angles below 30° due to high intensity levels that could damage the photomultiplier tubes. However, a scattering angle of 0° was necessary to properly align the detectors (see Section 4.3). As discussed in the theory, multiple scattering effects must be suppressed to correctly size particles. Although the majority of the suppression came from tilting the top fiber, some additional suppression was accomplished by the use of a polarizer. Single scattering of light is polarization preserving, while multiple scattered light generally does not maintain polarization. Therefore a polarizer that was oriented to transmit only vertically polarized light, i.e., polarized light from the laser, should suppress the multiply scattered signal left after the suppression caused by separating the detectors. The polarizer was mounted on the detection arm of the goniometer between the sample and the detector housing (Fig. 4).

The final pieces of equipment associated with the detection segment of the goniometer were the photomultiplier tubes (Fig. 4). The photomultiplier tubes were connected to the detector housing by single-mode fiber optic cables. Each fiber optic cable carried a scattered signal to one of the photomultiplier tubes. The photomultiplier tubes required two power supplies (see Appendix I). The power supplies were maintained at a constant 12 volts and 5 amps throughout the experiments. Each photomultiplier converted the incoming signal into usable electronic pulses. These pulses were then read and processed by a commercial digital correlator card (ALV-5000).

4.3 Alignment

Like the work done by Phillies (1981), Mos *et al.* (1986), and the other authors cited in the literature review, the success of the experiments described in this thesis depended on the alignment of the setup. Through a trial and error process of data collecting, a defined alignment procedure was developed. Some observations made during this process will be discussed in Chapter VI. The alignment procedure began with the light source itself, the laser. As mentioned previously, the laser was attached to a holder capable of small vertical adjustments. The holder consisted of an aluminum plate mounted on top of another plate. The top plate contained four screws, one at each corner. The screws allowed the laser to be raised uniformly or tilted slightly. A level was placed on the laser and the screws were manipulated until the laser was leveled at the proper height. As a second check in the alignment process, a reference point was then placed on the wall at the spot where the laser contacted it. This spot marked the level of the laser prior to the start of the experiments. The dot was also valuable during the alignment of other components on the goniometer. The alignment of the laser was done once, but was checked prior to realignment for each new experiment and prior to any needed adjustments. Realignment of the laser was usually not necessary, but occasionally was needed due to relaxation of the set screws used to control its positioning.

With the laser aligned, the next step was to align each fiber optic cable. For the alignment of the fiber optic cables, all components were removed from the setup. Alignment of the cables was accomplished by first moving the detector arm to 0°, so that the laser and detector housing were directly opposite of each other. This allowed for each fiber optic cable to see the incident light source directly through the use of the non-polarizing beamsplitter. The beamsplitter (see Appendix I) was designed to deliver 50 ± 3% of the incident beam's power both to the fiber seeing direct transmission and to the fiber seeing reflection (see Fig. 6). Each fiber optic cable was then manipulated by use of the micrometers or the screws (Figs. 7-10) until a beam of light was visible from its unattached end. Upon detection of a visible beam, the next step was to maximize the intensity of the beam exiting each fiber by moving the micrometers for channel 1 and by moving the set screws for channel 0. This was accomplished with the use of the previously mentioned power meter setup (see Appendix I). Holders, mounted on the optical table, were used to fix the position of both the wand of the power meter and the free end of the fiber optic cables during this step of the alignment procedure in order to ensure the consistency of the intensity measurements. With the intensity in each fiber maximized, the next step in the alignment process was to add all components to the goniometer.

The first components to be added to the goniometer were the water bath and the test tube. The water bath alone was added to the sample stand (Fig. 4) and positioned so that the beam passed through its center. Proper positioning was determined by both a visible check of the beam in the water bath as well as by checking for the strongest light from the fibers. The test tube was the next piece to be added. As described in the previous section, the water bath was equipped with a lid and base designed to vertically hold the test sample along the axis of rotation of the goniometer. If needed, the bath and sample were then repositioned by hand to allow the highest intensity light possible to reach the fibers.

The attenuator and polarizer were the next components added to the goniometer. The polarizer was positioned on a stand between the detector housing and the sample (Fig. 4). Alignment of the polarizer was determined by which position allowed for the brightest intensity light from the fiber optics. The attenuator was mounted to the laser arm in front of the laser beam. Since the purpose of the attenuator was to decrease the power of the laser beam, a different alignment criterion was needed. Proper positioning of the attenuator was determined when the back reflection of the laser was directed back onto the edge of the laser opening. Because of possible damage to the laser, direct back reflection into the laser was avoided. The use of the back reflection showed that the attenuator was as perpendicular as possible without introducing laser instabilities. This alignment was desired to limit any stray reflections (caused by misalignment) from being sent to the detection fibers.

The final component positioned onto the goniometer was the lens. The purpose of the lens was to focus the incident beam within the sample. As described in the theory, a tightly focused incident beam was valuable, because it was necessary to reduce the multiple scattering area within the sample. Therefore, proper alignment of the lens was critical in obtaining reliable data. The process of aligning the lens involved both the dot on the wall and the use of the ALV-5000 correlation package. Prior to the alignment of the lens, the detection arm of the goniometer had to be moved to the appropriate scattering angle for the upcoming experiment. Next, the lens holder was attached to the goniometer between the laser and the sample (Fig. 4). The first step in the alignment of the lens was to translate it both vertically and horizontally until the beam from the laser was directed through the center of the sample and on the dot on the wall. The lens was then adjusted along the length of the laser (x-direction) until the 'waist' of the beam was focused at the center of the sample. Due to diffraction effects, the focused beam could not be focused to a point with the lens, but instead was focused down to a condition where a 'waist' appeared. The 'waist' (Fig. 11) was considered the region where the smallest beam diameter occurred and was calculated by the following equation:

$$d \cong \frac{4 \cdot f \cdot \lambda}{D} = \frac{4 \cdot (33\,\text{mm}) \cdot (632.8\,\text{nm})}{(0.68\,\text{mm})} = 39.1\ \mu\text{m}\ , \qquad (4\text{-}1)$$

where d is the 'waist' diameter, D is the incident beam diameter, f is the focal length of the lens, and λ is the wavelength of the incident beam.

In order to complete the alignment of the lens, the fiber optic cables had to be connected to the photomultiplier tubes and the ALV-5000 computer program had to be setup. A discussion of the computer program and its settings will follow in Section 4.4. With the computer parameters set and the computer in the count rate mode, the final alignment of the lens could be completed. The count rate mode was used because it only displayed the intensities seen by the two photomultipliers, channel 0 and channel 1. The lens was adjusted vertically until the count rate of both channels was maximized. The maximized count rates showed that the detectors were looking at the center of the focused beam. After the maximization of the count rates, the intensity of the incident beam had to be attenuated to a workable range (50 to 250 kHz).

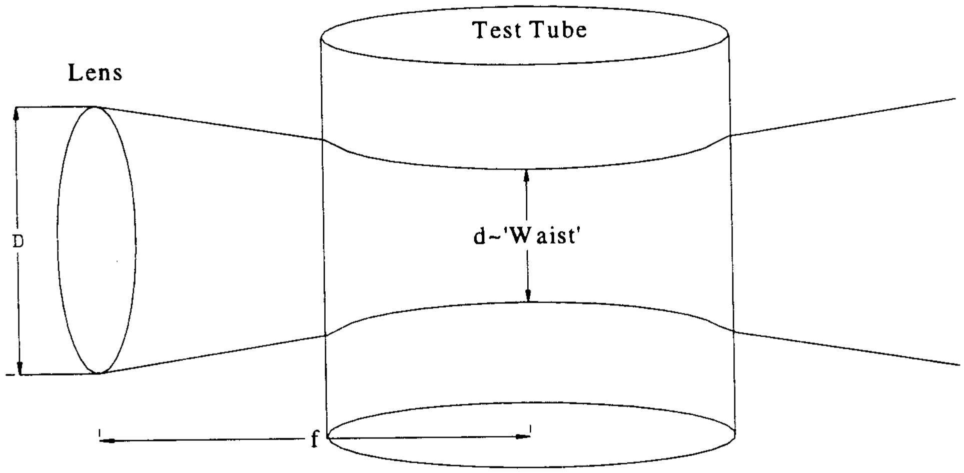

Figure 11: Representation of the beam 'waist' caused by diffraction effects in the test tube, where D is the incident beam diameter, d is the waist diameter, and f is the focal length of the lens. (Not shown to scale)

With all of the components added to the goniometer and aligned, the final adjustments could be made to channel 1. These adjustments were used to produce a signal-to-noise ratio near one and involved the top fiber. A high signal-to-noise ratio or y-intercept represented the level of useful input detected to the amount of background noise detected. It also implied that for a cross-correlation both fibers were looking at the same point in the sample from within the multiple scattering area. The ALV-5000 program was used in the run mode to determine when the top fiber was properly aligned. The program was set up to take multiple runs of 10 seconds per run. The short duration multiple runs were useful in giving immediate information on how a small adjustment of channel 1 affected the signal-to-noise ratio. Maximization of the signal-to-noise ratio was accomplished by adjusting the four micrometers of channel 1 (Figs. 7 and 8). The signal-to-noise ratio was generally maximized around a value of 0.900. With the alignment of channel 1 completed, the micrometer settings were recorded and the experiment could begin.

4.4 The ALV Computer Program

The correlation software package used in these experiments to read and analyze the data from the photomultiplier tubes was the ALV-5000 Multiple Tau Digital Correlator (see Appendix I). The software contains four main menus with several settings listed under each menu. Table 1 shows the parameters that were set at the beginning of each experiment. The rest of the settings were either kept at their default values or were not of interest to the research and therefore were not activated. Information on all parameters can be found in the ALV-5000 manual (1993) given in the reference section of this thesis.

Under the main menu, three subdirectories were useful in setting up the computer. The first subdirectory was the SampOpt subdirectory. This subdirectory allowed input of values that described the sample and setup. The first parameter was the wavelength of the laser used. For the static fluid experiments, the wavelength was 632.8 nm, while the wavelength used in the flowing fluid experiments was 532.5 nm. Other input parameters included refractive index of the sample, absolute temperature of the sample in K, and the type of solvent used in the sample. From these parameters, the ALV-5000 program calculated the viscosity of the sample. The other useful subdirectories under the main menu, were Angle and Multi. The subdirectory Angle allowed input of the scattering angle, θ, for each experiment. The subdirectory Multi was used to turn multiple runs on or off. This was valuable during the alignment of the setup (see Section 4.3).

Similar to the main menu, the control menu contained three subdirectories useful in the set up of the ALV-5000 program. The Scale subdirectory enabled the program to reduce the number of bits of information in the form of intensity that it was reading from each channel. This prevented intensity overflows in the two channels and allowed for an optimum performance of data fitting by the program. The Setup subdirectory contained several parameters that pertained to the type of experiment being performed. Duration was the amount of time each run would last. For the experiments performed in this thesis, a single correlation measurement was used, which had an initial sample time of 0.2 μs. Both auto- and cross-correlation measurements were performed, depending on the type of experiment being performed. During autocorrelation measurements, it was necessary to select which channel was to be used, channel 0 or channel 1. The final subdirectory of the control menu was the FileOpt subdirectory. This gave the user the option of saving information as an ASCII or a Binary data file. ASCII was useful in that it saved information in data sets containing the correlation data and its corresponding time. ASCII data was used to produce Figs. 22-25 in Section 6.5.1. Binary files were used the remainder of the time because they contained all of the pertinent information in a better disk space conserving manner.

Table 1: Input values for the ALV-5000 computer program.

Directory	Subdirectory	Parameter	Input Value or Setting
Main Menu			
F5	SampOpt	Wavelength	632.8 or 532.5
		Refractive Index	1.33
		Solvent Viscosity [cP]	Calculated by program using the input temp.
		Probe Temperature [K]	296
		AutoCorrect for Solvent	Water
F6	Angle	Scattering Angle, θ	30 to 150 degrees
F7	Multi	Enable Multiple Runs	On or Off
Shift Menu			
F9	GetWin	Get saved version of the display windows	c:/ryan.win
Alt Menu			
F8	FitPar	First Evaluated Channel	10
		Last Evaluated Channel	128
Control Menu			
F2	Scale	Autoscale	
F3	Setup	Duration [s]	120 to 600
		Single/Dual/Fast	Single
		Auto/Cross	Varied per experiment
		Input Channel	Ch 0 or Ch 1
F4	FileOpt	Data File Format	ASCII or Binary

4.5 Sample Preparation

The experiments performed using the static fluid setup dealt with particle sizing of nanometer spheres. Therefore, it was necessary to use special care when preparing the samples and not contaminate them. Duke Scientific supplied the core samples used in the experiments (see Appendix I). The core samples were polystyrene latex spheres at 10 percent solids by weight, which were then diluted down to a desired volume fraction for an upcoming experiment.

Preparation of the samples followed an established procedure to ensure consistency in the experiments. The first step was to wash a new test tube with deionized water to remove any dust. The deionized water came from an E-pure deionizer (see

Appendix I) and was stored in a sealed container. The storage of the water in the lab was done to allow the water to reach room temperature. With the test tube washed and dried, the next step was to weigh it and record the weight. This was done with an electronic lab scale (see Appendix I). The test tube was then filled with water and weighed again, with that weight also being recorded. When making these samples, a known volume fraction was desired. Therefore a calculation was made to determine the total weight of the test tube, the water and the sample necessary to produce that volume fraction. From that calculation, the required amount of the core sample by weight was then added using a pipette.

Hand calculations were used to compute the exact volume fraction using the weight of the test tube dry, the weight of the test tube and the water, the total weight of the test tube, water, and sample, and the percent solids of the core sample. These calculations are covered in Sundaresan (1999). The final step was to seal the test tube with Parafilm (see Appendix I) and label it with the volume fraction and the date prepared. The life expectancy of most samples was two to three weeks.

4.6 Experimental Procedure

The main goal of this thesis was to show how the two suppression techniques could be applied to a flowing multiple scattering sample for particle sizing. This chapter deals with the technique used to suppress the effects of multiple scattering. The previous sections described the procedure necessary to set up and align a non-flowing, dynamic light scattering experiment. This section describes the steps followed in carrying out the tilt angle sweep experiments. The purpose of these experiments was to separate the fibers enough to map the speckle profile from multiple to single scattering.

As described in the theory, the method used to suppress multiple scattering involved two single-mode fiber optic cables that were separated by milliradians. Referring to the alignment procedure (Section 4.3), both fiber optics were adjusted to look at the focused beam from within the multiple scattering area. This resulted in a signal-to-noise ratio near unity and an intercept of the correlation function, displayed by the correlation package, near its theoretical limit of 2.0 [Nobbmann (1997)]. It was from this position where the first run was taken for a duration of 120 seconds. For each run, the initial delay time was 200 nanoseconds, and was increased automatically by the software to an optimum value. Data from each run was stored as an intensity correlation, $g^2(\tau)$, and was converted by the software to the electric field correlation, $g^1(\tau)$, by Eq. (3-7). This data was then saved on disk.

The top fiber was then tilted one or two divisions by the use of the back micrometer (Figs. 7 and 8). The movement of the top micrometer was calibrated by reversing a laser back through the fiber optic and noting the change in position of the light on a screen at a known length from the fiber's axis of rotation. From this calibration, it was determined that one division on the micrometer equaled 0.1125 mrad. After each tilt, the fiber was translated along the scattering direction until the intensity of channel 1 was maximized (Figs. 5 and 7). The ALV-5000 program was used in the multiple run mode for a duration of 10 seconds to determine when the intensity was maximized. For each scattering angle tested, this procedure was repeated in both tilt angle directions until the signal-to-noise ratio became too small to give reliable data. The results from these experiments can be seen in Chapter VI.

CHAPTER V

FLOWING FLUID CONDITIONS: EXPERIMENTAL SETUP, ALIGNMENT, AND PROCEDURE

5.1 Introduction

Chapter IV explained the equipment used for multiple scattering suppression in a static fluid sample and its alignment. This chapter will focus on an experimental setup for flowing media capable of applying the same multiple scattering suppression technique. A technique for suppression of flow effects will also be discussed. The goniometer and flow circuit used in integrating the two suppression techniques were designed using the same principles as the static fluid setup. Details of the actual goniometer design are given in Sundaresan (1999). Therefore, this chapter will only give a brief description of the components used and any modifications that were made in switching from the static fluid setup. This will be followed by a discussion of the flow circuit and its design. Also discussed in this chapter will be the alignment of the setup and the experimental procedure used to collect data. The processes used to set up the ALV-5000 computer program and produce samples for the flowing setup were similar to the ones covered in Chapter IV. Any deviations from those processes will be mentioned.

5.2 Experimental Setup

Figure 12 gives a schematic diagram of the experimental setup used to perform particle sizing in a flowing fluid. Similar to the goniometer described in Chapter IV, this one can also be broken into three sections. The laser arm, the sample stand, and the detector arm were all modeled after the parts previously described in Chapter IV. A diagram of the dual detector setup used here can be seen in Figs. 5 and 6. However to accomplish both types of suppression, some of the equipment from the static fluid setup had to be replaced or modified. Since a detailed description of the goniometer design is presented in Sundaresan (1999), this section will give only a brief description of the equipment used and its general layout.

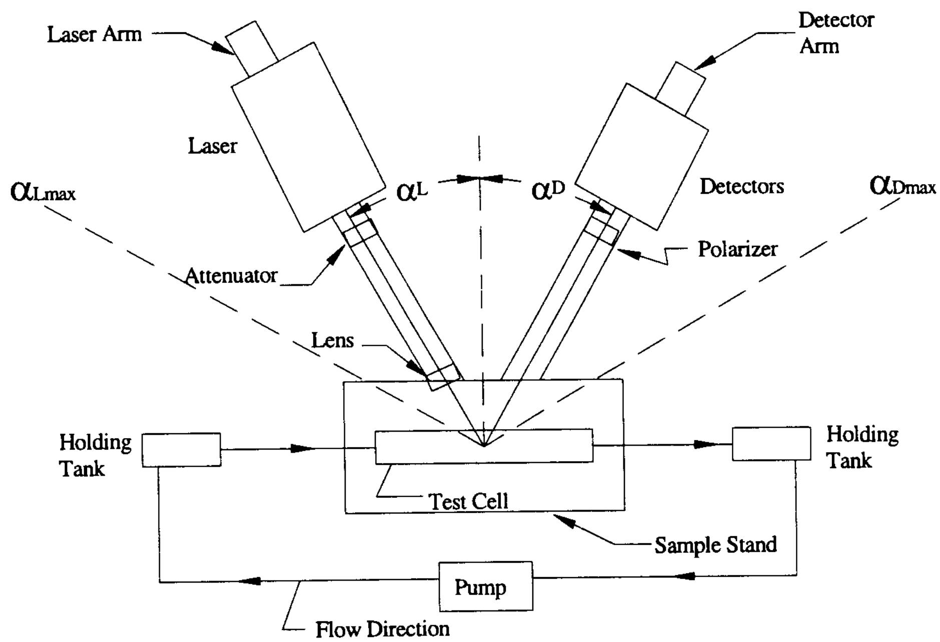

Figure 12: Experimental setup for simultaneous suppression of multiple scattering effects and of flow effects.

Like the static fluid setup, the first component of the setup was the light source. The light source was changed from the He-Ne laser used in the static fluid setup to a Neodymium-Yttrium-Aluminum-Garnet (Nd: YAG) laser (532.5 nm wavelength). The 100 mW Nd: YAG laser was vertically polarized and had an original beam diameter of 0.70 mm. As in the static fluid setup, a holder mounted the laser to the goniometer arm. The holder maintained the horizontal alignment of the laser, while being capable of vertical adjustments. The same adjustable attenuator, lens, and lens holder from the static fluid setup were the final components mounted to the laser arm (see Fig. 12). Unlike the static fluid setup, the laser arm for the flowing setup was mobile and could travel over a range of 0° to 48°. This range is marked as α_L and can be seen (Fig. 12) to run from a position where the laser points in the direction perpendicular to the test cell ($\alpha_L = 0°$) to where the sample stand interfered with the arm's movement ($\alpha_{Lmax} = 48°$).

For detection of the scattered signals, the same detector housing (see Fig. 6) was used as in the static fluid setup. This allowed the same technique of multiple scattering suppression to be utilized. The fiber optic cables and beamsplitter used in the static fluid setup were replaced with two new single-mode fiber optic cables specified for a 533 nm wavelength laser and a multi-band, nonpolarizing beamsplitter (see Appendix I) to accommodate the new laser. The new beamsplitter delivered 45 ± 5% of the laser's power to both channels equally. The same polarizer was used here as in the static fluid setup, and it was mounted in the detector housing in front of the beamsplitter. Like the laser arm, the detector arm was mobile over a range of 0° to 48°. This range started at the point where the detector arm was perpendicular to the test cell ($\alpha_D = 0°$ in Fig. 12) and ran to where the sample stand interfered with the arm's movement. This range is noted by α_D in Fig. 12. The photomultiplier tubes, the power supplies and the ALV-5000 correlation package described in Sections 4.2 and 4.3 were used in this setup as well.

The final section of the goniometer was the sample holder (Fig. 13). Like the static fluid setup, the sample holder was mounted on the axis of rotation of the goniometer. The sample holder for the flowing setup was a filter holder (see Appendix I) used to hold the rectangular test cell in place. The holder was mounted to a dovetail slide on top of the goniometer. The dovetail allowed the entire test cell to be moved in a direction that adjusted the depth of the laser inside the cell. The dovetail was equipped with a micrometer, so the position of the test cell could be marked and the depth of the laser within the test cell could be estimated (Fig. 13). The reason this depth was estimated will be discussed in Section 5.3. The slide portion of the dovetail carried the sample holder and contained a rotation stand made from Teflon. The rotation stand allowed the entire sample holder to be rotated through an angle of $\delta = \pm 60°$ (Fig. 13). The usefulness of this feature will be discussed in Chapter VI, where results will be shown for experiments in which δ was varied through $\pm 10°$.

The final component of the experimental setup was the flow system. The flow system was used to continuously circulate the fluids during the experiments. The flow system consisted of two holding tanks, a shuttle pump, the rectangular test cell, and Tygon tubing (see Appendix I). The holding tanks were fabricated from

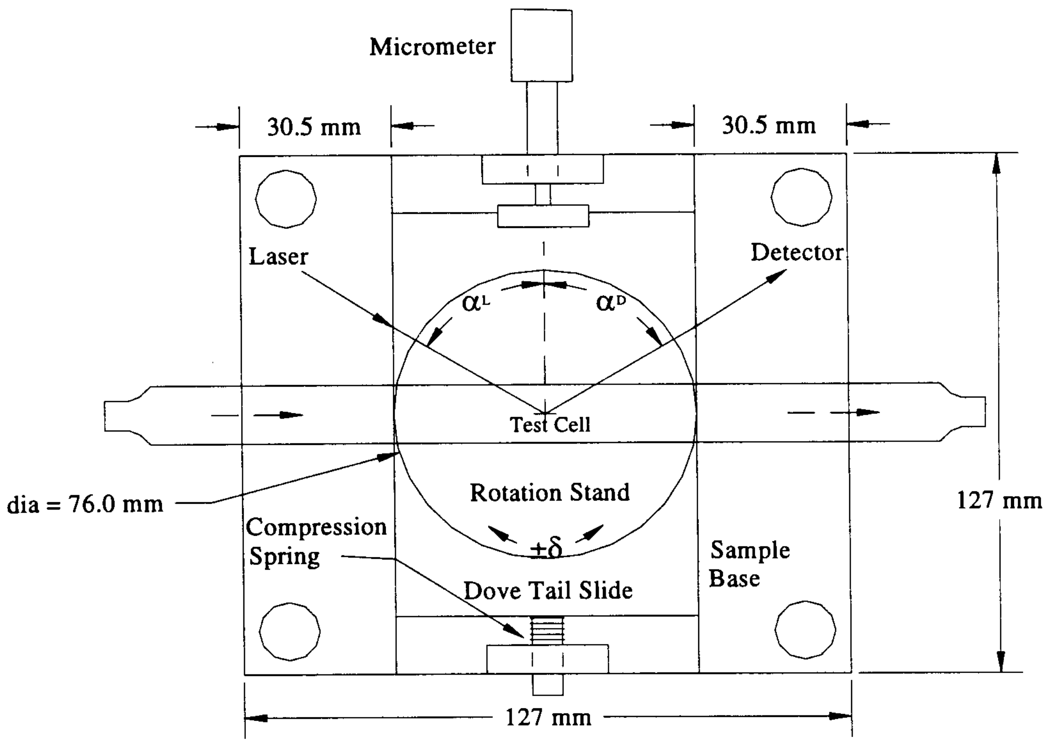

Figure 13: Diagram of the test cell mounted on the rotation stand and the angle of rotation, δ. A negative δ represented a rotation of the test cell toward the laser (counter clockwise), while a positive value meant a rotation toward the detector housing (clockwise). Also shown is the dovetail and micrometer used to move the test cell.

Plexiglas (see Appendix I). Both tanks were designed with large lids for easy filling and cleaning and had a capacity of 250 ml each (Fig. 14).

A dual channel shuttle pump was used to circulate the fluid throughout the system (see Appendix I). The shuttle pump was selected because it was capable of pumping at flow rates ranging from 1.25 to 25 ml/min without damaging the particles. This was a valuable aspect in the design of the flow system, because the theory used in determining the particle size was based on light scattering by spherical particles. The shuttle pump's design was similar to a peristaltic pump in that an oscillating mechanism squeezed the tubing to generate the flow.

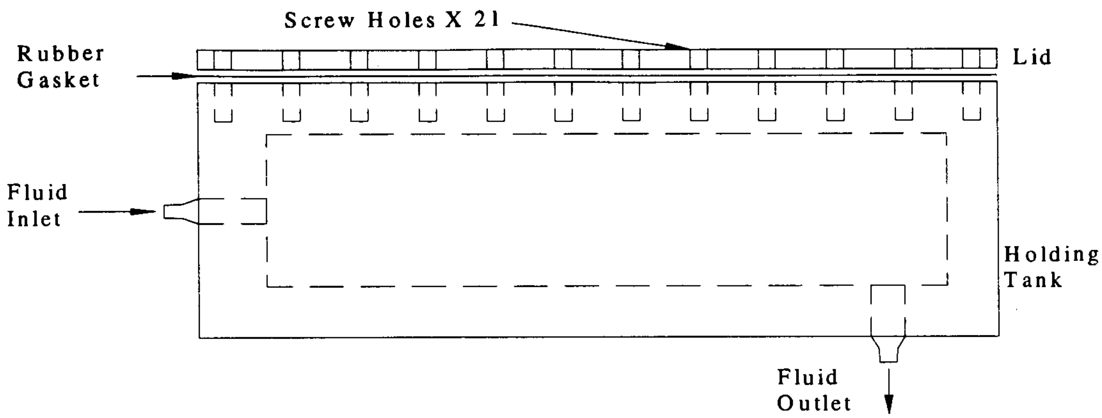

Figure 14: Side view of the holding tanks, lid, and gasket used in the flow circuit.

However, the shuttle pump's design produced flow without the tubes being squeezed to occlusion, which significantly reduced the possibility of damaging the micron sized test particles. Results from experiments utilizing the flow system will be presented in Chapter VI for various flow rates. Table 2 shows experimentally determined values for the different flow rates used throughout the research and the corresponding velocities to those flow rates. The average velocities were calculated by dividing the flow rate by the cross sectional area of the test cell (48 mm^2).

Table 2: Experimentally determined flow rates and their corresponding calculated average velocities.

Pump Settings	Calculated Flow Rate (ml/min)	Calculated Average Velocity (mm/sec)
0% Flow	0.00	0.00
50% Flow	9.46	3.28
75% Flow	15.07	5.23
100% Flow	22.40	7.78

The most vital component in the flow system was the rectangular test cell (see Appendix I). The test cell used in the flowing experiments was made from quartz glass and had dimensions of 6 mm x 8 mm x 30.48 cm. The length of the tube was necessary to produce a fully developed laminar flow profile and to reduce the possibility of entrance effects interfering with the experiments. The following simple calculations were performed to show that the flow system produced the situation described above. The Reynolds Number was first calculated with the following equation [Janna (1993)]:

$$\mathrm{Re} = \frac{D_h \varrho v}{\mu} =$$

$$\frac{(6.86 \times 10^{-3}\ \mathrm{m})(997.3\ \mathrm{kg/m^3})(7.78 \times 10^{-3}\ \mathrm{m/s})}{(947.95 \times 10^{-6}\ \mathrm{Pa \cdot s})} = 56, \qquad (5\text{-}1)$$

where ρ is the fluid density, μ is the dynamic viscosity of the fluid, v is the fluid velocity, and $D_h = \frac{4A}{P}$ is the hydraulic diameter with A being the cross-sectional area and P being the wetted perimeter. From the Reynolds Number, it was determined that the flow regime was laminar (Re < 2300), which was desired for suppression of flow effects. With the Reynolds Number determined, calculation of the length necessary for fully developed flow was performed using this equation [Janna (1993)]:

$$L_e = (0.06)(D_h)(\mathrm{Re}) = (0.06)(6.86\ \mathrm{mm})(56) = 23\ \mathrm{mm}. \qquad (5\text{-}2)$$

Experiments using the flowing fluid system were performed near the center (~150 mm from the entrance) of the test cell, and therefore were conducted in a region of fully developed flow. Further calculations depicting the fully developed flow profile can be seen in Appendix IV. Also contained in Appendix IV is a discussion of the time constants associated with fluid flow and Brownian motion of the particles.

5.3 Alignment

It has already been demonstrated in Chapter IV that the alignment of a dynamic light scattering device is critical. This setup is no different from any of the others that have been previously mentioned. The alignment process of the flow setup was very similar to the process described in Section 4.3.

The first component of the flowing setup to be aligned was the laser. To accomplish this, the laser arm (Fig. 12) was moved to $\alpha_L = 0°$ or the point were the laser arm was perpendicular to the test cell. To aid in the alignment of the laser and the fiber optics, a mirror was placed in the sample holder. With the mirror in place, the laser was adjusted until the back reflection was co-linear with the incident beam, which was determined by reflecting the beam almost back into the hole where the beam exits the laser. This positioning meant that the laser was aligned both horizontally and vertically. Once alignment was achieved, the laser was moved to the desired angle, α_L, for the upcoming experiment. Scattering angle calculations, corresponding to different laser and detector angles, are given in Section 5.4. The detector arm was then positioned at an angle that corresponded to $\alpha_L = \alpha_D$. As described in Chapter III, this allowed for the suppression of the flow effects by creating a scattering vector perpendicular to the flow vector. A second benefit of this positioning was apparent during the alignment of the multiple scattering suppression equipment (i.e., the detectors). Laser arm and detector arm positions corresponding to $\alpha_L = \alpha_D$ matched the angles necessary for the incident beam to be reflected into the detector housing by the mirror. This positioning was equivalent to that described in Section 4.3, where the detector arm was moved to $\theta = 0°$ in order to directly view the incident beam. A similar alignment procedure as that described in Section 4.3 was followed for the detectors. With the laser and the fiber optic cables aligned, the mirror could be removed, and the following components could be added: the attenuator, the polarizer, the lens, and the test cell.

The first components added to the setup were the attenuator and the polarizer (Fig. 12.). The alignment procedure for these two pieces was identical to that described in Section 4.3. After the addition of the polarizer and attenuator, the fiber optic cables were connected to the PMT's, and the computer was set up following the procedure previously described in Section 4.4.

The next component added to the setup was the test cell. Initially the test cell was placed in the holder so that the 8 mm wall appeared to be visibly perpendicular to the incident laser beam. Because of the use of a rectangular test cell, direct specular reflections from the front and back walls caused intensity levels too high for the PMT detectors (see Fig. 15). The reflections also caused heterodyning that interfered with the collection of data. To alleviate these problems, the test cell was slightly rotated from its vertical orientation (approximately 5.0° about an axis parallel to the cell's length) to direct the reflections away from the fiber optics. This method of reducing the reflections at the detector was only partially successful, and a second method had to be employed to suppress specular scattering.

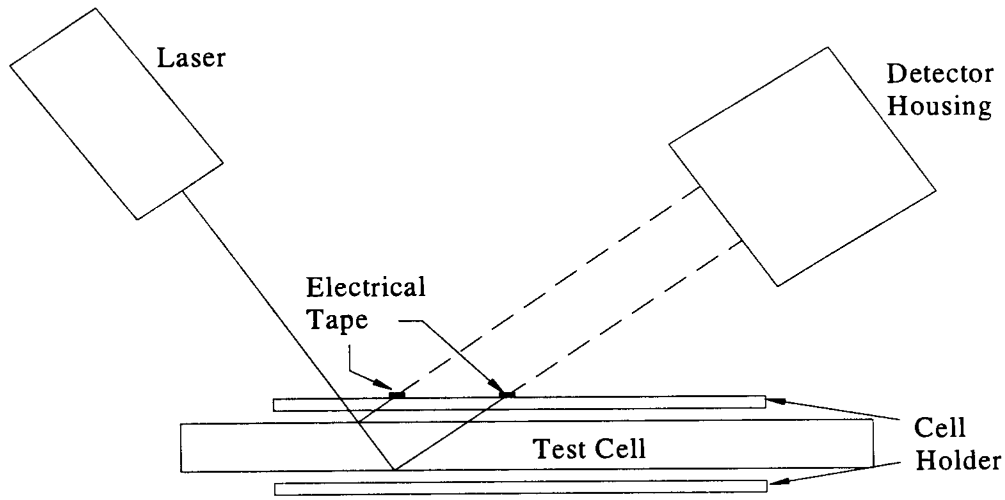

Figure 15: Schematic showing the positioning of the electrical tape to block reflections.

The second method consisted of applying two small strips of electrical tape to the sample holder (see Fig. 15). One strip blocked light reflecting from the front wall, while the second strip blocked the reflection from the back wall. The two strips had to be placed on the holder in a manner that blocked only the reflections and did not interfere with the scattered signal. The count rate mode, of the ALV-5000 software, was useful in applying the strips of tape to the holder by showing when a strip blocked out the scattered signal and not just the reflection. The last step in aligning the test cell was to move it so that the detection area was just inside the front wall. This was accomplished by moving the dovetail slide toward the laser and detectors with a micrometer while making autocorrelation readings with the ALV-5000 program (see Fig. 12). Readings of the signal-to-noise ratio were taken every 10 divisions turned on the micrometer (5 divisions = 0.05 mm). It was found that after approximately 100 divisions (1.0 mm), the signal-to-noise ratio had risen to a usable level near 0.9. All experimental results described in Chapter VI were performed at this approximate depth into the test cell.

With the test cell in place and the reflections blocked, the final component to be added to the setup was the lens. The lens was placed on the goniometer between the attenuator and the test cell. The lens was first adjusted vertically and horizontally until the count rate in both channels was maximized. The lens was then adjusted along the direction of the laser beam until the 'waist' of the laser beam was focused at the location where the detectors were looking. This alignment was determined also by maximizing the count rate of both channels. As in the static fluid setup, the ALV-5000 software was used during this process to determine the lens position that maximized the count rate. At this point, the last step in the alignment procedure was to repeat the steps outlined in Section 4.3 to maximize the signal-to-noise ratio.

5.4 Scattering Angle Calculations

Knowledge of the scattering angle is a necessary part in the success of any dynamic light scattering experiment in which the goal is to determine particle size. This is because Eq. (3-7) depends on the scattering angle to calculate particle size, and therefore an incorrect scattering angle would lead to an incorrect calculation of the particle size. For the flowing setup, the scattering angle had to be calculated before any runs could be made. The scattering angle is defined as the angle between the light directly transmitted through the sample volume and the direction from the sample volume to the detector and is given by the symbol θ in Fig. 16. The determination of the scattering angle is generally a straightforward process, but for the flowing system, it was complicated by refraction of the incident beam in the sample. As seen in Fig. 16, the scattering angle is altered by refraction effects at the boundary between the air and the sample. The air to glass and the glass to sample boundaries are assumed to be parallel. Therefore, the net refraction effects from those two boundaries sums to zero. Due to these refractive effects, the scattering angle becomes a function of several variables.

The following calculations were used to determine the different scattering angles used in the flowing experiments. The results of these calculations are summarized in Table 3. Also all variables used in the following section refer to Fig.

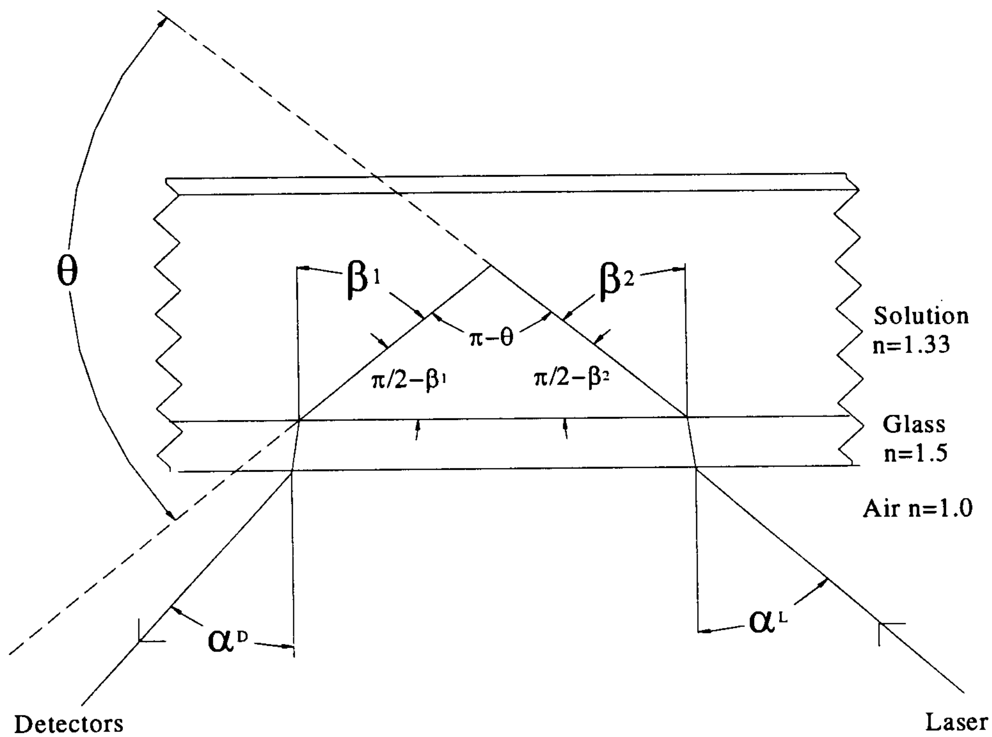

Figure 16: Refraction effects on the scattering angle in the flow cell. (Not drawn to scale)

16. Calculation of the scattering angle was governed by simple trigonometric functions as well as Snell's Law, which states:

$$n_{solution}\left[\sin(\beta_{1,2})\right] = n_{air}\left[\sin(\alpha_{L,D})\right]. \tag{5-3}$$

The scattering angle, θ was given as follows:

$$\theta = \pi - \beta_1 - \beta_2 = \pi - 2\beta , \tag{5-4}$$

where β_1 and β_2 were calculated by Snell's Law and were equal by the fact that $\alpha_L = \alpha_D$, and the bisector between those angles was perpendicular to the test cell in the experiments performed for this thesis.

5.5 Experimental Procedure

This chapter has dealt with the experimental setup used to apply two independent suppression techniques to a dense flowing suspension for particle sizing. The previous sections have described the equipment used as well as the alignment procedure necessary to obtain reliable data from the setup. This section describes the experimental procedures used to carry out different tests with the setup. The first type of experiment performed with the flowing setup was performed on single scattering samples to show how rotation of the test cell would affect flow suppression. The second type of experiment was performed to demonstrate how effective the suppression of multiple scattering would be in a flowing media.

Table 3: Summary of scattering angle calculation for experiments where $\alpha_L = \alpha_D$ and $\beta_1 = \beta_2$.

$\alpha_L = \alpha_D$		$\beta_1 = \beta_2$	θ (Degrees)	$\alpha_L = \alpha_D$		$\beta_1 = \beta_2$	θ (Degrees)
Degrees	Radians	(Degrees)		Degrees	Radians	(Degrees)	
20	0.35	14.90	150.20	46	0.80	32.74	114.52
21	0.37	15.63	148.74	47	0.82	33.36	113.28
22	0.38	16.36	147.28	48	0.84	33.97	112.06
23	0.40	17.08	145.83	49	0.86	34.57	110.85
24	0.42	17.81	144.39	50	0.87	35.17	109.66
25	0.44	18.53	142.95	51	0.89	35.75	108.49
26	0.45	19.24	141.51	52	0.91	36.33	107.33
27	0.47	19.96	140.08	53	0.93	36.90	106.19
28	0.49	20.67	138.66	54	0.94	37.47	105.07
29	0.51	21.38	137.24	55	0.96	38.02	103.96
30	0.52	22.08	135.84	56	0.98	38.56	102.88
31	0.54	22.78	134.43	57	0.99	39.09	101.81
32	0.56	23.48	133.04	58	1.01	39.62	100.77
33	0.58	24.17	131.65	59	1.03	40.13	99.75
34	0.59	24.86	130.27	60	1.05	40.63	98.74
35	0.61	25.55	128.90	61	1.06	41.12	97.76
36	0.63	26.23	127.54	62	1.08	41.60	96.81
37	0.65	26.90	126.19	63	1.10	42.06	95.88
38	0.66	27.57	124.85	64	1.12	42.52	94.97
39	0.68	28.24	123.52	65	1.13	42.96	94.09
40	0.70	28.90	122.20	66	1.15	43.38	93.23
41	0.72	29.56	120.89	67	1.17	43.80	92.41
42	0.73	30.21	119.59	68	1.19	44.20	91.61
43	0.75	30.85	118.30	69	1.20	44.58	90.83
44	0.77	31.49	117.03	70	1.22	44.95	90.09
45	0.79	32.12	115.76	71	1.24	45.31	89.38

5.5.1 Cell Rotation Effects

Preliminary experiments were performed with the flow setup to determine the sensitivity of the suppression technique to flow effects. These experiments were conducted on dilute samples, the results of which will be given in Chapter VI. From the alignment procedure (Section 5.3), the laser and detector arms were already positioned where $\alpha_L = \alpha_D$ and the test cell was perpendicular to the angular bisector between the two arms. The suppression experiments involved taking autocorrelation measurements over a range of cell rotation angles from δ = -10° to δ = +10° (Fig. 12). The first experiments were done for a cell rotation of δ = 0°. Autocorrelation measurements were taken for flow rates of 0 %, 50%, and 100% (see Table 2). The test cell was then rotated to -5°, -10°, +5°, and +10° and the same autocorrelation measurements at all of the flow rates listed above were taken at each rotation angle. A negative δ represented a rotation of the flow cell toward the laser, while a positive δ represented a rotation toward the detector housing (Fig. 13). Each time the test cell was rotated, the electrical tape used to block reflections was adjusted according to the procedure given in Section 5.3. This process was repeated for 0.204 μm and 0.300 μm PSL particles.

5.5.2 Particle Sizing Experiments

The experiments performed using the flow setup were done to show how both multiple scattering effects and flow effects could be suppressed in order to determine particle size. The same steps from the procedure used on the static fluid setup (Sections 4.3 and 4.6) were repeated with the flowing setup to accomplish the suppression of the multiple scattering effects. Many of the steps already described (see Section 5.3) during the alignment of the flow setup helped to ensure that the flow effects were suppressed. Those steps included positioning the laser (incident wave vector) and detector (scattered wave vector) arms where $\alpha_L = \alpha_D$ and having the bisector between the two arms perpendicular to the test cell. Both of these facts produced a scattering wave vector perpendicular to the flow vector. As described in Chapter III, suppression of flow effects was accomplished by the dot product of these two vectors equaling zero (Eq. (3-14)). Results from experiments with the flow setup on signal-to-noise ratio mapping and diameter mapping will be shown in Chapter VI for a variety of concentrations, particle sizes, and flow rates at a scattering angle of 112°.

CHAPTER VI

RESULTS AND DISCUSSION

6.1 Static Fluid Setup: Introduction

The purpose of this thesis is to show how two independent suppression techniques can be applied to a flowing system to determine particle size. The experimental setup described in Chapter IV was used to show how a single-beam, two detector system could be used to suppress multiple scattering in a static fluid sample. Several of the preliminary experiments performed using the static fluid setup did not yield the necessary data to determine particle size. However, these experiments were not failures, as they led to a discovery of nine characteristics of the static fluid setup. Four of these characteristics will be discussed in detail in Section 6.2 and the five other characteristics are discussed in Sundaresan (1999). The last 17 experiments performed using the static fluid setup did yield data usable to determine particle sizes. Three experiments were performed and repeated at a scattering angle of 90° on samples in a square cell. The experiments included various volume fractions of 0.107 μm PSL particles and are discussed in Sundaresan (1999). Also described in Sundaresan (1999) is a match of those experiments to Eq. (3-8) from the theory. The last 11 static fluid setup experiments were performed using a circular cell and a water bath. These experiments were performed at a variety of scattering angles on different volume fractions of 0.107 μm PSL particles (see Appendix I). Section 6.3 will review the results from experiments performed using the static fluid setup. Table 4 contains a summary of the last 17 static experiments performed, and Table 5 shows detailed results of the experimental data corresponding to the static fluid figures presented in this chapter. Both tables are given in Appendix II.

6.2 Static Fluid Setup Characteristics

As previously mentioned, the first static fluid experiments were performed to gain experience in employing the multiple scattering suppression technique. Through this experience, nine characteristics were discovered about the static fluid setup and are listed below. A discussion of the first four will follow the list, while the last five are covered by Sundaresan (1999).

1. Flaws in the beaker used to hold the water bath interfered with data collection.

2. To align the detectors properly, maximize the count rate in both channels at a scattering angle of 0° first. Then move the detector arm to the desired scattering angle and maximize the signal-to-noise ratio by adjusting channel 1. These steps should be performed prior to each new experiment.

3. During the tilt angle sweep, the intensity of channel 1 should be maximized by translating the fiber after each tilt as described in Section 4.6.

4. The theory describing the suppression of multiple scattering is based on the idea that the detection area of each fiber overlaps the area through which the incident beam passes in the sample. To ensure this all components should be aligned horizontally.

5. Measurements at scattering angles less than 60° were hard to align due to uncontrollable intensities detected due to direct transmission from the sample.

6. As explained in Section 4.3, the positioning and alignment of the lens is critical to the collection of usable data.

7. Also critical to the collection of usable data is the positioning of the detector housing.

8. The use of 0.107 μm PSL particles was found the most reliable diameter particles to work with.

9. Larger particles were thought to settle and therefore not behave as Brownian particles, which led to problems in the determination of their sizes.

The first characteristic that was found using the existing static fluid setup involved the water bath. It was originally contained in a 150 ml beaker that had been modified to hold the water bath. The top of the beaker had been cut off flat and a lid had been manufactured from Teflon to hold the test tube vertically at the center of the beaker. Several problems arose during the use of this beaker to hold the water bath, including interference of the incident beam by the labeling printed on the beaker's side. As previously mentioned in Chapter IV, component alignment was critical to the collection of reliable data. The writing on the beaker often interfered with that alignment, as special care was necessary to ensure that neither the incident nor the scattering light directions passed through the writing. A second similar problem stemmed from the lines in the beaker glass. These lines were a product of how the beaker was made and caused problems with the purity of the incident beam. To alleviate the problems, a piece of glass tubing (see Appendix I) was formed by the Oklahoma State University Glass Shop into a new container for the water bath. The new container was free of these problems and therefore helped to ease alignment and to provide data that was more reliable.

The second characteristic dealt with the alignment of the detectors. The preliminary experiments preformed with the static fluid setup led to the procedure described in Section 4.3. The fiber optic detectors were initially aligned at a scattering angle of 0° (θ in Fig. 4) to start each experiment. This was done to ensure that the detection areas of both fibers were coincident with the incident beam. Next, the detection arm was moved to the desired scattering angle, and the remaining steps of the alignment procedure were completed. With the alignment procedure completed, the final step was to maximize the signal-to-noise ratio, which is also described in Section 4.3. This step was performed in order to ensure that both channels were focused on the same location within the sample.

The third characteristic dealt with the alignment of the top fiber throughout the tilt angle sweep experiments described in Section 4.6. From the alignment described in Section 4.3, it was assumed that both channels were focused on the same point at the center of incident beam. This point should correspond to a maximum count rate in both channels. Each time that the detector for channel 1 was tilted, it was no longer looking at the same point as the detector for channel 0; and therefore it was translated in the proper x-direction (Fig. 5) until its count rate was maximized. If the detector for channel 1 was tilted upward, a translation towards the sample was necessary, while a downward tilt corresponded to a translation in the opposite direction.

Characteristic 4 dealt with the horizontal alignment of the components on the goniometer. As mentioned in Section 3.3, an overlap between the detection area of the fiber optics and the focused beam in the sample was necessary to achieve a correlation function. This alignment was controlled at several locations on the flow system. In particular, the lens and laser holders were useful in accomplishing the desired horizontal alignment. The laser holder controlled the height of the laser to begin the experiment.

The lens holder overcame any refraction problems from the water bath or sample by adjusting the height of the incident beam before it entered the water bath.

The four characteristics described above along with the five discussed in Sundaresan (1999) led to the procedural steps described in Section 4.3. The knowledge gained by performing these preliminary experiments with the static fluid setup developed a foundation for later success. The following section will describe the results from Experiments 38-48.

6.3 Static Fluid Setup Experiments

Although the experiments performed on the static fluid setup were not the primary focus of this research project, those experiments provided useful information and helped in the design of the flowing setup. The following sections will discuss the two types of experiments performed on the static fluid samples. A discussion of the results from a scattering angle sweep experiment is given in Section 6.3.1. Results from tilt angle experiments are shown in Section 6.3.2. Knowledge gathered from those two experimental processes was then used during the design of the flowing setup.

6.3.1 Scattering Angle Sweep

A scattering angle sweep was performed on a single scattering (dilute) sample of 0.107 μm PSL particles (see Appendix I). A scattering angle sweep requires no adjustment of the top fiber once alignment has been accomplished (see Section 4.3). For a scattering angle sweep experiment, autocorrelation measurements are taken (where in the data collected by each detector is self-correlated). If the sample is single scattering, the data should reveal the correct radius and the measured second cumulant should be near zero (see Section 3.3). Autocorrelation measurements utilizing both channels were taken for scattering angles ranging from 15° to 120°.

Two trends were discovered from the scattering angle sweep experiments. The first noticeable trend was seen in the intensity versus scattering angle plot of Fig. 17. The intensity remained relatively constant between 120° and 50°, seeing only a 10 kHz increase. As the scattering angle sweep decreased below 50°, the intensity in both channels increased by as much as 100+ kHz. A comparison of the two extreme scattering angles, 15° and 120°, showed that, at the smaller scattering angle, the intensities increased. The increase in intensities for channel 0 and channel 1 at 15° was 4.40 and 4.81 times the value measured at 120°, respectively.

Figure 18 is a plot of the intensity from Fig. 17 times the sine of the scattering angle versus the scattering angle. This was done to compensate for the larger detection area seen at the lower scattering angles. If larger detection areas were the only cause, compensating with the sin (θ) should produce a linear curve for intensity as a function of scattering angle, but Fig.18 shows the same trend as seen in Fig. 17. The intensity increased as the scattering angle decreased.

A plot of the radius versus the scattering angle (Fig. 19) showed the second trend associated with the static fluid setup. The radius determined from the data decreased as the scattering angle decreased until a minimum was reached around 40°. Data points for the remaining five scattering angles seem to show an upward trend with an exception

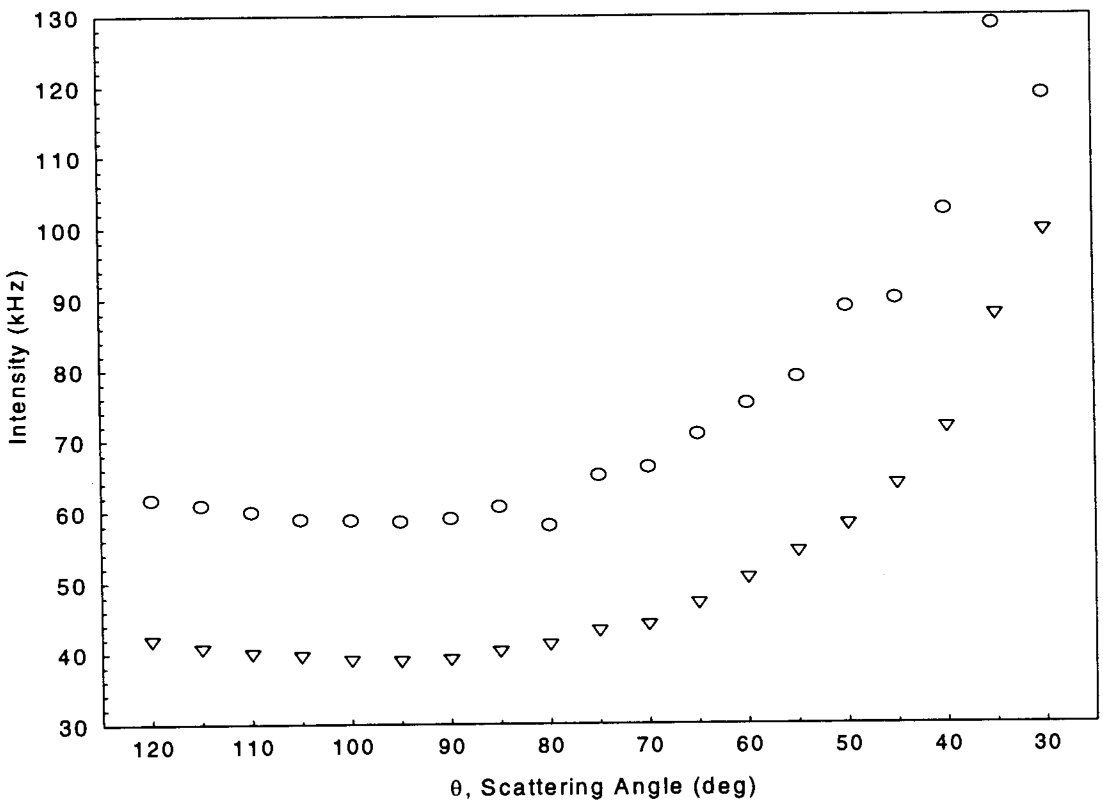

Figure 17: Intensity versus scattering angle for a single scattering sample of 0.107 μm PSL particles in water. Autocorrelation measurements were taken using both channel 0 (circles) and channel 1 (inverted triangles). Data corresponds to Experiment 42.

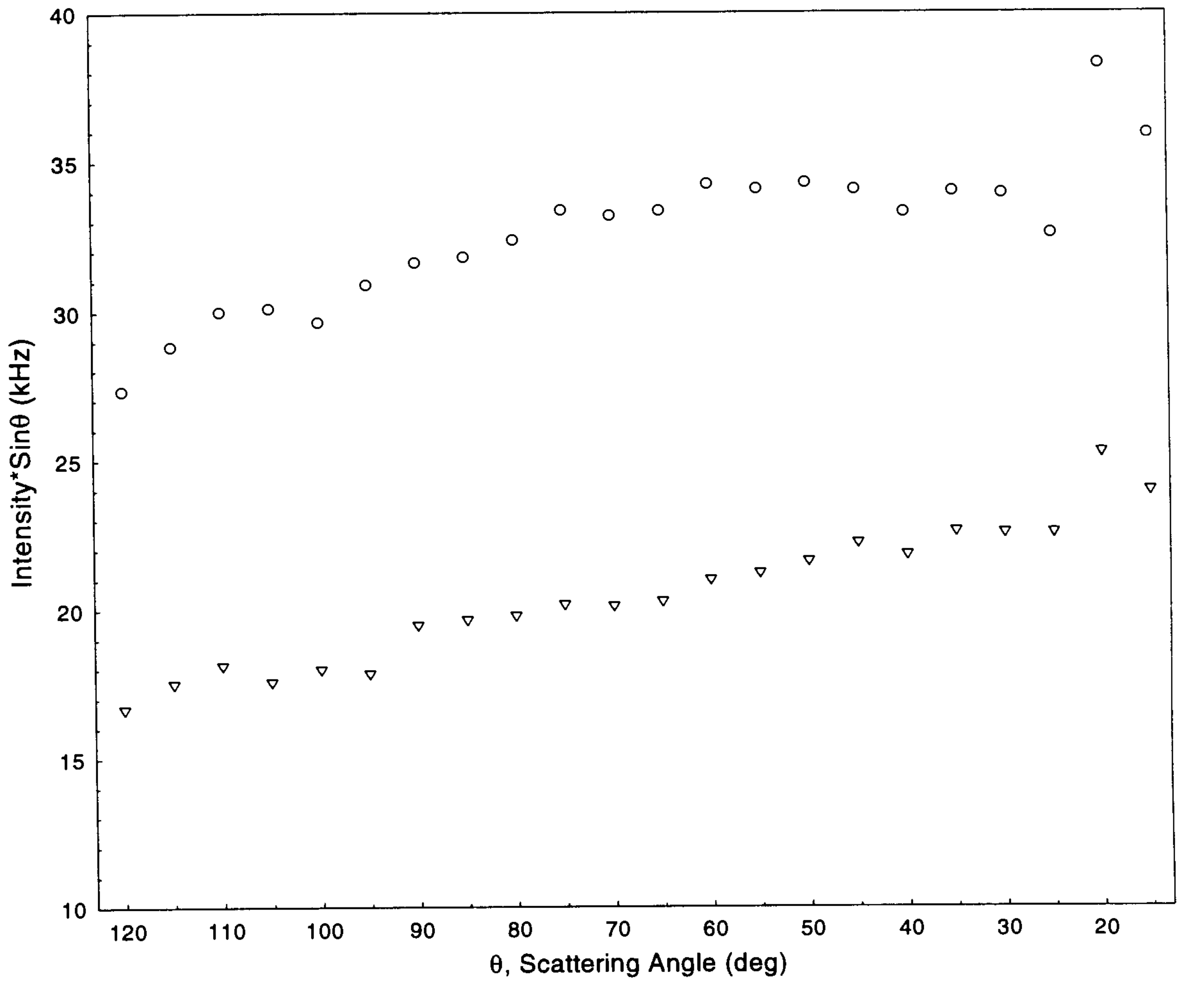

Figure 18: Intensity times sin (θ) versus scattering angle to determine effects of scattering angle for a single scattering sample of 0.107 μm PSL particles in water. Autocorrelation measurements were taken using both channel 0 (circles) and channel 1 (inverted triangles). Data corresponds to Experiment 42.

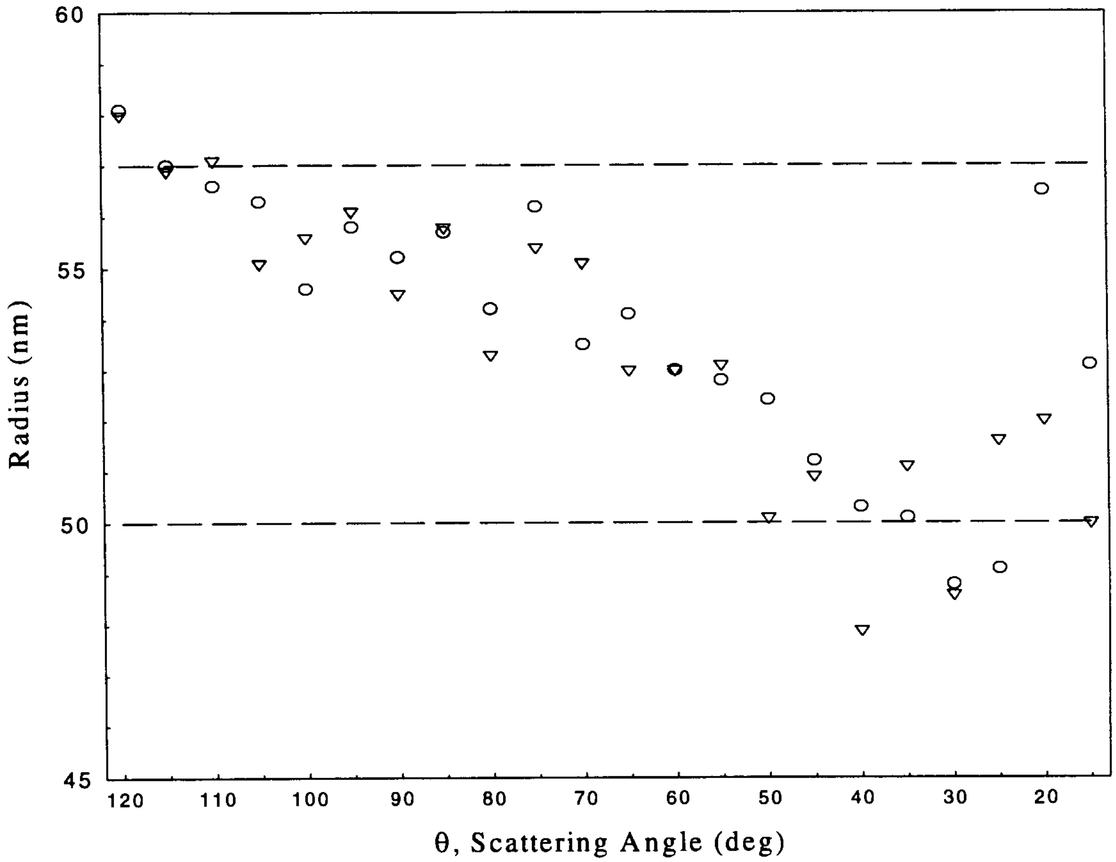

Figure 19: Radius versus scattering angle for a single scattering sample of 0.107 μm PSL particles in water. Autocorrelation measurements were taken using both channel 0 (circles) and channel 1 (inverted triangles). Data corresponds to Experiment 42.

occurring at 30°, which dropped back down. For the range of scattering angles from 105° to 45°, the autocorrelation data was accurate in calculating a radius within the acceptance range (shown by the horizontal dashed lines in Fig. 19). Problems arose at the extreme values of the scattering angle range, especially at the smaller angles ($\theta < 45°$). At the smaller angles, the diameter calculated from the data became erratic. This erratic behavior corresponded to the area where the intensity increased rapidly (Fig. 17). A second scattering angle sweep was performed on a different dilute sample and the data from that experiment (Exp. 45 in Appendix II) shows the same trends. The following discussion of the tilt angle sweep results will further illustrate the problems encountered at small scattering angles.

6.3.2 Tilt Angle Sweep

This section will discuss the result from the tilt angle sweep experiments. These experiments were conducted using the procedure described in Section 4.6. Cross-correlation experiments were performed on samples of 0.107 μm PSL particles (see Appendix I) at volume fractions ranging from 0.1330 to 0.5025 percent by weight. The data shows that the best results occurred at scattering angles of 90° and 120°, while scattering angles of 30°, 45°, and 60° gave poor results. These results agree with the ones given in the scattering angle sweep discussion.

Figure 20 shows the signal-to-noise ratio versus tilt angle sweep for the five different scattering angles listed above. The tilt angle sweep experiments were performed on samples of 0.107 μm PSL particles at volume fractions of approximately

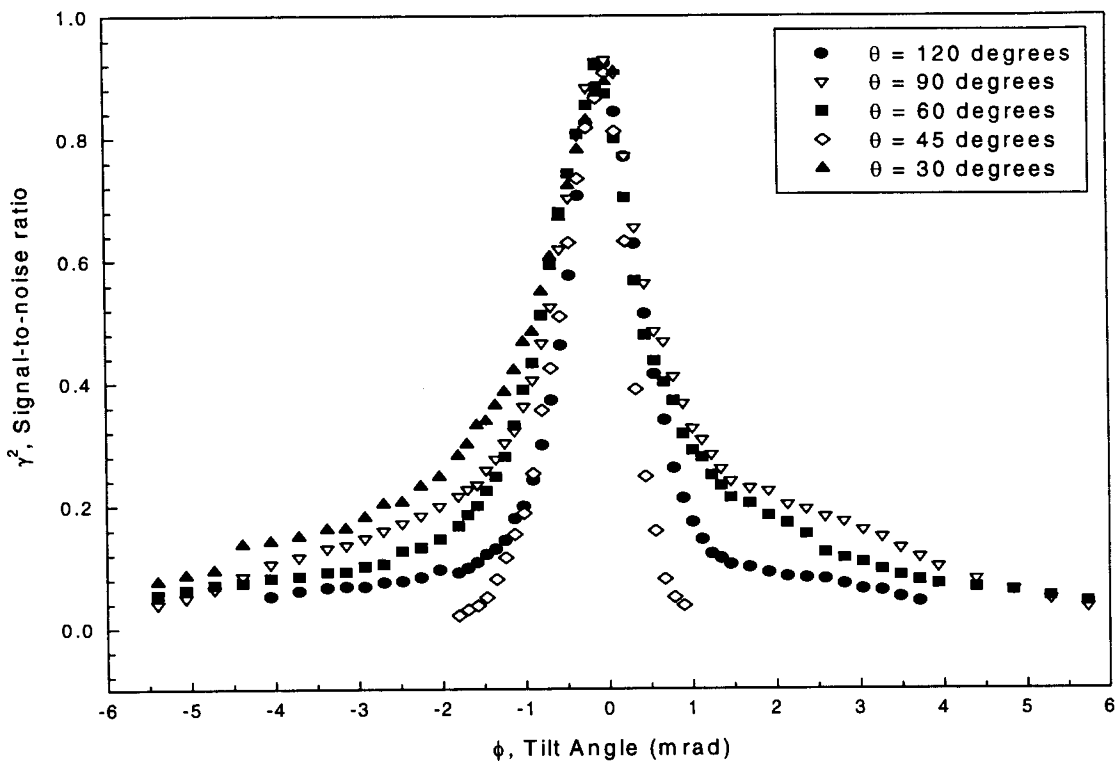

Figure 20: Signal-to-noise ratio versus tilt angle for cross-correlation measurements of 0.107 μm PSL particles at volume fractions of approximately 0.3 percent by weight for various scattering angles. Data corresponds to Experiments 39, 40, 43, 47, and 48.

0.30 percent by weight. The signal-to-noise ratio for all five scattering angles is shown to peak near 0.90. All of the curves with the exception of 45° show long 'shoulders', which should correspond to areas of single scattering. As will be shown in Fig. 21, this is not necessarily the case.

The second figure, Fig. 21, shows the radius as a function of tilt angle for the same five scattering angles. A comparison of Figs. 20 and 21 shows how multiple scattering effects are presumably more influential in forward scattering (scattering at small angles). These effects cause faster decay rates, which lead to apparently smaller diameters. For scattering angles of 30° and 60°, the 'shoulder' region (Fig. 20) was well defined and should correspond to single scattering results. However, in Fig. 21, the radius map for $\theta = 30°$ was lower than the expected range, while the radius map for $\theta = 60°$ barely reached the acceptance range. From all of the figures (17-21), the difficulties of dealing with a scattering angle around 45° can be seen as no 'shoulder' is present in Fig. 20 and the radius never reaches the acceptable range in Fig. 21. As discussed in Section 2.3, Meyer *et al.* (1997a) covered several scattering angles, with 60° being the smallest. Meyer reported no problems with taking data at any scattering angle.

The influences of concentration on the static fluid experiments performed with a water bath and circular test tube are limited. No more than two concentrations were used at one scattering angle (see Appendix II). However, some general trends can be seen in Figs. 22 and 23. Figure 22 shows the signal-to-noise ratio versus tilt angle for two different concentrations of 0.107 μm particles. The peaks for both concentrations are near the same point, but the more concentrated sample's signal-to-noise ratio drops much faster. This causes the peak region to be more pronounced. In addition, Fig. 22 shows

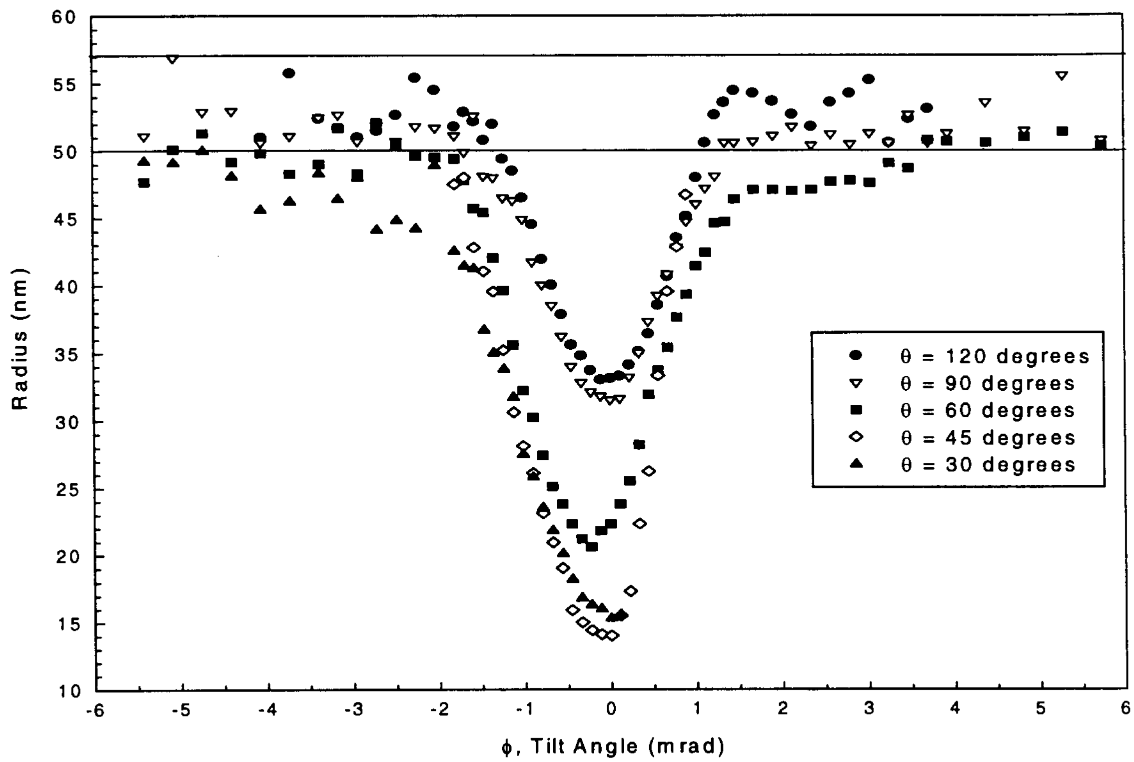

Figure 21: Radius versus tilt angle for cross-correlation measurements of 0.107 μm PSL particles at volume fractions of approximately 0.3 percent by weight various for scattering angles. Data corresponds to Experiments 39, 40, 43, 47, and 48.

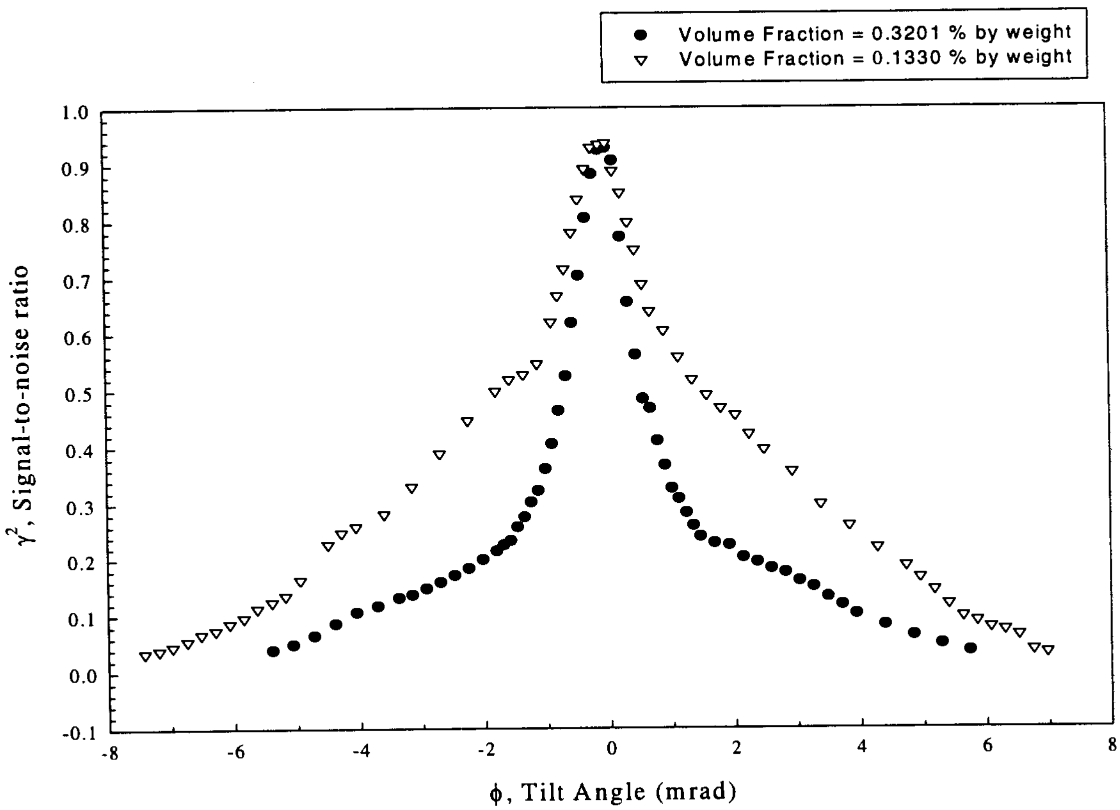

Figure 22: Signal-to-noise ratio versus tilt angle for cross-correlation measurements of 0.107 μm PSL particles at a scattering angle of 90° for two volume fractions. Data corresponds to Experiments 38 and 39.

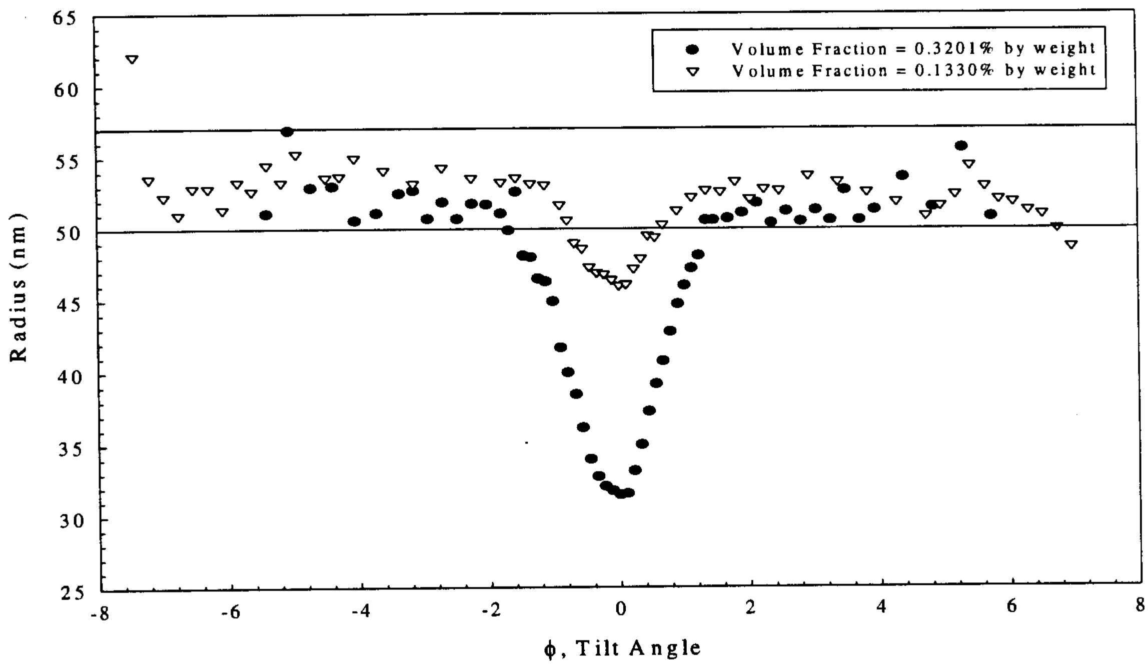

Figure 23: Radius versus tilt angle for cross-correlation measurements of 0.107 μm PSL particles at a scattering angle of 90° for two volume fractions. Data corresponds to Experiments 38 and 39.

that the shoulder region for the less concentrated sample extends 1.5 mrads farther in tilt angle than that of the more concentrated sample. The shoulder region begins at a higher signal-to-noise ratio for the less concentrated sample as well.

Figure 23 shows another trend that was connected to concentration level. The radius values given at the peak were much lower for the more concentrated sample, ~31 nm as compared to ~46 nm. This was due to the faster decay rates associated with higher concentrations. This fact meant that greater separation was necessary between the two detectors to achieve multiple scattering suppression. These trends were also seen at scattering angles of 60° and 120° (see Appendix II). Sundaresan (1999) contains further discussion on the effects of concentration.

6.4 Flowing Fluid Setup: Introduction

The goal of this thesis is to demonstrate that two independent suppression techniques can be used to determine particle size in a dense flowing system. The experimental setup depicted in Chapter V was used to suppress both multiple scattering effects and flow effects. Preliminary autocorrelation experiments were performed with the flowing setup to determine the sensitivity of measurements to a perpendicular alignment between the bisector (of the laser and detector arms) and the flow cell. These experiments were performed on 0.107 μm, 0.204 μm, and 0.300 μm PSL particles (see Appendix I) at cell rotation angles ranging from $\delta = -10°$ to $\delta = +10°$ (see Fig. 13). The results from these experiments are described in Section 6.5.1. After the rotation experiments, the test cell was returned to 0° (perpendicular to the bisector) so that the tilt angle sweep experiments could be performed.

As with the static setup, experiments were also performed through a tilt angle sweep to suppress multiple scattering effects. The purpose of these experiments was to show that both flow suppression and multiple scattering suppression could be used simultaneously to determine particle size. The following four parameters were investigated to determine their effects on particle sizing: flow velocity, particle size, concentration, and scattering angle. This thesis concentrates on varying the first three parameters at a scattering angle of 112°. The effects of varying the last parameter, scattering angle, is presented in Sundaresan (1999), where the effects of the first two parameters are studied for scattering angles of 122° and 136°. Preliminary tilt angle sweep experiments were conducted on samples of 0.107 μm PSL at volume fractions of 0.066 percent by weight and 0.198 percent by weight for various flow rates. The sample of 0.107 μm particles at a volume fraction of 0.198 percent by weight as well as two additional particles sizes, 0.098 μm and 0.203 μm PSL particles (see Appendix I) were used to conduct the remaining tilt angle experiments. Experiments were performed at two flow rates for the 0.098 μm and 0.203 μm particles, while the 0.107 μm particles were test at three flow rates. For the 0.098 μm particles, volume fractions of 0.30 percent and 0.86 percent by weight were used, while a volume fraction of 0.20 percent by weight was used for the 0.203 μm particles. All of these results are discussed in Section 6.5.2.

6.5 Flowing Fluid Setup Experiments

The experiments performed with the flowing fluid setup demonstrate that the two independent suppression techniques can be used together to determine particle size in a dense flowing system of particles. The following two sections will describe the results of the two experiments used to prove that the suppression techniques work. Section 6.5.1 shows the degree of sensitivity of the setup to cell rotation, which affects the relationship between the bisector of the laser and detector arms to the flow direction. Results from tilt angle sweep experiments are shown in Section 6.5.2. It was the results from those experiments, which showed that the two suppression techniques could be applied together to a dense flowing system of particles in order to determine particle size.

6.5.1 Cell Rotation Effects

As described in Chapters III and V, the alignment of the flowing fluid setup was critical to the success of flow effect suppression. The geometric alignment described in Chapter V allowed the flow vector and the scattering wave vector to be positioned perpendicular to each other. The sensitivity of this alignment is examined in this section. To test this sensitivity, autocorrelation measurements were performed on single scattering (dilute) samples of 0.107 μm, 0.204 μm, and 0.300 μm PSL particles. The first experiment was conducted on 0.107 μm PSL particles at a cell rotation angle of $\delta = 0°$ (see Fig. 13) for flow rates of 0%, 50% and 100% (see Table 2 for corresponding velocities). This section of the research was completed by five additional experiments that followed the procedure outlined in Section 5.5.1 for cell rotation angles of δ = -5°, -10°, +5°, and +10° and flow rates of 0%, 50% and 100%. To interpret the effects of flow on the data taken during these experiments, the natural logarithm of the normalized field autocorrelation function ($g^1(\tau)$) was plotted versus the delay time. To attain these values, the normalized field correlation function was found from the intensity field correlation data given by the ALV-5000 program using the following equation:

$$g^1(\tau) = \sqrt{\left(g^2(\tau) - 1\right)}, \tag{6-1}$$

which is Eq. (3-6) solved for $g^1(\tau)$ assuming $\gamma^2(\theta)$ is equal to 1.0. Substituting Eq. (3-13) into Eq. (6-1) gives:

$$\exp\left(-D_0 q^2 \tau + \left(i\bar{q} \bullet \bar{v}(r)\right) \tau\right) = \sqrt{\left(g^2(\tau) - 1\right)}. \tag{6-2}$$

In order to utilize this equation, the second term of the exponential on the left-hand side must be eliminated or suppressed. This is accomplished by forming the geometry described in Chapter V. If this term is suppressed, it can be seen that taking the natural logarithm and solving for the diffusion constant will lead to determination of the particle size by using the slope of the line as seen in Figs. 24-27. Therefore, the closer to linear that the plot of this equation is, the more reliable the data is and the better the determination of the particle size.

Figure 24 shows the natural logarithm of the normalized field autocorrelation function of channel 0 versus delay time using 0.107 μm PSL particles for no flow at five different cell rotation angles, δ. To allow the graphs to be clearer, data from only channel 0 is given as a representation of the effect of δ. However, a similar effect was found from the data collected by channel 1. From this graph, it can be seen that the cell rotation has very little effect on a static fluid case. Figure 25 shows the same information as Fig. 24, but for the case of 100% flow. The effect of flow can be seen to cause the plots represented by $\delta = \pm 10°$ to curve. The effect of flow is more suppressed in the three smaller rotation angles, $\delta = 0°$ and $\delta = \pm 5°$.

The effects of flow are even more pronounced when comparing Fig. 26 to Fig. 27, which are repeats of Figs. 24 and 25 except for the use of 0.204 μm PSL particles. Figure 26 is similar to Fig. 24 showing that cell rotation has little effect on static fluid conditions. Two facts are immediately apparent when viewing Fig. 27. The first fact is that as particle size is increased, rotating the cell away from a position perpendicular to the bisector had a greater effect on the influence of flow for the data taken. Secondly, rotation of the test cell toward the laser has a greater impact on the linearity of the data than rotation toward the detectors.

Experiments to determine the effects of test cell rotation on particle sizing of 0.300 μm particle samples were tried unsuccessfully. The intensity levels measured at scattering angles of 112°, 136°, and 150° were too low to produce useable correlations. This was determined to be due to the Rayleigh Gans form factor that is associated with 0.300 μm PSL particles. The Rayleigh Gans form factor is a measure of the amount of intensity scattered in a certain direction. Larger particles tend to be more forward scattering and the flow setup was built to take measurements from backscattering. Sundaresan (1999) contains calculations of the Rayleigh Gans form factors for the particles used in this research.

Three characteristics of the flowing fluid setup were found from the cell rotation experiments. First, the effect of flow can be suppressed if the bisector between the laser

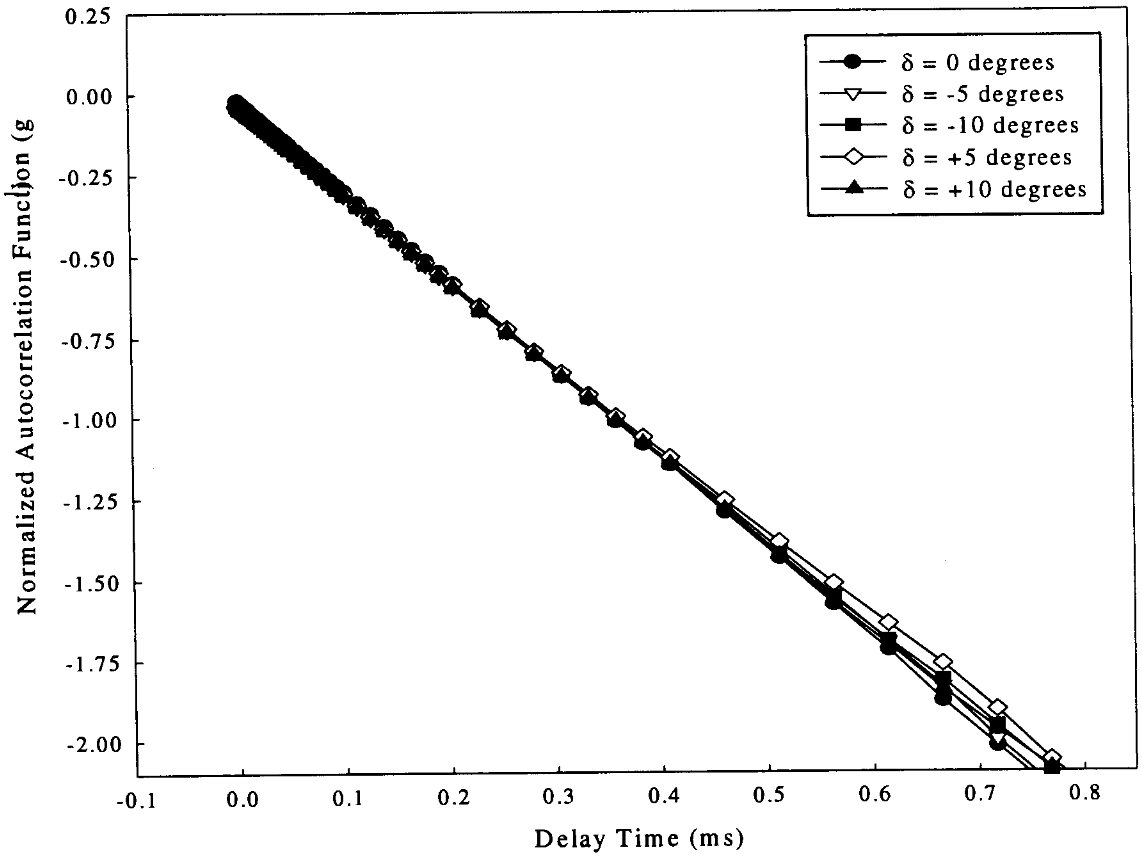

Figure 24: Normalized field autocorrelation function for channel 0 versus delay time for a dilute sample of 0.107 μm PSL particles at a 0% flow rate. Data corresponds to Experiment 58.

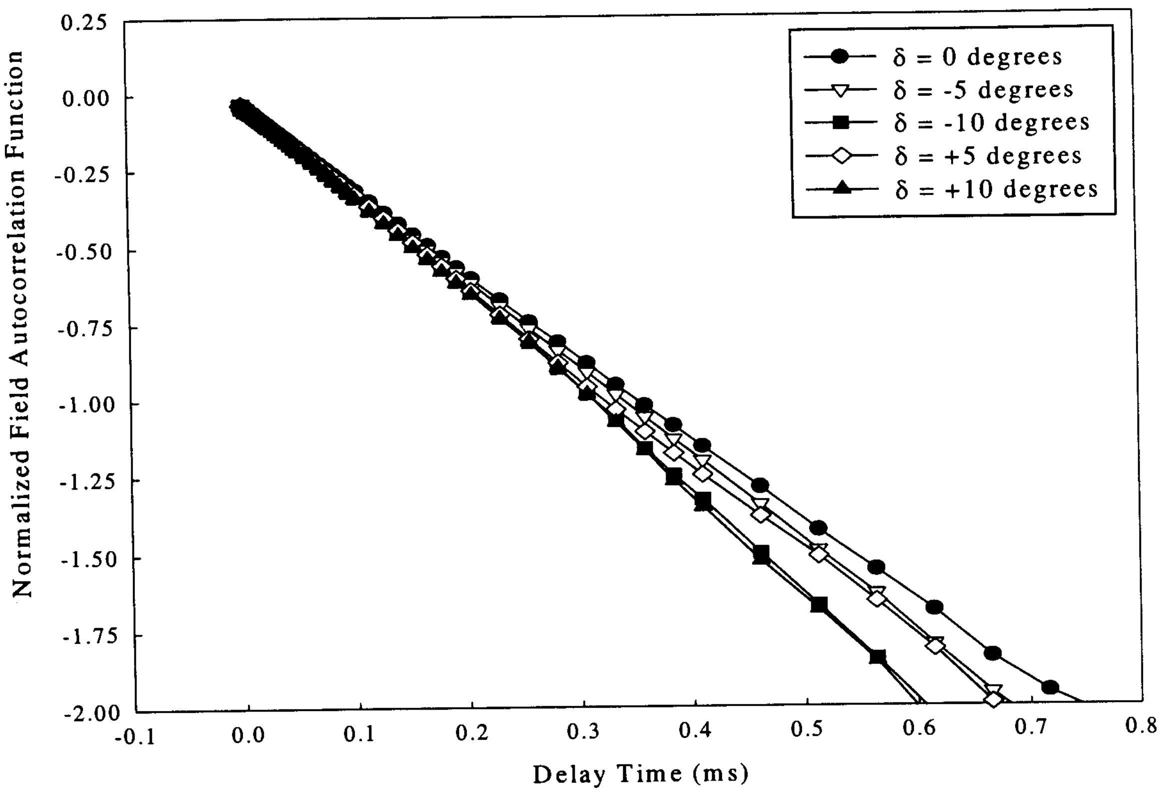

Figure 25: Normalized field autocorrelation function for channel 0 versus delay time for a dilute sample of 0.107 μm PSL particles at a 100% flow rate. Data corresponds to Experiment 58.

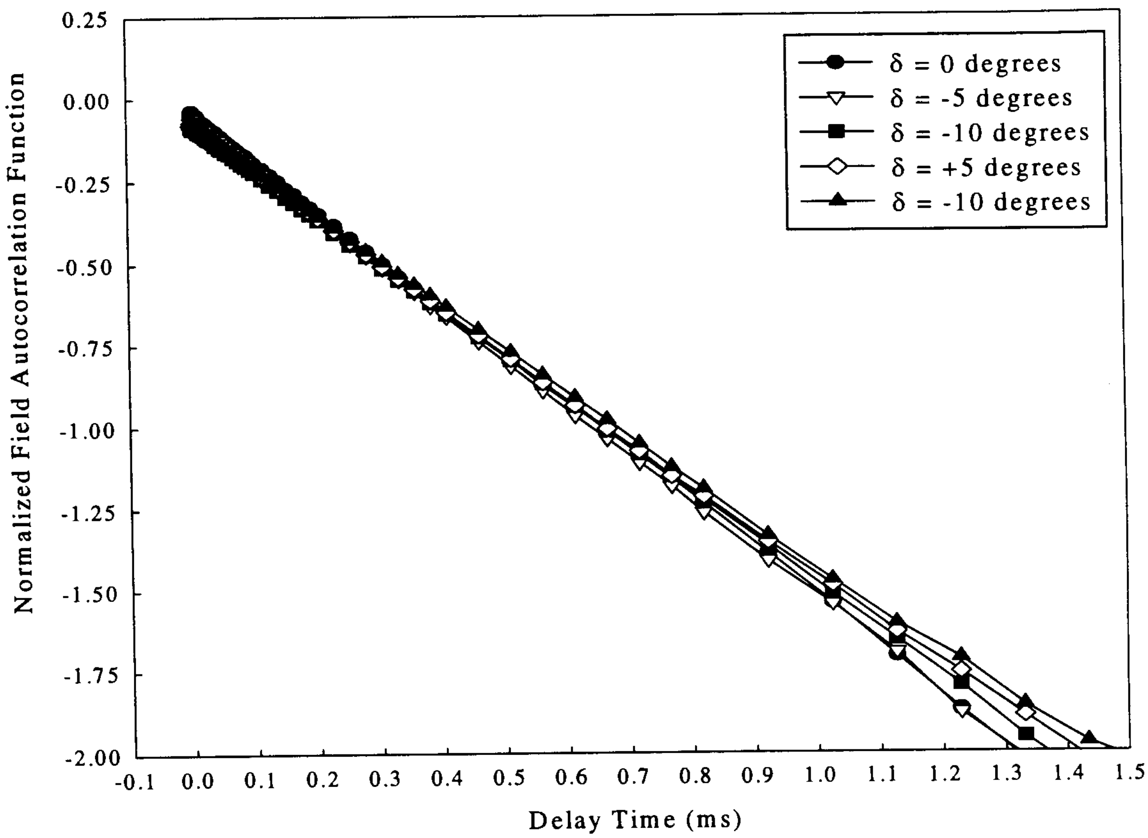

Figure 26: Normalized field autocorrelation function for channel 0 versus delay time for a dilute sample of 0.204 μm PSL particles at a 0% flow rate. Data corresponds to Experiment 60.

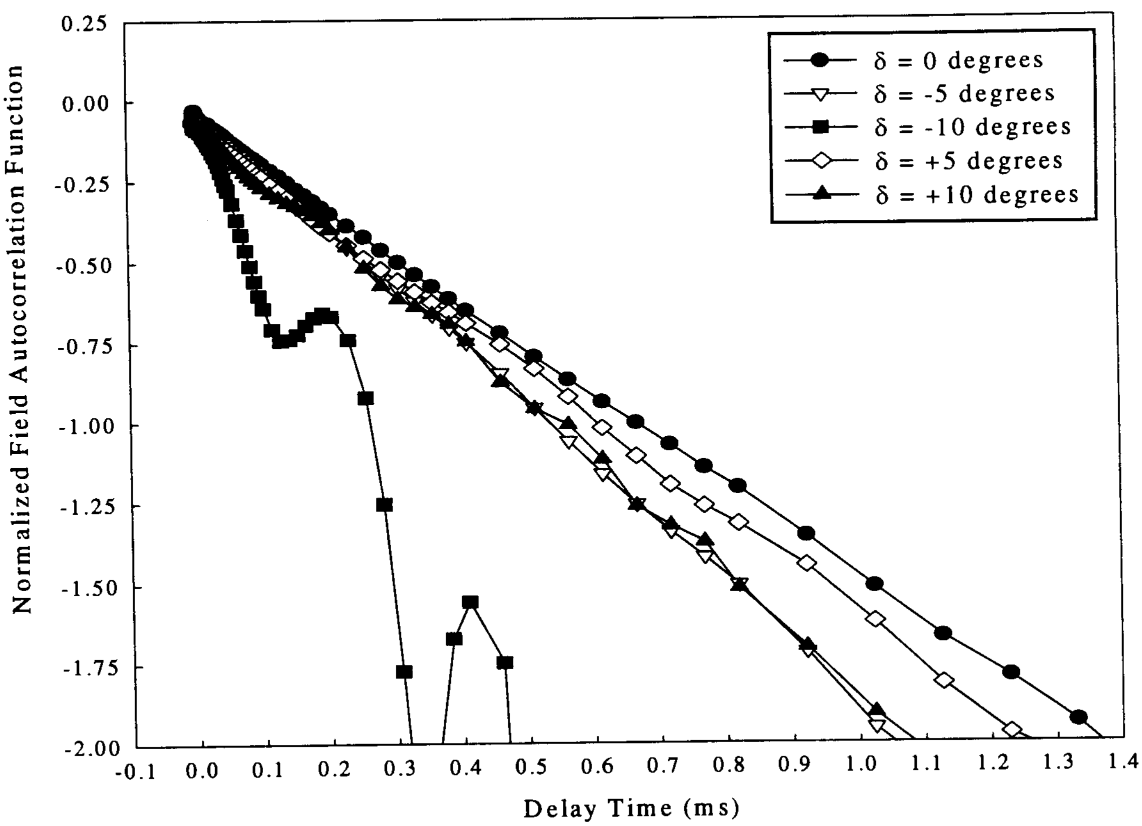

Figure 27: Normalized field autocorrelation function for channel 0 versus delay time for a dilute sample of 0.204 μm PSL particles at a 100% flow rate. Data corresponds to Experiment 60.

and detector arms is kept perpendicular to the flow direction. Second, the plots show that, while the setup is sensitive to cell rotation, this sensitivity is minor for cell rotation angles of $-5° \leq \delta \leq 5°$. The final characteristic is that cell rotation toward the laser has a greater impact on data collection than rotation toward the detector. This characteristic can be attributed to the fact that a rotation toward the laser caused the detection area to be move deeper within the cell where higher velocities were present (see Appendix IV).

6.5.2 Tilt Angle Sweep

Tilt angle sweep experiments for the flowing system were similar to the ones described in Section 4.6 for the static fluid setup. These experiments resulted in a means of mapping out the 'peak' and 'shoulders' associated with multiple and single scattering, respectively. As with the static fluid setup, the preliminary experiments performed on the useful data to determine particle size. Experiments 69-92 (see Appendix III) can be categorized as preliminary experiments. From those experiments, two characteristics about the flowing fluid setup were discovered.

The first characteristic of the flowing system dealt with the procedure used to take data. For the static fluid setup, each time the tilt angle was altered during a tilt angle sweep experiment, the top detector was translated to maximize the intensity. Through the preliminary experiments, it was determined that translation of the top detector to maintain intensity was more effective than maximizing intensity. As can be seen in Fig. 28, a plot of radius versus tilt angle for both maximizing and maintaining intensities, the maintaining intensity plot reaches the acceptable radius range first and stays there for a

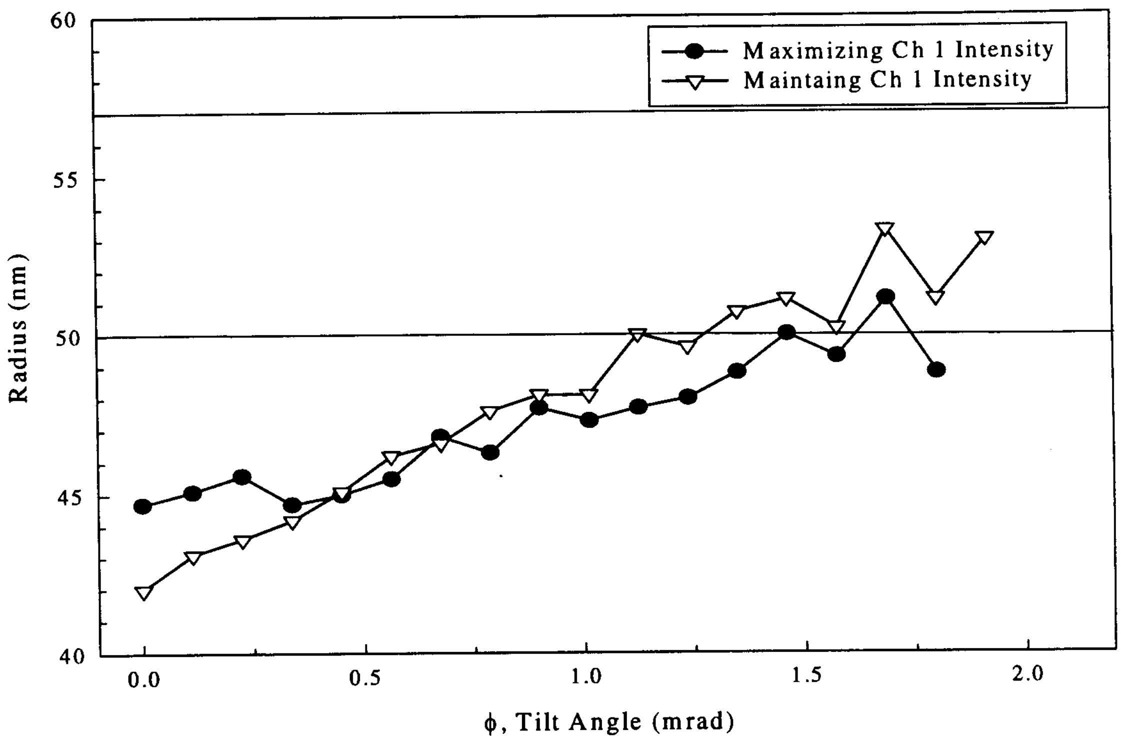

Figure 28: Radius versus tilt angle for cross-correlation measurements of 0.107 μm PSL particles at a volume fraction of 0.198 percent by weight and at a scattering angle of 112°. Data corresponds to Experiments 86 and 87.

larger range of tilt angles. Due to possible statistical errors in the data collected to produce Fig. 28, the differences between maximizing and maintaining intensities seen in Fig. 28 cannot be the lone reason for making the decision to maintain intensities. Due to personal experience, the technique of maintaining intensities in the top detector was adopted for use in all flowing fluid experiments.

The second characteristic involved the alignment of the system. A major focus of this paper was the fact that alignment of a dynamic light scattering system is crucial to collecting reliable data. The preliminary flowing experiments were performed with the lens improperly focused. The 'waist' of the incident beam inside the sample (Chapter IV) was focused in a way that allowed only part of the beam to be in the detection volume. The misalignment was caused by the lens being too close to the sample. This positioning greatly shortened the amount of tilt angle covered by the shoulder. Figure 29 shows this effect by comparing two curves of 0.107 μm PSL particles at a volume fraction of 0.198 percent by weight. One curve shows the signal-to-noise ratio versus tilt angle for data collected before the lens was repositioned, while the second curve uses data taken after the lens was refocused. The second curve produced a tilt angle range four times that of the first curve.

With these changes in alignment and procedure made, the last nine experiments listed in Table 6 were performed at a scattering angle of $\theta = 112°$. As mentioned in Section 6.4, the purpose of these experiments was to study the effects of three parameters on determining particle size. These three parameters are as follows: flow velocity, particle size, and concentration. Plots of the signal-to-noise ratio and the radius versus

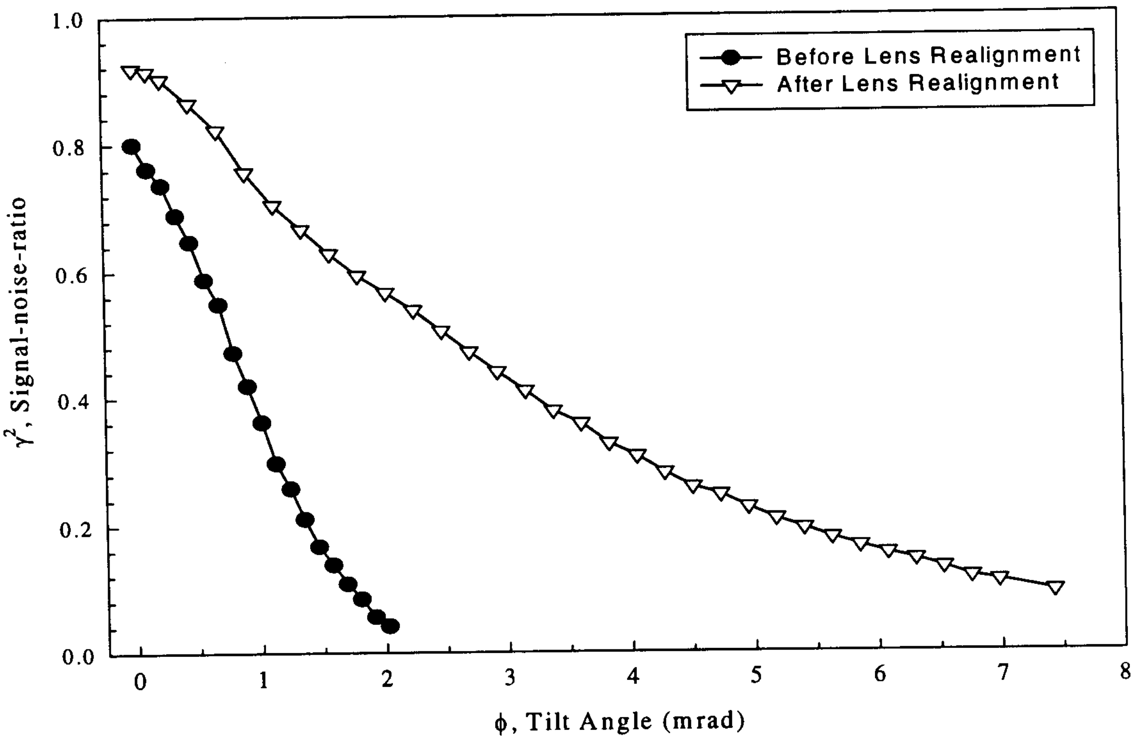

Figure 29: Signal-to-noise ratio versus tilt angle for cross-correlation measurements of 0.107 μm PSL particles at a volume fraction of 0.198 percent by weight and at a scattering angle of 112°. Data corresponds to Experiments 77 and 93.

tilt angle were created to illustrate the effect that each parameter had on particle measurements.

The flow velocity effect will be examined first. Three different particle sizes were used at various flow rates. The first particle size used in a tilt angle sweep experiment was 0.107 μm PSL at a volume fraction of 0.198 percent by weight. Figure 30 shows a plot of the radius as a function of tilt angle for 3 flow rates: 0%, 50%, and 100% (see Table 2 for corresponding velocities). From this plot, it can be seen that flow velocity affected the size computed for the multiple scattering area of the plot. As the velocity increased, the initial size given by the ALV-5000 program decreased. This also affected how much tilt was necessary to move into the single scattering area. These results were caused by the intermediate scattering wave vectors, **q**, not being perpendicular to the velocity vector, **v**. Due to this non-perpendicular alignment, the second term in the exponential of Eq. (3-14) was not suppressed and allowed the influence of the flow to affect the correct determination of particle size. In this way, the effect of velocity is similar to an increase in multiple scattering (compare Fig. 30. with Fig. 22 to see the effect of higher concentration).

In the peak region, the correlation function decays faster and therefore computations made from data within this region results in a smaller particle size. This effect can also be seen in Fig. 31, a plot of radius versus tilt angle for 0.203 μm PSL particles. Figure 31 shows a problem associated with the 0.203 μm PSL particles. The radii determined in the single scattering area by the ALV-5000 were slightly higher than the manufacturer's range of acceptance. At most, the determined radius was within 5 nm of the acceptance range. Therefore, it was decided that this error was acceptable.

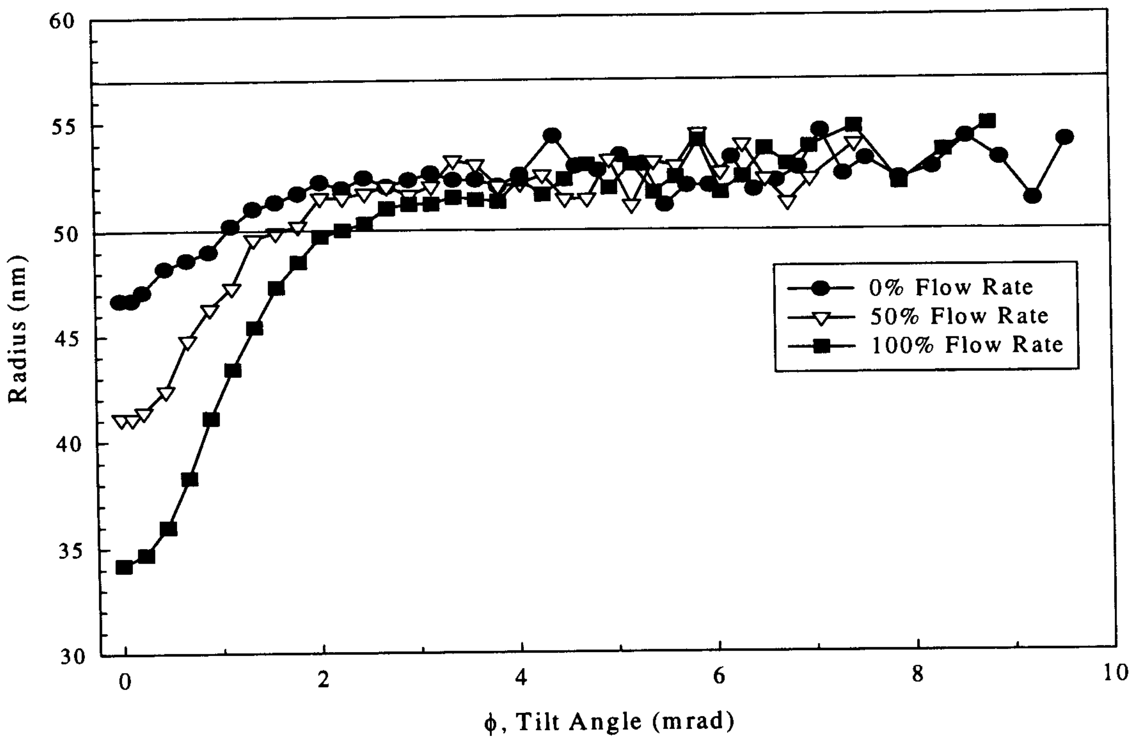

Figure 30: Radius versus tilt angle for cross-correlation measurements of 0.107 μm PSL particles at a volume fraction of 0.198 percent by weight and at a scattering angle of 112°. Data corresponds to Experiments 93, 94, and 95.

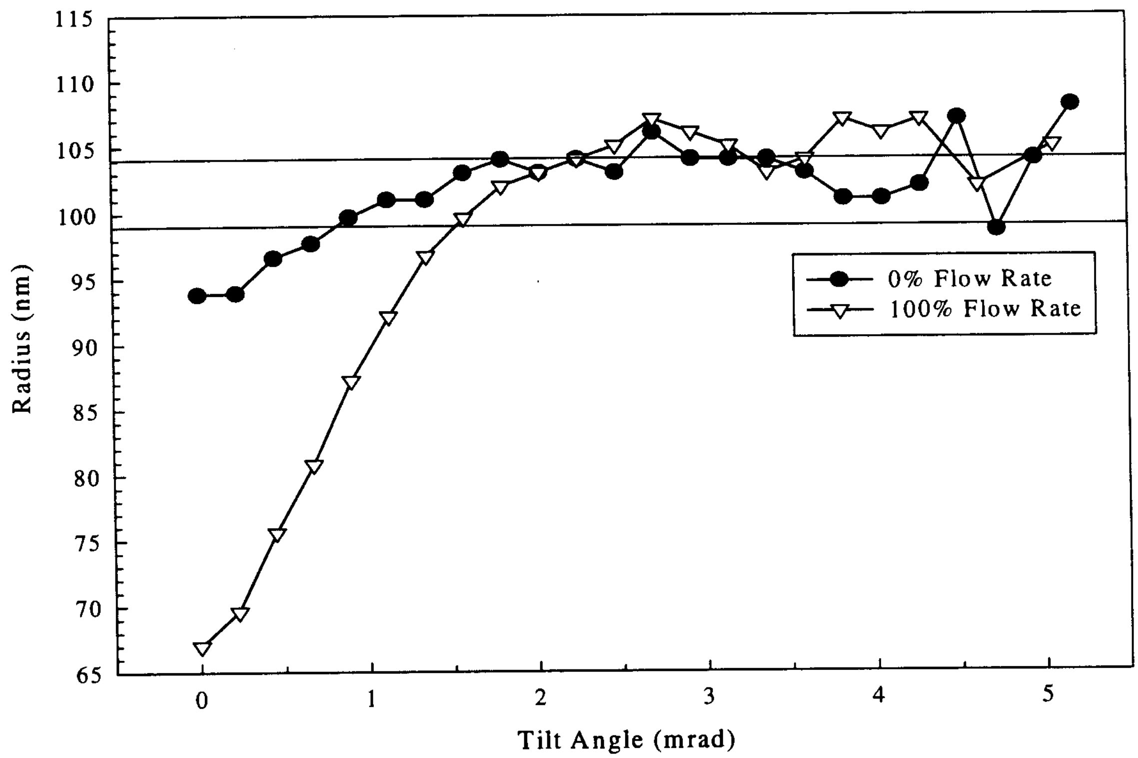

Figure 31: Radius versus tilt angle for cross-correlation measurements of 0.203 μm PSL particles at a volume fraction of 0.200 percent by weight and at a scattering angle of 112°. Data corresponds to Experiments 111 and 112.

The effect caused by the second parameter, particle size, was examined next. Figure 32 shows the normalized radius versus tilt angle for both 0.107 μm and 0.203 μm PSL particles at volume fractions of 0.198 and 0.200 percent by weight, respectively. The comparisons shown in Figs. 32 and 33 were based on the volume fraction and not the optical thickness of the sample, which was different. Figure 33 compares the two particle sizes with respect to their signal-to-noise ratios. The data for Figs. 32 and 33 was collected at a flow rate of 100%. For ease of comparison, the data collected from the ALV-5000 program for both particle sizes was normalized by dividing the data by the correct particle radius.

When comparing these two particle sizes, it can be seen that there is very little difference between the starting point of the two curves in Fig. 32. The peaks associated with both curves start at approximately the same value (0.65). Two major differences exist between the data used to produce the two curves in Fig. 32. The first difference is that, once the 0.107 μm PSL particles reach the acceptance range (the solid lines on Fig. 32) for their size, the radius determined by the data stays within the acceptance range for the remainder of the curve. The curve for the 0.203 μm particles does not stay within its acceptance range (the dashed lines on Fig. 32). The second difference is that the tilt angle range for the shoulder of the 0.107 μm particle curve is 4 mrads larger than the tilt angle range for the shoulder of the 0.203 μm particles. Figure 33 shows a greater effect of particle size. The curve for the 0.203 μm particles is much steeper and does not extend to as large of a tilt angle range as the curve for the 0.107 μm particles.

The final parameter studied was particle concentration. As with the static fluid setup, the data pertaining to this parameter was limited to Experiments 103-106. For a

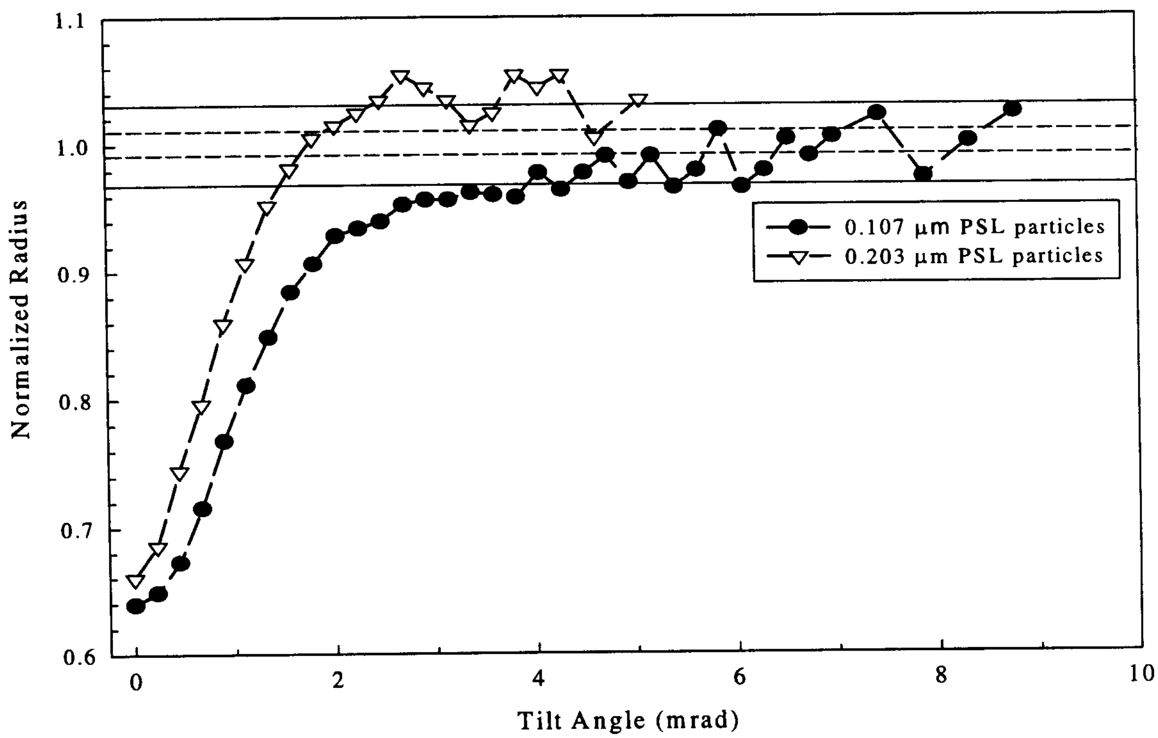

Figure 32: Normalized radius versus tilt angle for cross-correlation measurements taken at a scattering angle of 112° and flow rate of 100%. The samples were both at a volume fraction of approximately 0.200 percent by weight. Data corresponds to Experiments 95 and 112.

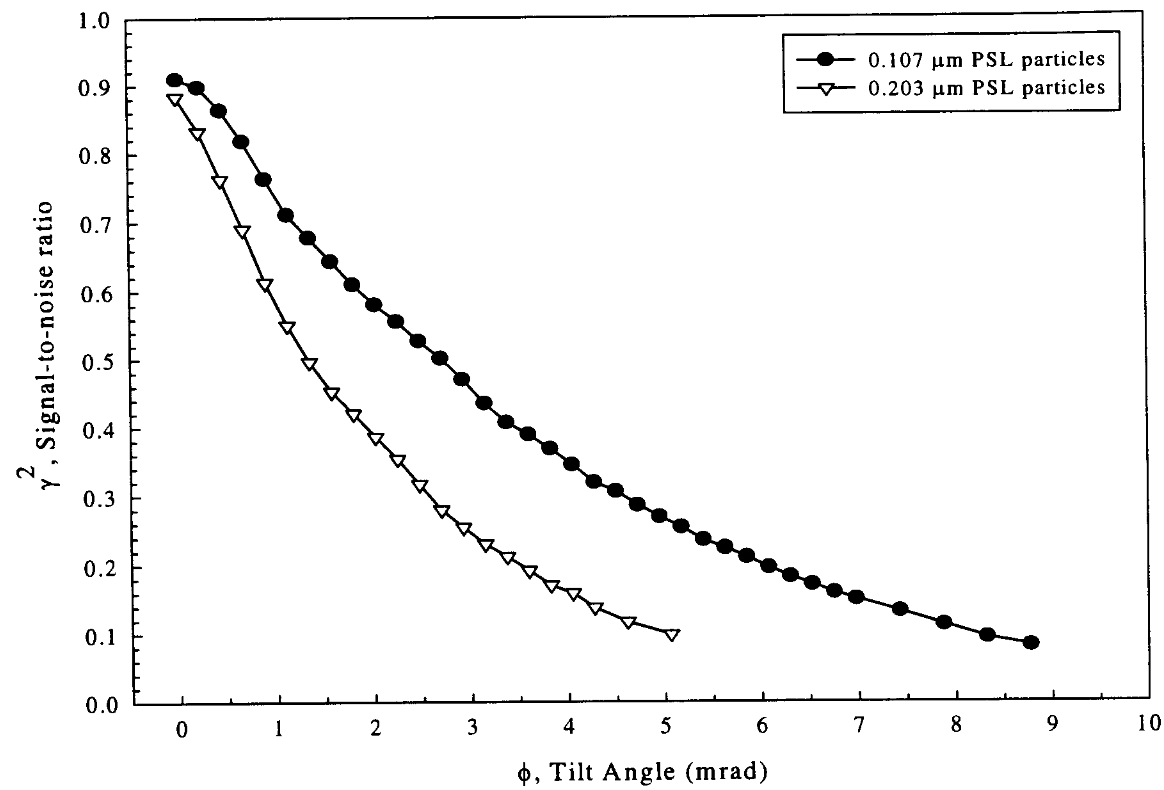

Figure 33: Signal-to-noise ratio versus tilt angle for cross-correlation measurements taken at a scattering angle of 112° and flow rate of 100%. Data corresponds to Experiments 95 and 112.

particle size of 0.098 μm, data from two volume fractions was available, 0.320 and 0.860percent by weight. Similar results were found for the flowing system as for the static fluid data shown in Figs. 22 and 23. Figure 34 shows the signal-to-noise ratio versus tilt angle for the samples listed above at a flow rate of 100%. As in Fig. 22, both curves in Fig. 34 peak at near the same signal-to-noise ratio, while the more concentrated sample shows a faster drop in its signal-to-noise ratio. This would give a narrower peak region if both shoulders were plotted. Additional effects of concentration can be seen in Fig. 35, where the radius is plotted as a function of tilt angle. The more concentrated sample gives a lower peak value for the radius of the particle, ~31 nm as compared to ~ 33 nm.

This effect is not as great as that seen in Fig. 36, where the same effect of concentration is shown for a flow rate of 0%. In Fig. 36, the radius given at the peak is ~39 nm for the more concentrated sample as compared to ~43 nm for the less concentrated sample. As in the static fluid sample, this difference in starting values is consistent with the less concentrated sample reaching the correct radius range at a smaller tilt angle than that of the more concentrated sample.

Results from the static fluid setup and flowing fluid setup are expanded upon in Sundaresan (1999). For the static fluid setup, the effects of concentration are examined for a sample of 0.107 μm PSL particles in a square test cell. For the flowing fluid setup, the effects of flow velocity, particle size, concentration, and cell rotation are covered in Sundaresan (1999) for scattering angles of $\theta = 122°$ and $\theta = 135°$.

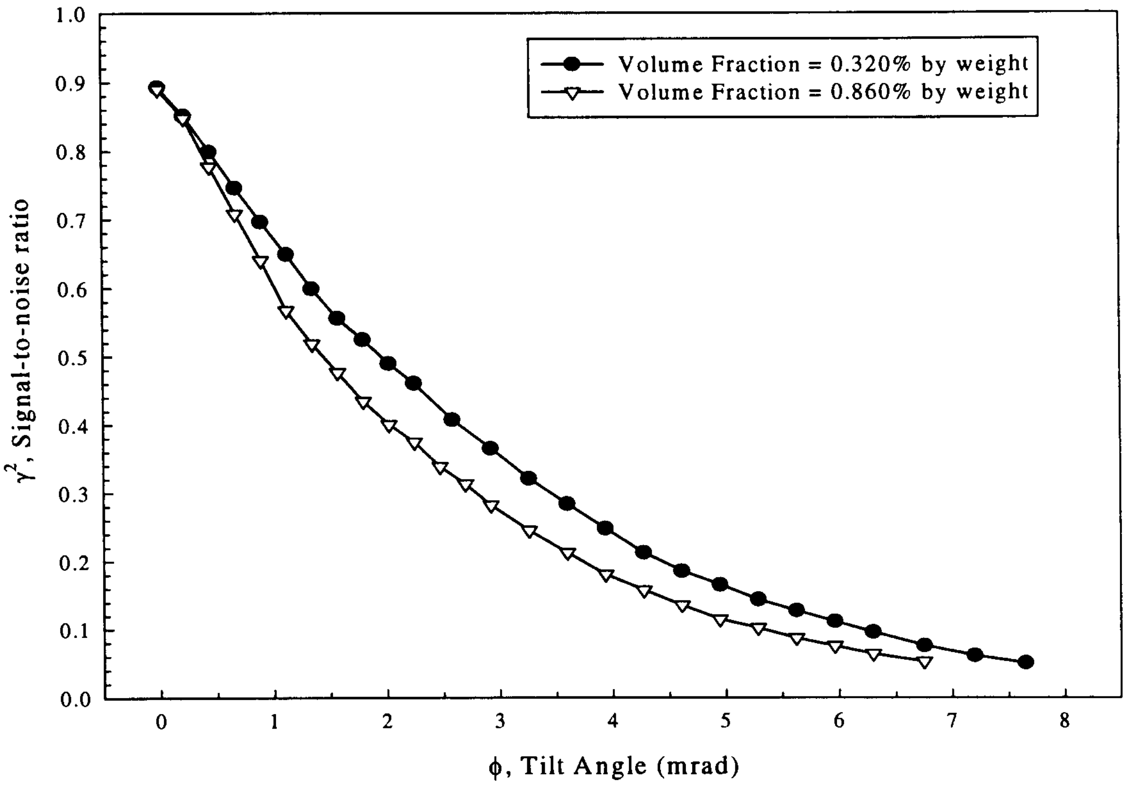

Figure 34: Signal-to-noise ratio versus tilt angle for cross-correlation measurements taken from a sample of 0.098 μm PSL particles at a scattering angle of 112° and flow rate of 100%. Data corresponds to Experiments 104 and 106.

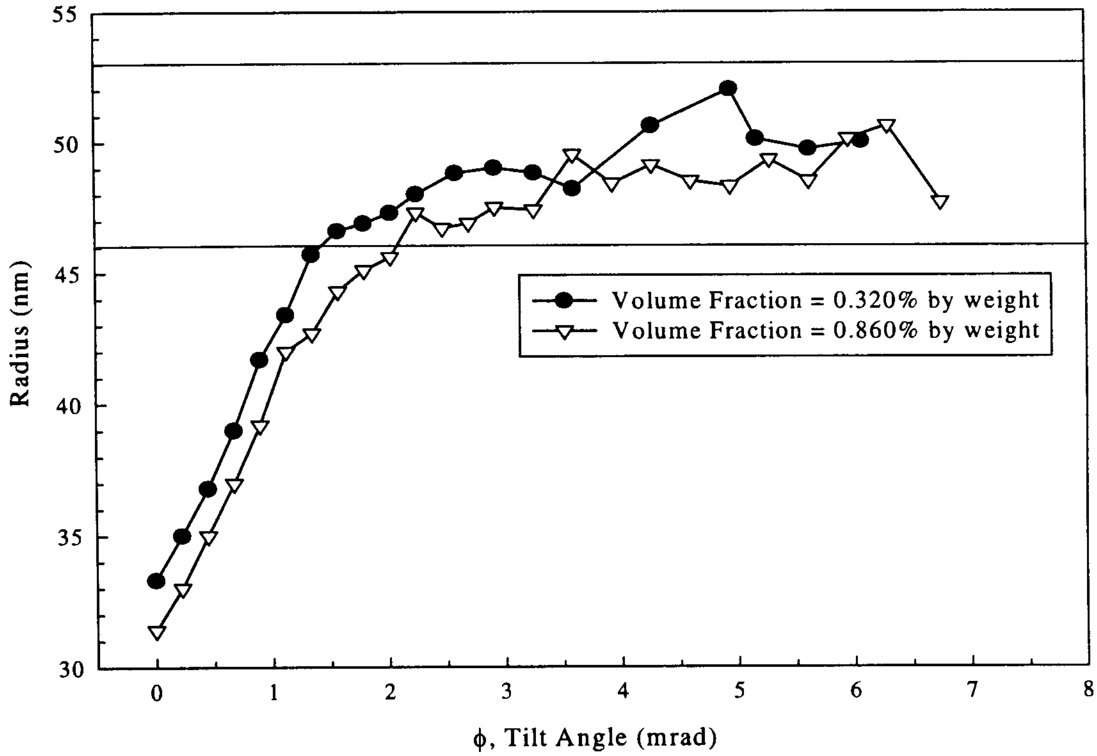

Figure 35: Radius versus tilt angle for cross-correlation measurements taken from a sample of 0.098 μm PSL particles at a scattering angle of 112° and flow rate of 100%. Data corresponds to Experiments 104 and 106.

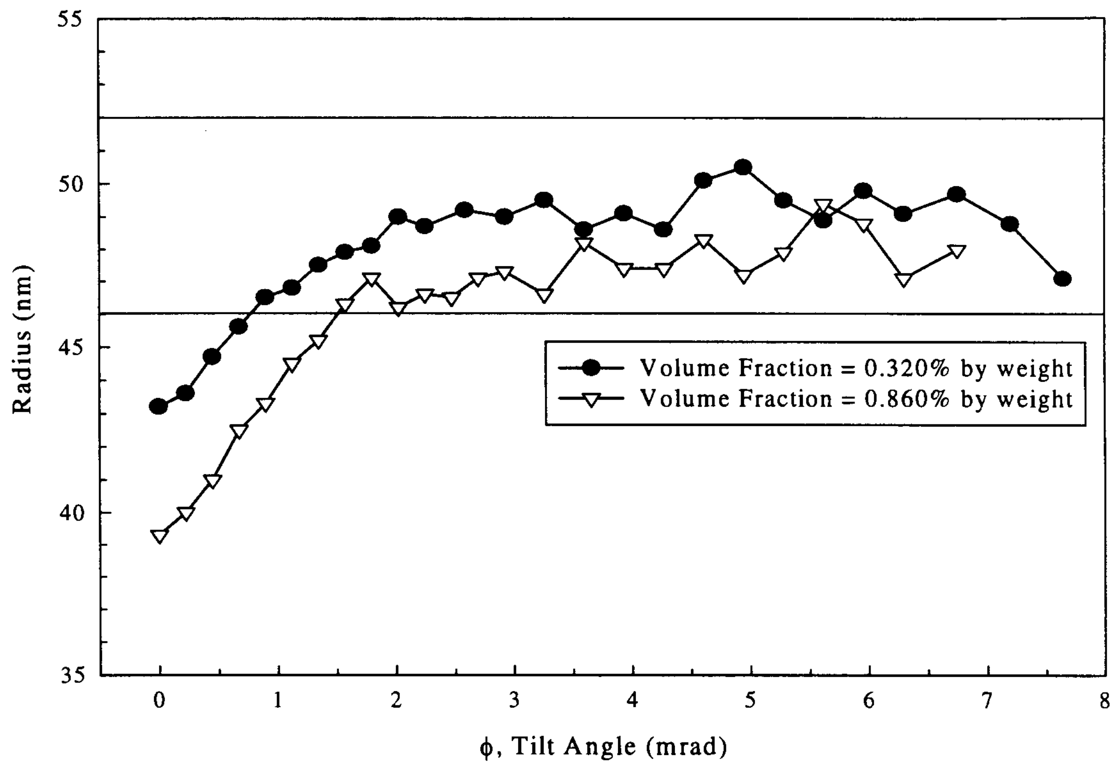

Figure 36: Radius versus tilt angle for cross-correlation measurements taken from a sample of 0.098 μm PSL particles at a scattering angle of 112° and flow rate of 0%. Data corresponds to Experiments 103 and 105.

CHAPTER VII

CONCLUSIONS AND RECOMENDATIONS

7.1 Conclusions

The use of dynamic light scattering data to determine particle characteristics is applicable to several industrial operations. Industries are looking for a method to accurately measure particle size without interrupting their operations. These types of measurements are termed non-intrusive in-situ and allow measurements to occur during normal production or testing operations. The research described in this thesis focused on a light scattering system that was capable of determining particle size in dense flowing solutions.

The purpose of this thesis was to demonstrate the feasibility of integrating two independent suppression techniques to determine particle size. One technique dealt with the suppression of multiple scattering effects. The second technique was used to suppress flow effects. The experimental setup, alignment, and procedure used for suppression of multiple scattering effects were discussed first. The essential components necessary to suppress multiple scattering effects from the static fluid setup were then integrated into a setup designed to suppress flow effects. This combined system was then used to determine particle size. Using both the static fluid and the flowing fluid setups, several parameters were studied to determine their effects on particle sizing. Those parameters include: scattering angle, sample concentration, particle size, flow rate, and alignment of the flowing setup test cell.

The first round of experiments involved the static fluid setup. The purpose of those experiments was twofold; the first purpose was to develop a familiarity with the suppression equipment and to develop the understanding of the suppression technique. The second purpose was to expand on the work done by Nobbmann *et al.* (1997). The static fluid experiments described within this thesis were conducted on 0.107 μm PSL particles at a variety of scattering angles ranging from 15° to 120° for volume fractions ranging from dilute to 0.5025 percent by weight. From the experiments performed on the static fluid setup, useful information about the characteristics of general dynamic light scattering and the data collected from it was discovered. Those characteristics include erratic behavior at small (forward) scattering angles and the system's sensitivity to misalignment. From these characteristics, a set procedure was adopted to deal with alignment of the system and for data collection. These characteristics as well as the others mentioned in Sections 6.2 and 6.3 led to the design of the flowing fluid setup.

The flowing fluid setup was designed to accomplish two forms of suppressions at once. First, the system utilized the same multiple scattering suppression procedure as that described in Chapter IV. Second, the system was aligned in a manner, which facilitated the suppression of flow effects. Various experiments were performed to demonstrate the suppression of flow effects and then the simultaneous suppression of multiple scattering and flow effects. The first set of experiments conducted with the flowing fluid setup demonstrated sensitivity to the system's alignment. The setup was positioned with the scattering wave vector perpendicular to the velocity vector of the fluid. The test cell was then rotated about the axis centered through its height to show the effect of non-perpendicular alignment between those two vectors. These experiments were conducted for various flow rates on samples of 0.107 μm and 0.204 μm PSL particles in a dilute (single scattering) solution. It was determined from these experiments that misalignment between ± 5° had little effect on the data collected. It was also determined that misalignment had a greater impact on the data used to determine the larger sized particles.

The second types of experiments performed with the flowing fluid setup were tilt angle mapping experiments (Sections 5.5.2 and 6.5.2). For cases of 0% flow, these experiments were similar to those performed with the static fluid setup of Chapter IV. When flow was added, the tilt angle experiments demonstrated the system's ability to suppress multiple scattering within flowing suspensions. Experiments were performed at a scattering angle of 112° on 0.098 μm, 0.107 μm, and 0.203 μm PSL particles at various volume fractions and for various flow rates. Several trends were discovered during these experiments concerning the nature of particle sizing in a flowing fluid. The first trend discovered dealt with the effect of fluid velocity. For higher velocities, larger tilt angles were required in order to suppress multiple scattering effects. This effect was similar to the effect caused by an increase in concentration. This effect held true for the flowing fluid setup as well as the static fluid setup. A final trend associated with the flowing fluid setup was that larger particle sizes (≥ 0.2 μm) appear to be more difficult to correctly size.

7.2 Recommendations

The theories utilized by the research described within this thesis are relatively new, and, to the knowledge of those involved in the experiments, have never been used together to determine particle characteristics. This thesis only discusses the use of the suppression techniques to determine one particle characteristic, particle size or diameter. Although several parameters (particle size, concentration, scattering angle, and flow velocity) were studied in order to evaluate their effects on the determination of particle size, many more parameters exist that were not researched. Parameters such as more scattering angles so that bigger particle sizes can be used, polarization, index of refraction, scattering/absorbing particles, higher velocity, etc., should be investigated. Also, more real world situations should be covered, such as solutions involving particle distributions instead of just monodisperse solutions. The current system must be modified if some of these recommendations are to be realized.

Some realistic minor modifications to the current setup are necessary to further the research. The first change would be to replace the current rear fiber mount (Figs. 9 and 10) with one similar in design to that of the top mount (Figs. 7 and 8). The ability to record the starting position as well as the position of alignment (through the micrometers on the top mount) would be of great benefit in the alignment process for the back mount.

The second change would be to modify the body of the goniometer (specifically the sample stand of Fig. 12) to allow the arms to achieve a wider range of angular travel. The current setup allows for each arm to travel to a maximum angle of 48°, which corresponds to a scattering angle of 112°. Due to the Rayleigh-Gans form factors associated with larger particles [Sundaresan (1999)] this scattering angle is not large enough to produce useable intensity levels for particles larger than the 0.2 μm particles. A modification of the setup to allow detector and laser arm to move to angles of $\delta = 70°$ (corresponding to a scattering angle of $\theta = 90°$ from Table 3) would improve the chance of achieving useable intensities. Although this increase should be enough, I believe the goniometer should be redesigned to allow for enough movement from the arms to be positioned across from each other ($\alpha_L = \alpha_D = 90°$). This positioning would allow the detectors direct view of the incident beam for alignment. This is similar to the alignment discussed in Section 4.3 for the static fluid setup. Doing so would allow for direct alignment of the detectors with respect to the incident beam.

A device utilizing a micrometer for precise cell rotations needs to be added to the current flowing fluid setup. The current system employs angles marked on the rotation disk, which carries the test cell holder. This method of positioning the test cell holder only allows for estimated rotation angles. The new system would allow exact cell rotation measurements to be conducted to determine a better-defined range of acceptable cell rotation angles.

The final recommendations for the redesign of the flowing fluid setup deal with the test cell holder. To use the current setup, the test cell is tilted approximately 5° from vertical in the holder to redirect reflections away from the detector housing. A better design would be to allow the entire top section (Fig. 13) to be tilted. A micrometer could be added to the rear of the device to allow for measuring of how much of a tilt is necessary in order to keep direct reflections away from the detectors. This information would also allow for the calculation of the actual depth of the incident laser beam into the cell.

A second recommendation for improving the current setup deals with the method employed to block reflections from reaching the detector. Strips of electrical tape are currently used to accomplish this task. The tape has a tendency to stretch during application and come loose from the holder during an experiment. This allows reflections to interfere with the measurements. A second problem with the use of electrical tape is the repeatability of replacing the tape on the cell holder in the same spot each time. An improvement would be the addition of slits to the test cell holder, which would be a more reliable method to block the reflections.

REFERENCES

Aberle, L.B. Hülstede, P., Wiegand, S., Schröer, W., and Staude, W. (1998), "Effective Suppression of Multiply Scattered Light in Static and Dynamic Light Scattering," **Applied Optics**, Vol. 37, No. 27, pp. 6511-6524.

Ackerson, B.J. and Clark, N.A. (1981), "Dynamic Light Scattering at Low Rates of Shear," **Journal of Physique**, Vol. 42, pp. 929-936.

Ackerson, B.J., Dougherty, R.L., Reguigui, N.M., and Nobbmann, U. (1992), "Correlation Transfer: Application of Radiative Transfer Solution Methods to Photon Correlation Problems," **Journal of Thermophysics and Heat Transfer**, Vol. 6, No 4, pp. 577-588.

ALV-Laser Vertiebsgesellschaft m.b.H., *ALV-5000 Multiple Tau Digital Correlator Reference Manual for Software Version 5.0*, June 1993.

Berne, B.J. and Pecora, R. (1976), *Dynamic Light Scattering*, John Wiley and Sons, Inc., New York.

Brown, W. (1993), *Dynamic Light Scattering: The Method and Some Applications*, Clarendon Press, Oxford.

Dhont, J.K.G. and de Kruif, C. G. (1983), "Scattered Light Intensity Cross Correlation. I. Theory," **Journal of Chemical Physics**, Vol. 79, pp.1658-1663.

Dorri-Nowkoorani, F., Nobbmann, U., Reguigui, N.M., Ackerson, B.J., and Dougherty, R.L. (1993), "Correlation Measurements of a Multiply Scattered Laser Beam by Fluid/Particle Suspensions," AIAA 93-2745, AIAA 28th Thermophysics Conference, Orlando, FL, July 6-9.

Dorri-Nowkoorani, F., Nobbmann, U., Reguigui, N.M., Ackerson, B.J., and Dougherty, R.L. (1994), "Improved P_N Approximation for One-Dimensional Scattering and Absorbing Media with Application to Correlation Transfer," AIAA 94-2096, AIAA 6th AIAA/ASME Joint Thermophysics and Heat Transfer Conference, Colorado Springs, CO, June 20-23.

Dorri-Nowkoorani, F. (1995), "Multiple Scattering Correlation Measurements in Fluid/Particle Suspensions: Application to Particle Characterization," Ph.D. Thesis, Oklahoma State University, Stillwater, Oklahoma.

Gougeon, P., Le Toulouzan, J. N., Gouesbet, G., and Thénard, C. (1987), "Optical Measurements of Particle Size and Concentration in Densely Laden Media Using a Visible/Infrared Double Extinction Technique," **Journal of Physics E: Science Instrumentation**, Vol. 20, pp. 1235-1242.

Hoppenbrouwers, M. and van de Water, W. (1998), "Dynamic Light Scattering in Shear Flow," **Physics of Fluids**, Vol. 10, No. 9, pp. 2128-2136.

Janna, W.S. (1993), *Introduction to Fluid Mechanics*, PWS Publishing Company, Boston, MA.

Lock, J. A. (1997a), "Theory of Multiple Scattering Suppression in Cross-Correlated Light Scattering Employing a Single Laser Beam," in *Light Scattering and Photon Correlation Spectroscopy*, Pike, E. R. and Abbiss, J. B., eds., NATO Series, (Kluwer, Dordrcht, The Netherlands), pp. 51-64.

Lock, J. A. (1997b), "Role of Multiple Scattering in Cross-Correlated Light Scattering With a Single Laser Beam," **Applied Optics**, Vol. 36, No. 30, pp. 7559-7570.

Mandel, L. and Wolf, E. (1995), *Optical Coherence and Quantum Optics*, Cambridge University Press, New York.

Meyer, W. V., Cannell, D. S., Smart, A. E., Taylor, T. W., and Tin, P. (1997a), "Suppression of Multiple Scattering Using a Single Beam Cross-Correlation Method," in *Light Scattering and Photon Correlation Spectroscopy*, Pike, E. R. and Abbiss, J. B., eds., NATO Series, (Kluwer, Dordrcht, The Netherlands), pp. 39-50.

Meyer, W. V., Cannell, D. S., Smart, A. E., Taylor, T. W., and Tin, P. (1997b), "Multiple-Scattering Suppression By Cross-Correlation," **Applied Optics**, Vol. 36, No. 30, pp. 7551-7558.

Mos, H. J., Pathmamonoharan, C., Dhont, J. K. G., and de Kruif, C. G. (1986), "Scattered Light Intensity Cross-Correlation. II. Experimental," **Journal of Chemical Physics**, Vol. 84, pp. 45-49.

Nobbmann, U. (1991), "Light Scattering From Micron Sized Particles," Masters' Thesis, Oklahoma State University, Stillwater, Oklahoma.

Nobbmann, U. (1997), "Multiple Light Scattering From Colloidal Samples," Ph.D. Thesis, Oklahoma State University, Stillwater, Oklahoma.

Nobbmann, U., Jones, S.W., and Ackerson, B.J. (1997), "Multiple-Scattering Suppression: Cross-Correlation With Tilted Singled-Mode Fibers," **Applied Optics**, Vol. 36, No. 30, pp. 7571-7576.

Pecora, R. (1985), *Dynamic Light Scattering Applications of Photon Correlation Spectroscopy*, Plenum Press, New York.

Phillies, G. D. J. (1981a), "Suppression of Multiple Scattering Effects in Quasielastic Light Scattering by Homodyne Cross-Correlation Techniques," **Journal of Chemical Physics**, Vol. 74, pp. 260-262.

Phillies, G. D. J. (1981b), "Experimental Demonstration of Multiple Scattering Suppression in Quasielastic-Light-Scattering Spectroscopy by Homodyne Coincidence Techniques," **Physical Review A**, Vol. 24, No. 4, pp. 1939-1943.

Pine, D. J., Weitz, D. A., Chaikin, P.M., and Herbolzheimer, E. (1988), "Diffusing-Wave Spectroscopy," **Physical Review Letters**, Vol. 60, No. 12, pp. 1134-1137.

Schätzel, K., Drewel, M., and Ahrens, J. (1990), "Suppression of Multiple Scattering in Photon Correlation Stectroscopy," **Journal of Physics: Condensed Matter 2**, SA393-SA398.

Segrè, P. N., van Megen, P., Pusey, P. N., Schätzel, K., and Peters, W. (1995), "Two-Colour Dynamic Light Scattering," **Journal of Modern Optics**, Vol. 42, No. 9, pp. 1929-1952.

Sundaresan, S. (1999), "Multiple Scattering Suppression Applied to Particle Sizing in Nonflowing/Flowing Media," Masters' Thesis, Oklahoma State University, Stillwater, Oklahoma.

van de Hulst, H. C. (1957), *Light Scattering by Small Particles*, Dover Publications, Inc., New York.

Welty, J., Wicks, C., and Wilson, R. (1984), *Fundamentals of Momentum, Heat and Mass Transfer*, 3rd Edition, John Wiley and Sons, Inc., New York.

White, F.M. (1991), *Viscous Fluid Flow*, 2nd Edition, McGraw-Hill, Inc., New York.

Wiese, H. and Horn, D. (1991), "Single-Mode Fibers in Fiber-Optic Quasielastic Light Scattering: A Study of the Dynamics of Concentrated Latex Dispersions," **Journal of Chemical Physics**, Vol. 94, pp. 6429-6443.

APPENDICES

APPENDIX I

Equipment List

1. 20mW Helium Neon laser manufactured by Uniphase with a wavelength of 632.5 nm, Model No. 1135P.

2. 100 mW Neodymium-Yttrium-Silver laser manufactured by Adlas with a wavelength of 532.5 nm, Model No. DPY315II.

3. Optical Power Meter manufactured by Newport Inc., Model No. 840 with wand Model No. 818-ST.

4. Test tube manufactured by Fisher Scientific from borosilicate glass with dimensions of 10 mm x 75 mm, Catalog No. 14-961-25.

5. Fiber Optic Cables manufactured by Oz Optics LTD. Part No. LPC-02-532-4/125-P-0.7-3.2GR-30-1-3-3.

6. Translation stages, Model No. 426a, manufactured by Newport and equipped with SM-25 micrometers were used for the top fiber mount. Dimensions of the stages were 89 mm x 89 mm x 25.4 mm with a 50.8 mm diameter hole in the center. The aluminum tilt plates were produced by the OSU Chemistry/Physics Machine Shop and had dimensions of 127 mm x 134 mm x 10 mm.

7. The back fiber mount was manufactured by the OSU Chemistry/Physics Machine Shop and had two main pieces, the mount plate and the piece that carried the set screws. The dimensions of the mount plate were 101.6 mm x 101.6 mm x 12.7 mm with a 34.5 mm diameter hole in the center. The dimensions of the second piece were 101.6 mm x 101.6 mm x 22.9 mm with a 34.5 mm diameter hole in the center.

8. Two power supplies produced by Global Specialties, Model Nos. 1310 and 1302.

9. 632.5 nm wavelength specific beamsplitter from Newport, Model No. 05BC16-NP.4, for the non-flowing setup.

10. ALV-5000 Multiple Tau Digital Correlator by ALV-Laser Vertriebsgesellschaft m.b.H Germany.

11. E-pure deionizer, Model No. D4641, manufactured by Barnstead and Thermolyne.

12. Electronic lab scale, Model No. 31205, by Sartorious.

13. Multi-band (400-700 nm), nonpolarizing beamsplitter, Model No. 05FC16-PB.3, by Newport for the flowing setup.

14. Filter holder manufactured by Newport, Model No. FH-1.

15. Shuttle pump manufactured by Instech Labs, Model No. S20P.

16. 6 mm x 8 mm 30.5 cm rectangular test cell with a 0.9 mm wall thickness, manufactured by Wilmad Glass from clear fused quartz, Catalog No. WQR-0608.

17. 1/8" x 1/16" tubing manufactured by Tygon, S-50-HL, Class VI.

18. Water bath container formed from 64-stock glass tubing in Oklahoma State Glass Shop with dimensions of 6.35 cm outside diameter having a wall thickness of 2.4 mm and a height of 8.89 cm.

19. Photomultiplier tubes manufactured by Thorn EMI Electron Tubes Inc., Model No. EBA-805.

20. Holding tanks with dimensions of 215 mm x 69.5 mm x 49.5 mm were manufactured from Plexiglas by the Oklahoma State University Physics Machine Shop. The side walls were 12 mm thick, while the lid and base were 9 mm thick. The lid was sealed to the base by 21 screws and a rubber gasket.

21. Core samples of polystyrene latex (PSL) particles from Duke Scientific:

    A. 0.107 μm diameter; 10 percent solids by weight; 5.6% Coefficient of Variation, Catalog No. 5010A-Lot No. 16456
    B. 0.098 μm diameter; 10 percent solids by weight; 6.2% C.V., Catalog No. 5010A-Lot No. 20259
    C. 0.203 μm diameter; 10 percent solids by weight; 2.1% C.V., Catalog No. 5020A-Lot No. 20500
    D. 0.204 μm ± 6 nm diameter; 1 percent solids by weight; Catalog No. 3200A-Lot No. 20613
    E. 0.300 μm ± 5 nm diameter; 1 percent solids by weight; Catalog No. 3300A-Lot No. 20286.

20. Parafilm laboratory film manufactured by American National Can was used to seal test tubes.

APPENDIX II

Static Fluid: Experimental Data

Table 4: Summary of the static fluid experiments discussed in Sundaresan (1999) and in this thesis.

Experiment Number	Scattering Angle (deg)	Test Cell Type	Volume Fraction (% by weight)	Particle Diameter (μm)
32	90	Square	0.3239	0.107
33	90	Square	0.3239	0.107
34	90	Square	0.1536	0.107
35	90	Square	0.1536	0.107
36	90	Square	0.4285	0.107
37	90	Square	0.4285	0.107
38	90	Circular	0.1330	0.107
39	90	Circular	0.3201	0.107
40	30	Circular	0.3201	0.107
41	30	Circular	0.3201	0.107
42	Sweep	Circular	Single Scatt.	0.107
43	60	Circular	0.3271	0.107
44	60	Circular	0.1545	0.107
45	Sweep	Circular	Single Scatt.	0.107
46	120	Circular	0.5025	0.107
47	120	Circular	0.3795	0.107
48	45	Circular	0.3795	0.107

Note: Detailed data for Experiments 32-37 appear in Sundaresan (1999), and detailed data for Experiments 38-48 appear in Table 5.

Table 5: Detailed description of experiments 38-48 described in summary Table 4.

Exp 38 Circular Cell 0.107 μm PSL V.F. = 0.133% θ = 90 deg
Front Tilt = 16.91 div. Rear Translation = 11.23 div.

Rear Tilt (div)	Side Translation (div)	Tilt Angle (mrad)	Intensity (kHz) Ch 0	Intensity (kHz) Ch 1	Y-Intercept	Decay Rate (1/msec)	Radius (nm)	Normalized Second Cumulant	Time (sec)
16.68	11.84	-7.425	221.485	167.417	0.0350	1.23	62.1	-0.2900	300
16.70	11.92	-7.200	222.044	165.552	0.0396	1.43	53.6	-0.0019	300
16.72	12.00	-6.975	222.858	164.413	0.0460	1.47	52.3	0.0280	300
16.74	12.10	-6.750	223.251	160.046	0.0559	1.50	51.0	0.0091	300
16.76	12.19	-6.525	223.600	160.302	0.0674	1.45	52.9	0.0560	300
16.78	12.29	-6.300	224.735	162.080	0.0748	1.45	52.9	0.0061	300
16.80	12.41	-6.075	227.312	165.040	0.0862	1.49	51.4	0.0170	300
16.82	12.48	-5.850	215.699	170.612	0.0964	1.48	53.3	-0.0061	300
16.84	12.59	-5.625	216.424	168.351	0.1130	1.49	52.7	0.0330	120
16.86	12.67	-5.400	217.390	165.495	0.1240	1.44	54.5	0.0170	300
16.88	12.77	-5.175	217.082	162.023	0.1350	1.48	53.3	0.0320	120
16.90	12.93	-4.950	219.400	159.414	0.1640	1.43	55.3	-0.0210	120
16.94	13.15	-4.500	219.450	170.152	0.2280	1.47	53.6	0.0150	120
16.96	13.27	-4.275	219.451	171.163	0.2480	1.47	53.7	0.0200	120
16.98	13.35	-4.050	220.289	166.459	0.2590	1.43	55.0	0.0064	120
17.02	13.49	-3.600	219.408	168.211	0.2820	1.46	54.1	0.0170	120
17.06	13.70	-3.150	219.829	163.177	0.3300	1.48	53.2	0.0300	120
17.10	13.90	-2.700	213.072	170.496	0.3880	1.45	54.3	0.0016	120
17.14	14.14	-2.250	222.806	171.898	0.4460	1.47	53.6	0.0120	120
17.18	14.34	-1.800	215.328	165.455	0.4980	1.48	53.3	0.0370	120
17.20	14.40	-1.575	222.773	174.563	0.5180	1.47	53.6	0.0200	120
17.22	14.42	-1.350	214.396	166.929	0.5270	1.48	53.2	0.0290	120
17.24	14.47	-1.125	222.837	163.309	0.5450	1.48	53.1	0.0240	120
17.26	14.61	-0.900	221.006	167.366	0.6190	1.52	51.7	0.0270	120
17.27	14.68	-0.788	223.399	170.716	0.6650	1.56	50.6	0.0400	120
17.28	14.73	-0.675	229.111	174.544	0.7130	1.61	49.0	0.0490	120
17.29	14.79	-0.563	223.647	171.153	0.7790	1.62	48.6	0.0630	120
17.30	14.84	-0.450	231.247	178.654	0.8370	1.67	47.3	0.0750	120
17.31	14.90	-0.338	223.532	169.284	0.8910	1.68	46.9	0.0720	120
17.32	14.96	-0.225	225.221	169.094	0.9280	1.68	46.8	0.0810	120
17.33	15.00	-0.113	238.175	178.087	0.9340	1.70	46.4	0.0720	120
17.34	15.03	0.000	223.847	207.015	0.9370	1.67	46.0	0.0880	120
17.35	15.10	0.113	223.897	211.382	0.8880	1.66	46.1	0.0740	120
17.36	15.16	0.225	225.348	214.338	0.8490	1.63	47.2	0.0720	120
17.37	15.22	0.338	224.310	214.517	0.7970	1.60	47.9	0.0620	120
17.38	15.29	0.450	224.986	216.072	0.7480	1.55	49.5	0.0560	120
17.39	15.33	0.563	213.781	195.927	0.6850	1.55	49.4	0.0550	120
17.40	15.42	0.675	229.206	203.753	0.6380	1.53	50.3	0.0460	120
17.42	15.48	0.900	220.696	194.896	0.6030	1.49	51.3	0.0240	120
17.44	15.57	1.125	217.499	186.720	0.5570	1.47	52.2	0.0210	120
17.46	15.68	1.350	219.748	187.649	0.5170	1.45	52.7	0.0047	120
17.48	15.79	1.575	219.727	189.240	0.4900	1.46	52.6	0.0330	120
17.50	15.90	1.800	210.688	191.171	0.4670	1.44	53.3	0.0280	120
17.52	15.97	2.025	223.077	194.545	0.4540	1.47	52.1	0.0520	120
17.54	16.12	2.250	223.289	188.619	0.4210	1.45	52.8	0.0170	120
17.56	16.21	2.475	224.628	185.381	0.3940	1.45	52.7	-0.0120	120
17.60	16.41	2.925	227.158	185.976	0.3550	1.43	53.7	0.0150	120
17.64	16.59	3.375	228.177	192.643	0.2970	1.44	53.3	0.0270	120
17.68	16.74	3.825	230.986	188.780	0.2590	1.46	52.6	0.0260	120
17.72	16.94	4.275	229.023	183.630	0.2190	1.48	51.9	0.0200	120
17.76	17.14	4.725	230.248	186.504	0.1860	1.51	50.9	0.0490	120
17.78	17.26	4.950	231.853	188.501	0.1650	1.48	51.6	0.0630	120
17.80	17.37	5.175	230.712	187.176	0.1430	1.46	52.4	0.0250	120
17.82	17.52	5.400	232.443	181.634	0.1180	1.41	54.4	0.0190	120
17.84	17.69	5.625	232.644	174.714	0.0961	1.45	53.0	0.0230	120
17.86	17.75	5.850	232.546	181.706	0.0883	1.46	52.1	-0.0360	120
17.88	17.86	6.075	231.698	185.053	0.0769	1.48	51.9	0.0780	120
17.90	17.92	6.300	231.402	193.843	0.0718	1.49	51.3	0.0260	120
17.92	17.99	6.525	228.680	204.385	0.0631	1.48	51.0	-0.0110	300
17.94	18.37	6.750	225.741	226.926	0.0371	1.53	50.0	0.0400	300
17.96	18.38	6.975	223.530	237.697	0.0321	1.57	48.7	-0.1100	300

<u>Exp 39</u> Circular Cell 0.107 µm PSL V.F. = 0.3201% θ = 90 deg

Front Tilt = 16.92 div. Rear Translation = 11.23 div.

Rear Tilt (div)	Side Translation (div)	Tilt Angle (mrad)	Intensity (kHz)		Y-Intercept	Decay Rate (1/msec)	Radius (nm)	Normalized Second Cumulant	Time (sec)
			Ch 0	Ch 1					
16.78	12.84	-6.3000	190.974	138.293	0.0320	2.61	47.6	0.1500	300
16.85	12.65	-5.5125	191.773	136.145	0.0402	2.50	51.1	0.0110	300
16.88	12.80	-5.1750	193.137	133.760	0.0499	2.35	56.9	-0.0500	300
16.91	12.99	-4.8375	194.167	135.453	0.0642	2.45	52.9	-0.0530	300
16.94	13.12	-4.5000	196.272	143.100	0.0854	2.45	53.0	-0.0600	300
16.97	13.36	-4.1625	195.062	141.545	0.1060	2.52	50.6	0.0220	120
17.00	13.48	-3.8250	194.487	143.382	0.1170	2.50	51.1	-0.0580	120
17.03	13.61	-3.4875	194.066	143.984	0.1310	2.46	52.5	-0.0430	120
17.05	13.69	-3.2625	193.207	143.644	0.1360	2.46	52.7	-0.0270	120
17.07	13.75	-3.0375	191.789	143.692	0.1470	2.51	50.7	-0.0200	120
17.09	13.85	-2.8125	192.159	142.517	0.1590	2.48	51.9	-0.0420	120
17.11	13.91	-2.5875	191.361	140.449	0.1710	1.51	50.7	0.0170	120
17.13	14.00	-2.3625	198.755	146.124	0.1830	1.48	51.8	0.0590	120
17.15	14.11	-2.1375	191.943	140.886	0.1990	1.48	51.7	-0.0320	120
17.17	14.21	-1.9125	191.921	142.451	0.2150	1.50	51.1	0.0180	120
17.18	14.26	-1.8000	192.468	142.909	0.2260	1.54	49.9	0.0570	120
17.19	14.31	-1.6875	192.696	143.023	0.2340	1.46	52.6	-0.0230	120
17.20	14.40	-1.5750	193.111	144.261	0.2580	1.59	48.1	0.0620	120
17.21	14.45	-1.4625	195.315	140.741	0.2760	1.60	48.0	0.0530	120
17.22	14.50	-1.3500	196.486	144.521	0.3020	1.65	46.5	0.0530	120
17.23	14.54	-1.2375	194.597	144.546	0.3220	1.66	46.3	0.0830	120
17.24	14.60	-1.1250	199.877	144.530	0.3610	1.71	44.9	0.0870	120
17.25	14.65	-1.0125	200.553	144.123	0.4040	1.84	41.7	0.1100	120
17.26	14.69	-0.9000	201.878	144.548	0.4640	1.92	40.0	0.1200	120
17.27	14.74	-0.7875	202.547	143.611	0.5240	1.99	38.5	0.1500	120
17.28	14.79	-0.6750	202.694	143.524	0.6180	2.12	36.2	0.1500	120
17.29	14.83	-0.5625	202.290	142.237	0.7020	2.25	34.0	0.1700	120
17.30	14.89	-0.4500	201.857	142.968	0.8050	2.34	32.8	0.1700	120
17.31	14.93	-0.3375	199.960	140.740	0.8820	2.39	32.1	0.1800	120
17.32	14.97	-0.2250	200.994	144.334	0.9250	2.41	31.8	0.1900	120
17.33	15.00	-0.1125	199.800	140.067	0.9280	2.43	31.5	0.1800	120
17.34	15.03	0.0000	197.733	137.942	0.9060	2.43	31.6	0.1800	120
17.35	15.13	0.1125	183.733	131.087	0.7710	2.31	33.2	0.1800	120
17.36	15.20	0.2250	189.266	135.814	0.6540	2.19	35.0	0.1700	120
17.37	15.26	0.3375	190.043	137.176	0.5620	2.05	37.3	0.1400	120
17.38	15.31	0.4500	201.283	144.362	0.4840	1.98	39.2	0.1400	120
17.39	15.34	0.5625	201.671	143.886	0.4670	1.88	40.8	0.1200	120
17.40	15.40	0.6750	201.879	143.758	0.4100	1.79	42.8	0.1100	120
17.41	15.46	0.7875	200.451	141.430	0.3660	1.72	44.7	0.0920	120
17.42	15.53	0.9000	200.537	138.728	0.3260	1.67	46.0	0.0690	120
17.43	15.56	1.0125	200.330	137.650	0.3070	1.63	47.2	0.0640	120
17.44	15.63	1.1250	199.679	135.287	0.2830	1.59	48.1	0.0720	120
17.45	15.72	1.2375	199.200	133.505	0.2600	1.52	50.6	0.0360	120
17.46	15.80	1.3500	197.722	131.054	0.2400	1.52	50.6	0.0430	120
17.48	15.90	1.5750	196.559	131.539	0.2290	1.51	50.7	0.0110	120
17.50	15.93	1.8000	196.285	133.635	0.2240	1.50	51.1	0.0320	120
17.52	16.07	2.0250	195.547	129.260	0.2020	1.48	51.8	-0.0100	120
17.54	16.17	2.2500	193.781	128.697	0.1940	1.52	50.4	0.0500	120
17.56	16.24	2.4750	191.672	129.836	0.1820	1.50	51.2	0.0067	120
17.58	16.33	2.7000	191.585	131.905	0.1740	1.52	50.5	-0.0160	120
17.60	16.40	2.9250	192.785	133.651	0.1600	1.49	51.3	0.0660	120
17.62	16.47	3.1500	191.442	133.943	0.1490	1.52	50.6	0.0390	120
17.64	16.60	3.3750	190.962	141.031	0.1310	1.46	52.7	-0.0013	120
17.66	16.71	3.6000	189.416	145.103	0.1170	1.52	50.6	-0.0360	180
17.68	16.84	3.8250	188.678	147.104	0.1010	1.49	51.3	0.0650	180
17.72	17.07	4.2750	194.181	131.148	0.0803	1.43	53.6	-0.0027	180
17.76	17.28	4.7250	190.555	129.179	0.0630	1.49	51.5	0.0290	180
17.80	17.44	5.1750	184.284	135.242	0.0475	1.38	55.6	0.1100	180
17.84	17.65	5.6250	183.606	134.728	0.0342	1.51	50.8	0.0660	180
17.88	17.77	6.0750	182.395	133.023	0.0260	1.55	49.6	0.0910	180

Exp 40 Circular Cell 0.107 μm PSL V.F. = 0.3201% θ = 30 deg

Front Tilt = 16.92 div. Rear Translation = 11.23 div.

Rear Tilt (div)	Side Translation (div)	Tilt Angle (mrad)	Intensity (kHz) Ch 0	Intensity (kHz) Ch 1	Y-Intercept	Decay Rate (1/msec)	Radius (nm)	Normalized Second Cumulant	Time (sec)
17.33	15.00	0.0000	216.628	160.471	0.9060	0.699	14.7	0.2800	120
17.32	14.97	-0.1125	214.462	161.398	0.9020	0.697	14.7	0.2800	120
17.31	14.94	-0.2250	214.538	167.347	0.8710	0.677	15.2	0.2800	120
17.30	14.90	-0.3375	215.131	166.873	0.8180	0.646	15.9	0.2800	120
17.29	14.83	-0.4500	216.336	161.059	0.7250	0.596	17.2	0.2900	120
17.28	14.79	-0.5625	212.607	165.244	0.6500	0.530	19.4	0.2800	120
17.27	14.76	-0.6750	214.100	169.244	0.5870	0.500	20.6	0.2800	120
17.26	14.70	-0.7875	211.671	168.166	0.5110	0.411	25.0	0.2700	120
17.25	14.65	-0.9000	213.418	169.385	0.4570	0.372	27.4	0.2600	120
17.24	14.61	-1.0125	216.881	168.940	0.4330	0.330	31.1	0.2300	120
17.23	14.55	-1.1250	218.751	170.740	0.4000	0.291	35.3	0.1900	120
17.22	14.49	-1.2375	219.905	168.390	0.3720	0.289	35.6	0.1800	120
17.21	14.43	-1.3500	221.660	166.660	0.3430	0.280	36.6	0.1600	120
17.20	14.38	-1.4625	218.276	167.876	0.3320	0.270	38.0	0.1600	120
17.19	14.34	-1.5750	218.327	169.400	0.3050	0.279	36.9	0.1200	120
17.18	14.28	-1.6875	220.253	167.796	0.2980	0.267	38.5	0.1500	120
17.17	14.22	-1.8000	221.263	168.496	0.2880	0.262	39.2	0.1500	120
17.16	14.18	-1.9125	209.687	180.986	0.2780	0.261	39.4	0.1400	120
17.15	14.13	-2.0250	207.231	171.480	0.2670	0.261	39.3	0.1500	120
17.14	14.08	-2.1375	245.728	168.922	0.2530	0.257	40.0	0.0910	120
17.13	14.04	-2.2500	235.476	183.883	0.2430	0.253	40.7	0.0740	120
17.12	13.99	-2.3625	211.871	207.831	0.2290	0.246	42.5	0.0840	120
17.11	13.86	-2.4750	236.293	183.982	0.2000	0.247	42.2	0.0310	240
17.10	13.80	-2.5875	238.336	180.935	0.1890	0.252	41.6	0.0920	300
17.09	13.76	-2.7000	238.444	181.848	0.1800	0.239	43.7	0.0480	300
17.08	13.72	-2.8125	237.080	183.789	0.1680	0.252	41.5	0.0850	300
17.07	13.66	-2.9250	236.960	184.653	0.1550	0.240	43.5	0.0640	300

Exp 41 Circular Cell 0.107 μm PSL V.F. = 0.3201% θ = 30 deg

Front Tilt = 16.92 div. Rear Translation = 11.23 div.

Rear Tilt (div)	Side Translation (div)	Tilt Angle (mrad)	Intensity (kHz) Ch 0	Intensity (kHz) Ch 1	Y-Intercept	Decay Rate (1/msec)	Radius (nm)	Normalized Second Cumulant	Time (sec)
17.33	15.00	0.0000	198.197	177.236	0.9090	0.69	15.6	0.2800	120
17.32	14.96	-0.1125	189.354	169.819	0.0892	0.70	15.3	0.2800	120
17.31	14.93	-0.2250	189.943	170.720	0.0874	0.67	16.0	0.2800	120
17.30	14.90	-0.3375	188.337	170.884	0.8300	0.66	16.3	0.2900	120
17.29	14.88	-0.4500	187.077	170.576	0.7810	0.64	16.8	0.2900	120
17.28	14.85	-0.5625	186.659	107.722	0.7230	0.59	18.2	0.2900	120
17.27	14.82	-0.6750	186.497	170.030	0.6710	0.53	20.1	0.2900	120
17.26	14.79	-0.7875	185.173	168.427	0.6060	0.49	21.8	0.3000	120
17.25	14.76	-0.9000	183.106	165.743	0.5500	0.46	23.5	0.2800	120
17.24	14.71	-1.0125	185.146	173.731	0.4830	0.42	25.8	0.3000	120
17.23	14.69	-1.1250	176.123	152.719	0.4670	0.39	27.5	0.2900	120
17.22	14.62	-1.2375	174.775	155.426	0.4200	0.34	31.7	0.2600	120
17.21	14.54	-1.3500	176.500	159.048	0.3850	0.32	33.8	0.2400	120
17.20	14.50	-1.4625	170.662	151.994	0.3640	0.31	35.0	0.2200	120
17.19	14.45	-1.5750	175.844	160.166	0.3380	0.29	36.7	0.2100	120
17.18	14.38	-1.6875	175.429	161.412	0.3310	0.26	41.2	0.1700	120
17.17	14.31	-1.8000	180.032	160.396	0.3000	0.26	41.4	0.1600	120
17.16	14.26	-1.9125	172.730	164.351	0.2810	0.25	42.5	0.1400	120
17.15	14.16	-2.0250	168.626	163.146	0.2470	0.22	48.9	0.0460	120
17.14	14.08	-2.1375	173.109	157.109	0.2320	0.24	44.2	0.1100	120
17.13	14.02	-2.2500	177.866	152.325	0.2060	0.23	44.8	0.0890	120
17.12	13.98	-2.3625	173.438	152.232	0.2030	0.24	44.1	0.0990	120
17.11	13.92	-2.4750	169.144	159.735	0.1810	0.22	48.0	0.0180	120
17.10	13.88	-2.5875	167.207	165.030	0.1630	0.23	46.4	0.0910	120
17.09	13.84	-2.7000	167.867	163.191	0.1620	0.22	48.3	0.0810	120
17.08	13.80	-2.8125	170.571	161.822	0.1500	0.23	46.2	0.0830	300

Exp 42   Circular Cell   0.107 μm PSL   θ = Sweep   Tilt Angle (mrad) = 0.000

Volume Fraction = Single Scattering

Scattering Angle (deg)	Intensity (kHz) Ch 0	Ch 1	Y-Intercept	Decay Rate (1/msec)	Radius (nm)	Normalized Second Cumulant	Time (sec)
120.00	31.540	0.000	0.883	1.9900	58.1	0.0150	60
115.00	31.785	0.000	0.886	1.9200	57.0	0.0170	60
110.00	31.905	0.000	0.889	1.8200	56.6	-0.0059	60
105.00	31.165	0.000	0.890	1.7200	56.3	0.0100	60
100.00	30.084	0.000	0.879	1.6500	54.6	0.0230	60
95.00	31.011	0.000	0.884	1.5000	55.8	-0.0047	60
90.00	31.629	0.000	0.890	1.3900	55.2	-0.0047	60
85.00	31.939	0.000	0.895	1.2600	55.7	0.0047	60
80.00	32.865	0.000	0.897	1.1700	54.2	0.0096	60
75.00	34.536	0.000	0.908	1.0100	56.2	-0.0036	60
70.00	35.323	0.000	0.907	0.9430	53.5	0.0180	60
65.00	36.797	0.000	0.912	0.8180	54.1	0.0310	60
60.00	39.536	0.000	0.918	0.7230	53.0	0.0450	60
55.00	41.602	0.000	0.903	0.6200	52.8	0.0360	60
50.00	44.747	0.000	0.923	0.5230	52.4	0.0470	60
45.00	48.165	0.000	0.930	0.4390	51.2	0.0850	60
40.00	51.805	0.000	0.933	0.3570	50.3	0.0350	60
35.00	59.273	0.000	0.936	0.2770	50.1	0.0860	60
30.00	67.845	0.000	0.904	0.2110	48.8	0.0990	60
25.00	77.111	0.000	0.916	0.1460	49.1	0.1000	60
20.00	111.859	0.000	0.937	0.0819	56.5	0.1400	60
15.00	138.699	0.000	0.900	0.0492	53.1	0.0099	60
120.00	0.000	19.260	0.942	1.9900	58.0	0.0170	60
115.00	0.000	19.325	0.943	1.9200	56.9	0.0080	60
110.00	0.000	19.286	0.940	1.8100	57.1	0.0046	60
105.00	0.000	18.196	0.932	1.7600	55.1	0.0190	60
100.00	0.000	18.266	0.933	1.6200	55.6	-0.0079	60
95.00	0.000	17.914	0.936	1.4900	56.1	0.0060	60
90.00	0.000	19.447	0.936	1.4100	54.5	0.0260	60
85.00	0.000	19.730	0.940	1.2500	55.8	0.0130	60
80.00	0.000	20.104	0.942	1.1900	53.3	0.0440	60
75.00	0.000	20.884	0.943	1.0300	55.4	0.0240	60
70.00	0.000	21.416	0.953	0.9150	55.1	0.0030	60
65.00	0.000	22.375	0.941	0.8350	53.0	0.0220	60
60.00	0.000	24.252	0.945	0.7230	53.0	0.0180	60
55.00	0.000	25.911	0.948	0.6150	53.1	0.0054	60
50.00	0.000	28.239	0.939	0.5470	50.1	0.0790	60
45.00	0.000	31.444	0.948	0.4410	50.9	0.0720	60
40.00	0.000	33.966	0.935	0.3740	47.9	0.0880	60
35.00	0.000	39.407	0.969	0.2710	51.1	0.1100	60
30.00	0.000	45.108	0.947	0.2120	48.6	0.1200	60
25.00	0.000	53.391	0.9520	0.1390	51.6	0.1300	60
20.00	0.000	73.847	0.8850	0.0889	52.0	0.1900	60
15.00	0.000	92.572	0.9390	0.0523	50.0	0.1500	60

Exp 43 Circular Cell 0.107 μm PSL V.F. = 0.3045% θ = 60 deg

Front Tilt = 16.92 div. Rear Translation = 11.23 div.

Rear Tilt (div)	Side Translation (div)	Tilt Angle (mrad)	Intensity (kHz) Ch 0	Intensity (kHz) Ch 1	Y-Intercept	Decay Rate (1/msec)	Radius (nm)	Normalized Second Cumulant	Time (sec)
17.04	13.51	-3.2625	163.332	98.935	0.0480	0.946	41.2	0.1100	180
17.05	13.57	-3.1500	163.879	98.558	0.0559	0.841	47.7	0.0200	180
17.06	13.62	-3.0375	166.555	99.080	0.0635	0.794	50.1	0.0900	180
17.07	13.67	-2.9250	167.512	99.986	0.0712	0.774	51.3	-0.0160	180
17.08	13.71	-2.8125	167.869	98.943	0.0746	0.808	49.2	0.0590	180
17.09	13.74	-2.7000	170.751	98.133	0.0822	0.798	49.8	0.0550	300
17.10	13.77	-2.5875	173.652	98.939	0.0850	0.821	48.3	0.0600	300
17.11	13.80	-2.4750	173.115	95.832	0.0921	0.811	49.0	0.0190	300
17.12	13.82	-2.3625	179.398	104.382	0.0928	0.779	51.7	-0.0800	300
17.13	13.89	-2.2500	182.377	105.658	0.1010	0.834	48.3	0.0520	300
17.14	13.94	-2.1375	185.377	109.776	0.1050	0.773	52.1	-0.0340	300
17.15	13.99	-2.0250	173.833	102.341	0.1260	0.803	50.4	0.0800	300
17.16	14.05	-1.9125	175.688	104.995	0.1320	0.816	49.6	0.0660	300
17.17	14.10	-1.8000	179.041	103.804	0.1460	0.817	49.5	0.0400	300
17.18	14.17	-1.6875	181.803	104.938	0.1670	0.819	49.4	0.0160	300
17.19	14.27	-1.5750	176.887	105.533	0.1850	0.847	47.8	0.0550	300
17.20	14.34	-1.4625	173.526	107.272	0.2000	0.886	45.7	0.0800	300
17.21	14.39	-1.3500	176.078	108.545	0.2240	0.890	45.4	0.0790	120
17.22	14.44	-1.2375	177.891	108.136	0.2470	0.963	42.0	0.1200	120
17.23	14.50	-1.1250	179.997	107.705	0.2800	1.020	39.6	0.1500	120
17.24	14.57	-1.0125	181.581	109.587	0.3310	1.140	35.6	0.1800	120
17.25	14.65	-0.9000	182.177	107.734	0.3890	1.260	32.2	0.2200	120
17.26	14.68	-0.7875	181.588	107.700	0.4320	1.340	30.2	0.2300	120
17.27	14.74	-0.6750	171.099	102.415	0.5110	1.470	27.4	0.2300	120
17.28	14.78	-0.5625	176.482	104.478	0.5930	1.610	25.1	0.2500	120
17.29	14.83	-0.4500	178.808	107.210	0.6790	1.700	23.8	0.2500	120
17.30	14.87	-0.3375	187.333	114.901	0.7430	1.820	22.3	0.2400	120
17.31	14.92	-0.2250	184.195	115.343	0.8070	1.800	21.2	0.2500	120
17.32	14.95	-0.1125	184.603	116.222	0.8540	1.860	20.6	0.1600	120
17.33	15.00	0.0000	174.626	110.801	0.9190	1.760	21.8	0.2500	120
17.34	15.06	0.1125	181.189	115.671	0.8730	1.720	22.3	0.2600	120
17.35	15.11	0.2250	173.986	112.051	0.8000	1.610	23.8	0.2500	120
17.36	15.18	0.3375	174.775	114.132	0.7040	1.500	25.5	0.2500	120
17.37	15.27	0.4500	174.529	115.138	0.5680	1.360	28.2	0.2300	120
17.38	15.35	0.5625	174.823	114.732	0.4780	1.200	31.9	0.2300	120
17.39	15.37	0.6750	179.472	118.442	0.4360	1.140	33.7	0.2100	120
17.40	15.40	0.7875	174.985	114.761	0.4010	1.080	35.4	0.1700	120
17.41	15.44	0.9000	173.497	113.580	0.3710	1.020	37.6	0.1600	120
17.42	15.49	1.0125	165.504	108.787	0.3170	0.977	39.3	0.1400	120
17.43	15.54	1.1250	165.466	114.179	0.2900	0.927	41.4	0.1400	120
17.44	15.57	1.2375	164.993	108.413	0.2790	0.905	42.4	0.1400	120
17.45	15.64	1.3500	163.863	108.294	0.2500	0.859	44.6	0.0780	120
17.46	15.69	1.4625	174.031	107.427	0.2330	0.858	44.7	0.0980	120
17.47	15.73	1.5750	165.064	109.015	0.2130	0.826	46.4	0.0540	120
17.48	15.78	1.6875	165.408	108.125	0.2040	0.814	47.1	0.0290	120
17.49	15.85	1.8000	165.135	108.259	0.1840	0.815	47.1	0.0630	300
17.50	15.90	1.9125	166.160	107.914	0.1720	0.816	47.0	0.0810	300
17.51	16.00	2.0250	167.723	105.975	0.1540	0.814	47.1	0.1000	300
17.52	16.05	2.1375	184.502	107.562	0.1240	0.804	47.7	0.0560	300
17.53	16.11	2.2500	185.472	105.696	0.1150	0.803	47.8	0.1100	300
17.54	16.21	2.3625	170.026	101.422	0.1080	0.806	47.6	0.0570	300
17.55	16.26	2.4750	173.602	104.330	0.0966	0.781	49.1	0.0360	300
17.56	16.32	2.5875	171.936	102.644	0.0869	0.788	48.7	0.0320	300
17.57	16.37	2.7000	173.918	101.464	0.0791	0.754	50.8	-0.0054	300
17.58	16.42	2.8125	177.909	106.383	0.0731	0.756	50.7	0.0220	300
17.59	16.47	2.9250	182.680	107.160	0.0670	0.757	50.6	-0.0230	300
17.60	16.52	3.0375	185.526	109.364	0.0625	0.752	51.0	0.0450	300
17.61	16.57	3.1500	188.553	111.130	0.0526	0.746	51.4	0.0028	300
17.62	16.60	3.2625	191.031	108.706	0.0437	0.760	50.4	-0.0023	300
17.63	16.67	3.3750	184.565	109.328	0.0357	0.878	43.6	0.0440	300

Exp 44 Circular Cell 0.107 μm PSL V.F. = 0.1545% θ = 60 deg

Front Tilt = 16.92 div. Rear Translation = 11.23 div.

Rear Tilt (div)	Side Translation (div)	Tilt Angle (mrad)	Intensity (kHz) Ch 0	Intensity (kHz) Ch 1	Y-Intercept	Decay Rate (1/msec)	Radius (nm)	Normalized Second Cumulant	Time (sec)
16.89	12.72	-4.9500	188.501	113.884	0.0262	0.638	61.7	0.096	300
16.91	12.34	-4.7250	189.840	115.051	0.0407	0.731	53.9	0.0750	240
16.93	12.93	-4.5000	188.748	114.986	0.0513	0.374	53.3	-0.0870	240
16.95	13.04	-4.2750	189.572	114.984	0.0613	0.776	50.7	0.1000	240
16.97	13.12	-4.0500	188.930	113.088	0.0685	0.761	51.8	0.0150	240
16.99	13.22	-3.8250	188.623	113.767	0.0799	0.788	50.0	0.0180	180
17.01	13.28	-3.6000	187.220	111.350	0.0903	0.780	50.5	0.0013	180
17.03	13.37	-3.3750	187.280	113.600	0.1170	0.709	55.5	0.0580	180
17.05	13.47	-3.1500	187.792	113.325	0.1310	0.765	51.5	0.0420	120
17.07	13.56	-2.9250	185.859	114.551	0.1640	0.776	50.7	0.0028	120
17.09	13.64	-2.7000	184.452	113.456	0.1870	0.772	51.0	0.0480	120
17.11	13.73	-2.4750	183.871	112.671	0.2070	0.776	50.7	0.0580	120
17.13	13.80	-2.2500	184.022	110.686	0.2300	0.788	50.0	0.0760	120
17.15	13.92	-2.0250	183.123	113.562	0.2690	0.773	50.9	0.0077	120
17.16	13.97	-1.9125	182.749	112.708	0.2750	0.757	52.0	0.0084	120
17.17	14.02	-1.8000	182.572	111.684	0.3040	0.771	51.1	0.0470	120
17.18	14.12	-1.6875	193.628	113.771	0.3500	0.772	51.0	0.0420	120
17.19	14.15	-1.5750	191.148	113.770	0.3680	0.782	50.3	0.0770	120
17.20	14.19	-1.4625	190.044	112.460	0.3770	0.753	52.3	-0.0025	120
17.21	14.23	-1.3500	190.830	111.003	0.3950	0.793	49.6	0.0770	120
17.22	14.36	-1.2375	185.740	113.178	0.4510	0.804	49.0	0.0440	120
17.23	14.42	-1.1250	184.952	113.051	0.4790	0.801	49.2	0.0840	120
17.24	14.50	-1.0125	183.584	114.410	0.5250	0.843	46.7	0.0780	120
17.25	14.57	-0.9000	182.540	114.476	0.5950	0.866	45.5	0.1100	120
17.26	14.62	-0.7875	181.238	113.594	0.6320	0.884	44.5	0.1100	120
17.27	14.67	-0.6750	180.832	111.593	0.6680	0.918	42.9	0.1400	120
17.28	14.74	-0.5625	180.647	111.328	0.7490	0.972	40.5	0.1600	120
17.29	14.77	-0.4500	180.025	109.751	0.7890	1.010	39.2	0.1700	120
17.30	14.83	-0.3375	180.376	109.879	0.8420	1.040	37.7	0.1800	120
17.31	14.91	-0.2250	179.764	110.894	0.9190	1.080	36.5	0.1900	120
17.32	14.96	-0.1125	182.306	112.601	0.9310	1.100	35.9	0.1800	120
17.33	15.00	0.0000	186.309	116.340	0.9270	1.100	35.9	0.1800	120

Exp 45 Circular Cell 0.107 μm PSL θ = Sweep Tilt Angle (mrad) = 0.000

V.F. = Single Scattering

Scattering Angle (deg)	Intensity (kHz) Ch 0	Intensity (kHz) Ch 1	Y-Intercept	Decay Rate (1/msec)	Radius (nm)	Normalized Second Cumulant	Time (sec)
120.00	61.675	0.000	0.958	2.170	55.3	0.00440	60
115.00	60.878	0.000	0.950	2.080	54.6	0.01400	60
110.00	60.021	0.000	0.955	1.980	54.0	0.01200	60
105.00	58.945	0.000	0.952	1.850	54.3	0.02400	60
100.00	58.808	0.000	0.952	1.750	53.5	0.03000	60
95.00	58.630	0.000	0.941	1.640	52.9	0.00830	60
90.00	59.109	0.000	0.942	1.480	53.9	-0.00052	60
85.00	60.722	0.000	0.938	1.400	52.1	0.02000	60
80.00	58.110	0.000	0.940	1.270	52.1	0.01400	60
75.00	65.162	0.000	0.948	1.130	52.4	0.05200	60
70.00	66.242	0.000	0.942	0.999	52.6	0.00650	60
65.00	70.873	0.000	0.939	0.911	50.6	0.03100	60
60.00	75.175	0.000	0.937	0.787	50.8	0.01100	120
55.00	79.033	0.000	0.938	0.676	50.4	0.04500	120
50.00	88.918	0.000	0.949	0.549	52.0	0.11000	120
45.00	90.126	0.000	0.938	0.481	48.6	0.06600	120
40.00	102.658	0.000	0.946	0.380	49.1	0.12000	120
35.00	128.749	0.000	0.973	0.250	57.8	0.21000	120
30.00	118.902	0.000	0.944	0.199	53.7	0.17000	120
120.00	0.000	42.037	0.962	2.200	54.6	0.02900	60
115.00	0.000	40.941	0.958	2.080	54.5	0.01100	60
110.00	0.000	40.053	0.965	1.990	54.0	0.04100	60
105.00	0.000	39.832	0.963	1.880	53.4	0.02800	60
100.00	0.000	39.184	0.970	1.740	53.9	0.00840	60
95.00	0.000	39.111	0.957	1.640	53.0	0.01700	60
90.00	0.000	39.295	0.959	1.480	54.0	-0.01800	60
85.00	0.000	40.480	0.953	1.370	53.1	0.00460	60
80.00	0.000	41.395	0.951	1.280	51.7	0.01500	60
75.00	0.000	43.381	0.947	1.150	51.3	0.02600	60
70.00	0.000	44.198	0.956	1.020	51.3	0.02500	60
65.00	0.000	47.204	0.961	0.920	50.1	0.01400	60
60.00	0.000	50.774	0.971	0.804	49.7	0.05200	120
55.00	0.000	54.505	0.947	0.684	49.8	0.06800	120
50.00	0.000	58.292	0.961	0.590	48.3	0.06600	120
45.00	0.000	63.990	0.961	0.483	48.4	0.08500	120
40.00	0.000	71.897	0.952	0.394	47.5	0.12000	120
35.00	0.000	87.921	0.956	0.291	49.6	0.09900	120
30.00	0.000	99.764	0.966	0.206	52.0	0.18000	120

<u>Exp 46</u> Circular Cell 0.107 μm PSL V.F. = 0.50255% θ = 120 deg

Front Tilt = 16.92 div. Rear Translation = 11.72 div.

Rear Tilt (div)	Side Translation (div)	Tilt Angle (mrad)	Intensity (kHz)		Y-Intercept	Decay Rate (1/msec)	Radius (nm)	Normalized Second Cumulant	Time (sec)
			Ch 0	Ch 1					
17.35	15.04	0.0000	156.721	100.844	0.9010	5.16	22.9	0.210	120
17.34	14.99	-0.1125	157.468	101.650	0.8840	5.14	23.0	0.210	120
17.33	14.95	-0.2250	161.346	104.309	0.7920	4.96	23.8	0.200	120
17.32	14.90	-0.3375	161.785	104.385	0.6630	4.90	24.1	0.210	120
17.31	14.86	-0.4500	162.250	105.025	0.5220	4.74	24.9	0.210	120
17.30	14.80	-0.5625	162.265	106.094	0.3530	4.44	26.6	0.200	120
17.29	14.74	-0.6750	160.324	103.418	0.2270	4.00	29.5	0.190	120
17.28	14.67	-0.7875	160.816	103.462	0.1490	3.52	33.6	0.180	120
17.27	14.61	-0.9000	157.853	102.419	0.1010	3.22	36.7	0.180	120
17.26	14.56	-1.0125	157.184	102.815	0.0811	3.04	38.9	0.180	120
17.25	14.51	-1.1250	159.558	103.692	0.0685	2.68	44.1	0.074	300
17.24	14.46	-1.2375	163.422	102.924	0.0564	2.58	45.8	0.011	300
17.23	14.42	-1.3500	161.738	103.037	0.0505	2.48	47.7	0.100	300
17.22	14.35	-1.4625	160.432	104.361	0.0424	2.35	50.2	0.032	420

Exp 47 Circular Cell 0.107 μm PSL V.F. = 0.3795% θ = 120 deg

Front Tilt = 16.92 div. Rear Translation = 11.23 div.

Rear Tilt (div)	Side Translation (div)	Tilt Angle (mrad)	Intensity (kHz) Ch 0	Ch 1	Y-Intercept	Decay Rate (1/msec)	Radius (nm)	Normalized Second Cumulant	Time (sec)
17.06	13.53	-3.2625	92.551	58.181	0.0426	2.07	57.0	-0.12000	420
17.08	13.66	-3.0375	92.767	59.478	0.0520	2.32	51.0	0.02300	420
17.10	13.74	-2.8125	92.895	60.895	0.0608	2.12	55.8	-0.01400	420
17.12	13.82	-2.5875	92.613	60.892	0.0660	2.26	52.4	0.06200	420
17.13	13.85	-2.4750	92.699	61.088	0.0677	2.29	51.7	0.00970	420
17.14	13.93	-2.3625	92.154	61.162	0.0685	2.32	51.0	0.03200	420
17.15	13.97	-2.2500	92.921	61.525	0.0751	2.30	51.5	0.04800	420
17.16	14.04	-2.1375	93.191	61.250	0.0769	2.24	52.7	0.04800	420
17.17	14.07	-2.0250	93.590	61.347	0.0822	2.13	55.4	0.01200	420
17.18	14.11	-1.9125	94.406	61.500	0.0949	2.17	54.5	-0.02100	420
17.19	14.16	-1.8000	94.249	61.475	0.0903	2.28	51.8	0.02500	300
17.20	14.20	-1.6875	94.028	61.550	0.0975	2.23	52.9	0.01500	300
17.21	14.25	-1.5750	94.512	61.697	0.1070	2.26	52.2	0.03000	300
17.22	14.33	-1.4625	94.881	62.582	0.1200	2.33	50.8	0.06200	300
17.23	14.38	-1.3500	94.411	62.643	0.1290	2.27	52.0	0.03300	300
17.24	14.45	-1.2375	94.250	63.053	0.1430	2.39	49.4	0.04900	300
17.25	14.53	-1.1250	94.830	63.270	0.1780	2.44	48.5	0.03600	300
17.26	14.59	-1.0125	94.416	62.259	0.1980	2.54	46.5	0.07300	120
17.27	14.65	-0.9000	94.599	62.215	0.2410	2.66	44.5	0.07300	120
17.28	14.71	-0.7875	94.073	61.186	0.2980	2.82	41.9	0.14000	120
17.29	14.75	-0.6750	95.199	61.752	0.3710	2.96	40.0	0.12000	120
17.30	14.80	-0.5625	94.710	60.309	0.4610	3.12	37.8	0.16000	120
17.31	14.84	-0.4500	95.231	60.953	0.5750	3.32	35.6	0.15000	120
17.32	14.88	-0.3375	95.902	60.904	0.7060	3.40	34.8	0.16000	120
17.33	14.94	-0.2250	94.763	90.100	0.8250	3.51	33.7	0.17000	120
17.34	14.98	-0.1125	94.991	59.076	0.8830	3.58	33.0	0.17000	120
17.35	15.04	0.0000	93.645	58.386	0.9220	3.57	33.1	0.17000	120
17.36	15.09	0.1125	92.084	56.589	0.8430	3.55	33.3	0.16000	120
17.37	15.14	0.2250	92.289	56.873	0.7700	3.46	34.1	0.17000	120
17.38	15.18	0.3375	92.049	56.356	0.6270	3.36	35.1	0.15000	120
17.39	15.23	0.4500	92.411	56.531	0.5130	3.25	36.4	0.16000	120
17.40	15.27	0.5625	92.090	56.687	0.4130	3.07	38.5	0.14000	120
17.41	15.30	0.6750	92.341	56.695	0.3390	2.91	40.6	0.13000	120
17.42	15.36	0.7875	92.258	56.808	0.2610	2.72	43.5	0.10000	120
17.43	15.41	0.9000	91.953	56.814	0.2110	2.62	45.1	0.08100	120
17.44	15.47	1.0125	92.092	57.287	0.1730	2.46	48.0	0.08000	120
17.45	15.54	1.1250	92.496	58.246	0.1440	2.33	50.6	0.04200	300
17.46	15.64	1.2375	92.543	58.369	0.1210	2.24	52.7	0.03000	300
17.47	15.70	1.3500	97.946	59.616	0.1140	2.21	53.6	0.00460	300
17.48	15.77	1.4625	97.291	59.404	0.1040	2.17	54.5	-0.02000	300
17.49	15.86	1.5750	96.951	57.960	0.0985	2.18	54.3	0.01200	300
17.50	15.93	1.6875	95.474	56.937	0.0904	2.20	53.7	-0.00026	300
17.51	16.00	1.8000	93.921	56.528	0.0848	2.24	52.7	0.05100	300
17.52	16.05	1.9125	94.095	56.753	0.0823	2.28	51.8	0.03200	300
17.53	16.08	2.0250	95.189	56.818	0.0801	2.21	53.6	0.01000	300
17.55	16.17	2.2500	94.894	57.078	0.0723	2.18	54.3	-0.02600	300
17.57	16.27	2.4750	95.537	54.335	0.0635	2.14	55.3	-0.00015	300
17.59	16.33	2.7000	97.177	54.765	0.0613	2.34	50.6	0.06400	300
17.61	16.43	2.9250	97.702	54.228	0.0509	2.25	52.4	0.05200	300
17.63	16.53	3.1500	98.370	55.510	0.0428	2.23	53.1	0.00460	300
17.65	16.67	3.3750	97.348	55.062	0.0350	1.96	60.4	-0.01700	300

Exp 48 Circular Cell 0.107 μm PSL V.F. = 0.3795% θ = 45 deg

Front Tilt = 16.92 div. Rear Translation = 11.23 div.

Rear Tilt (div)	Side Translation (div)	Tilt Angle (mrad)	Intensity (kHz)		Y-Intercept	Decay Rate (1/msec)	Radius (nm)	Normalized Second Cumulant	Time (sec)
			Ch 0	Ch 1					
17.19	14.29	-1.8000	107.519	66.934	0.0205	0.499	47.5	0.170	300
17.20	14.33	-1.6875	106.929	66.240	0.0302	0.494	48.0	0.038	300
17.21	14.37	-1.5750	117.776	71.795	0.0369	0.553	42.8	0.093	300
17.22	14.42	-1.4625	117.407	71.182	0.0501	0.578	41.0	0.220	300
17.23	14.49	-1.3500	117.730	71.963	0.0797	0.600	39.5	0.140	300
17.24	14.56	-1.2375	116.807	71.892	0.1150	0.673	35.2	0.230	120
17.25	14.61	-1.1250	117.496	71.988	0.1530	0.774	30.6	0.240	120
17.26	14.65	-1.0125	117.397	71.905	0.1870	0.843	28.1	0.260	120
17.27	14.70	-0.9000	117.545	72.305	0.2520	0.908	26.1	0.260	120
17.28	14.77	-0.7875	117.539	72.107	0.3550	1.030	23.1	0.280	120
17.29	14.80	-0.6750	118.275	72.059	0.4230	1.130	20.9	0.270	120
17.30	14.83	-0.5625	116.934	70.877	0.5090	1.250	19.0	0.280	120
17.31	14.89	-0.4500	95.834	58.459	0.6290	1.460	15.9	0.270	120
17.32	14.93	-0.3375	95.202	57.811	0.7340	1.530	15.0	0.270	120
17.33	14.97	-0.2250	97.229	59.374	0.8170	1.600	14.4	0.270	120
17.34	15.01	-0.1125	95.749	58.322	0.8650	1.630	14.1	0.270	120
17.35	15.04	0.0000	93.631	57.130	0.9060	1.650	14.0	0.270	120
17.36	15.11	0.1125	114.548	83.647	0.8110	1.530	15.5	0.270	120
17.38	15.20	0.3375	113.055	82.046	0.6310	1.370	17.3	0.270	120
17.40	15.33	0.5625	112.781	83.176	0.3890	1.060	22.3	0.270	120
17.42	15.43	0.7875	111.094	82.259	0.2470	0.903	26.2	0.260	120
17.44	15.52	1.0125	111.310	81.246	0.1590	0.712	33.3	0.230	120
17.46	15.66	1.2375	99.378	79.271	0.0797	0.603	39.5	0.140	120
17.47	15.73	1.3500	107.423	74.826	0.0505	0.554	42.8	0.130	120
17.48	15.77	1.4625	108.206	75.337	0.0370	0.508	46.7	0.029	120
17.49	15.87	1.5750	109.300	75.985	0.0153	0.781	30.4	0.370	120

APPENDIX III

Flowing Fluid: Experimental Data

Table 6: Summary of the flowing fluid experiments conducted at a scattering angle of $\theta = 112°$. N/A means temperature was not available.

Experment Number	Volume Fraction (% by weight)	Particle Diameter (μm)	Flow Rate (%)	Rotation Angle (degrees)	Temperature (K)
58	Single Scattering	0.107	Sweep	Sweep	N/A
60	Single Scattering	0.107	Sweep	Sweep	N/A
69	0.066	0.107	25	0	N/A
70	0.066	0.107	25	0	N/A
71	0.066	0.107	50	0	N/A
72	0.066	0.107	50	0	N/A
73	0.066	0.107	75	0	296
74	0.066	0.107	75	0	296
75	0.066	0.107	100	0	296
76	0.066	0.107	100	0	296
77	0.198	0.107	0	0	295
78	0.198	0.107	0	0	295
79	0.198	0.107	25	0	N/A
80	0.198	0.107	25	0	N/A
81	0.198	0.107	75	0	N/A
82	0.198	0.107	75	0	N/A
83	0.198	0.107	100	0	295
84	0.198	0.107	100	0	295
86	0.198	0.107	25	0	295
87	0.198	0.107	25	0	295
93	0.198	0.107	0	0	295
94	0.198	0.107	50	0	295
95	0.198	0.107	100	0	295
103	0.320	0.098	0	0	296
104	0.320	0.098	100	0	296
105	0.860	0.098	0	0	296
106	0.860	0.098	100	0	296
111	0.200	0.203	0	0	296
112	0.200	0.203	100	0	296

Note: The experiments not listed in this summary table did not contain any pertinent information to the subjects discussed in this thesis.

Table 7: Detailed description of experiments described in summary Table 6.

Exp 58 — Flow Cell — θ = 112 deg — 0.107 μm PSL — Flow Rate = 0%, 50%, and 100% — Single Scattering

Cell Rotation Angle (deg)	Intensity (kHz) Ch 0	Intensity (kHz) Ch 1	Y-Intercept	Decay Rate (1/ms)	Radius (nm)	Normalized Second Cumulant	Flow Rates (%)
0.00	76.195	0.000	0.9860	2.81	54.1	0.01000	0
0.00	0.000	68.559	0.9420	2.79	54.6	0.01200	0
0.00	76.560	0.000	0.9460	2.80	54.4	0.00610	50
0.00	0.000	68.941	0.9670	2.80	54.4	0.02300	50
0.00	78.015	0.000	0.9430	2.83	53.9	0.01900	100
0.00	0.000	69.045	0.9630	2.83	53.9	0.02100	100
-5.00	66.491	0.000	0.9370	2.80	54.4	0.02600	0
-5.00	0.000	64.592	0.9670	2.78	54.9	0.01400	0
-5.00	65.630	0.000	0.9380	2.83	53.9	0.02300	50
-5.00	0.000	64.439	0.9620	2.80	54.3	-0.00340	50
-5.00	66.112	0.000	0.9410	2.87	53.0	-0.00072	100
-5.00	0.000	63.928	0.9670	2.93	52.0	0.01800	100
-10.00	68.111	0.000	0.9390	2.78	54.8	0.01300	0
-10.00	0.000	63.425	0.9610	2.80	54.4	0.01700	0
-10.00	67.795	0.000	0.9350	2.81	54.2	-0.03800	50
-10.00	0.000	62.906	0.9640	2.83	53.9	-0.01100	50
-10.00	67.566	0.000	0.9380	2.94	51.9	-0.05800	100
-10.00	0.000	62.826	0.9700	2.97	51.3	0.00540	100
5.00	81.401	0.000	0.9450	2.79	54.6	0.02900	0
5.00	0.000	71.979	0.9670	2.77	55.1	0.00770	0
5.00	80.152	0.000	0.9390	2.79	54.6	-0.02100	50
5.00	0.000	71.183	0.9700	2.79	54.6	0.00041	50
5.00	79.958	0.000	0.9430	2.88	52.9	-0.05700	100
5.00	0.000	70.287	0.9620	2.91	52.4	-0.00026	100
10.00	79.734	0.000	0.9460	2.81	54.2	0.02200	0
10.00	0.000	69.144	0.9640	2.81	54.2	0.03200	0
10.00	80.633	0.000	0.9440	2.81	54.2	-0.03300	50
10.00	0.000	68.921	0.9690	2.84	53.7	0.00130	50
10.00	79.413	0.000	0.9470	3.00	50.7	-0.04200	100
10.00	0.000	68.090	0.9650	3.00	50.8	-0.01500	100

Exp 60 Flow Cell 0.204 μm PSL Single Scattering
θ = 112 deg Flow Rate = 0%, 50%, and 100%

Cell Rotation Angle (deg)	Intensity (kHz) Ch 0	Ch 1	Y-Intercept	Decay Rate (1/ms)	Radius (nm)	Normalized Second Cumulant	Flow Rates (%)
0.00	30.727	0.000	0.9210	1.52	103	0.0320	0
0.00	0.000	30.458	0.9470	1.47	106	0.0350	0
0.00	30.724	0.000	0.9270	1.53	103	0.0220	50
0.00	0.000	30.413	0.9530	1.50	104	0.0150	50
0.00	31.272	0.000	0.9180	1.52	103	0.0460	100
0.00	0.000	31.717	0.9570	1.52	103	0.0230	100
-5.00	29.934	0.000	0.8940	1.50	104	0.0130	0
-5.00	0.000	29.716	0.9420	1.48	106	0.0200	0
-5.00	30.444	0.000	0.8980	1.52	103	-0.0600	50
-5.00	0.000	29.136	0.9430	1.52	103	-0.0230	50
-5.00	30.051	0.000	0.8970	1.68	92.3	-0.0460	100
-5.00	0.000	28.735	0.9430	1.65	94.9	0.0220	100
-10.00	24.397	0.000	0.8570	1.44	108	0.0260	0
-10.00	0.000	25.618	0.9360	1.46	107	0.0140	0
-10.00	27.348	0.000	0.9500	3.45	45.4	0.2100	50
-10.00	0.000	25.833	0.9440	1.70	92.0	-0.0400	50
-10.00	27.128	0.000	0.9690	6.44	24.3	0.3300	100
-10.00	0.000	25.803	0.9360	1.89	82.9	-0.5900	100
5.00	29.538	0.000	0.8710	1.44	109	0.0200	0
5.00	0.000	26.857	0.9360	1.46	107	0.0450	0
5.00	29.107	0.000	0.8750	1.48	106	-0.0033	50
5.00	0.000	27.213	0.9360	1.49	105	0.0280	50
5.00	29.082	0.000	0.8700	1.67	93.5	0.0930	100
5.00	0.000	26.325	0.9380	1.58	99.1	0.0530	100
10.00	29.134	0.000	0.8690	1.41	111	0.0290	0
10.00	0.000	24.449	0.9330	1.44	109	0.0360	0
10.00	28.701	0.000	0.8780	1.65	95.0	0.0910	50
10.00	0.000	24.627	0.9380	1.80	86.8	0.1200	50
10.00	28.747	0.000	0.8640	1.76	89.1	0.0530	100
10.00	0.000	24.523	0.9280	1.70	91.8	0.0720	100

Exp 69	Flow Cell Front Tilt = 18.01 div.		0.107 μm PSL Rear Translation = 12.23 div.		V.F.= 0.066%			θ = 112 deg Flow Rate = 25%	
Rear Tilt (div.)	Side Translation (div.)	Tilt Angle (mrad)	Intensity (kHz) Ch 0	Ch 1	Y-Intercept	Decay Rate (1/ms)	Radius (nm)	Normalized Second Cumulant	Time (sec.)
15.99	11.63	0.0000	96.383	97.181	0.8130	3.23	48.6	0.06300	120
16.00	11.71	0.1125	93.988	97.796	0.8050	3.20	49.0	0.05900	120
16.01	11.75	0.2250	93.341	96.512	0.7800	3.19	49.2	0.05200	120
16.02	11.78	0.3375	93.682	99.646	0.7620	3.14	50.1	0.03000	120
16.03	11.80	0.4500	93.520	99.253	0.7260	3.11	50.5	0.04000	120
16.04	11.84	0.5625	92.885	97.347	0.6760	3.12	50.4	0.03300	120
16.05	11.87	0.6750	92.482	99.978	0.6220	3.09	50.8	0.03300	120
16.06	11.92	0.7875	91.579	96.562	0.5440	3.07	51.2	0.02600	120
16.07	11.96	0.9000	92.280	97.020	0.4770	3.03	51.9	0.01700	120
16.08	11.96	1.0125	92.401	107.209	0.4700	3.02	52.0	0.00970	120
16.09	12.00	1.1250	92.117	105.475	0.3990	3.00	52.3	-0.00140	120
16.10	12.03	1.2375	92.327	107 .345	0.3430	3.01	52.1	0.02000	120
16.11	12.08	1.3500	92.233	102.482	0.2780	2.97	52.8	-0.00079	180
16.12	12.12	1.4625	92.314	102.029	0.2240	2.90	54.1	-0.04700	180
16.13	12.15	1.5750	91.943	102.598	0.1810	2.92	53.8	-0.01800	300
16.14	12.19	1.6875	91.896	98.486	0.1420	2.96	53.0	-0.02200	300
16.15	12.21	1.8000	91.903	100.762	0.1190	2.94	53.5	0.02600	300
16.16	12.25	1.9125	91.972	101.419	0.0924	2.84	54.4	0.00820	300
16.17	12.28	2.0250	91.750	101.364	0.0690	2.99	52.5	-0.00017	420
16.18	12.32	2.1375	90.057	96.931	0.0497	2.95	53.3	0.02400	420
16.19	12.35	2.2500	89.846	98.880	0.0334	2.87	54.8	-0.03000	420
16.20	12.39	2.3625	89.836	98.270	0.0199	3.25	48.4	-0.01200	420

Exp 70 — Repeat of Exp 69 at random points to verify repeatability

15.99	11.63	0.0000	89.4580	92.030	0.8030	3.26	48.2	0.06600	120
16.02	11.77	0.3375	92.9670	98.257	0.7520	3.16	49.7	0.05200	120
16.05	11.85	0.6750	87.8050	99.354	0.6460	3.09	50.8	0.02900	120
16.08	11.94	1.0125	89.5980	102.565	0.4730	3.06	51.4	0.02500	120
16.11	12.07	1.3500	89.2930	103.931	0.2900	2.96	53.1	-0.00280	180
16.14	12.17	1.6875	89.2890	105.570	0.1630	2.90	54.2	0.01000	300
16.17	12.27	2.0250	89.2790	104.906	0.0710	3.00	52.4	0.06900	420
16.20	12.39	2.3625	88.4870	101.755	0.0201	3.37	46.6	0.21000	420

Exp 71 — Flow Cell — 0.107 μm PSL — V.F. = 0.066% — θ = 112 deg
Front Tilt = 18.01 div. — Rear Translation = 12.23 div. — Flow Rate = 50%

Rear Tilt (div.)	Side Translation (div.)	Tilt Angle (mrad)	Intensity (kHz) Ch 0	Intensity (kHz) Ch 1	Y-Intercept	Decay Rate (1/ms)	Radius (nm)	Normalized Second Cumulant	Time (sec.)
15.99	11.63	0.0000	100.176	101.437	0.7980	3.37	46.7	0.0870	120
16.00	11.70	0.1125	97.312	104.902	0.7950	3.34	47.1	0.0750	120
16.01	11.76	0.2250	96.200	101.725	0.7620	3.31	47.5	0.0720	120
16.02	11.79	0.3375	95.908	102.120	0.7370	3.24	48.4	0.0580	120
16.03	11.83	0.4500	95.617	99.653	0.6960	3.21	49.0	0.0500	120
16.04	11.86	0.5625	95.605	99.746	0.6480	3.16	49.2	0.0390	120
16.05	11.90	0.6750	95.159	96.444	0.5880	3.15	49.9	0.0300	120
16.06	11.93	0.7875	94.733	99.015	0.5490	3.12	50.4	0.0190	120
16.07	11.97	0.9000	93.787	99.072	0.4720	3.02	53.0	0.0140	120
16.08	12.00	1.0125	95.925	99.561	0.4190	3.03	51.8	0.0110	120
16.09	12.04	1.1250	94.757	100.585	0.3620	2.99	52.5	0.0034	120
16.10	12.08	1.2375	94.487	99.915	0.2980	3.07	51.1	0.0014	120
16.11	12.11	1.3500	94.517	100.707	0.2590	3.03	51.8	0.0430	180
16.12	12.15	1.4625	94.234	99.278	0.2110	3.03	51.9	0.0081	180
16.13	12.18	1.5750	93.878	97.993	0.1670	2.95	53.3	-0.0260	300
16.14	12.21	1.6875	93.758	102.544	0.1380	3.06	51.3	0.0110	300
16.15	12.25	1.8000	93.443	98.108	0.1080	2.96	53.1	-0.0230	300
16.16	12.28	1.9125	93.203	101.821	0.0843	2.91	53.1	-0.0250	420
16.17	12.33	2.0250	92.889	95.301	0.0560	2.98	52.7	0.0240	420
16.18	12.36	2.1375	92.405	95.602	0.0413	2.84	55.2	-0.1800	420

Exp 72 — Repeat of Exp 71 at random points to verify repeatability

16.00	11.70	0.1125	92.3340	101.821	0.7950	3.34	47.1	0.0620	120
16.03	11.82	0.4500	92.0590	100.387	0.7000	3.26	48.2	0.0550	120
16.06	11.93	0.7875	91.0770	93.234	0.5300	3.14	50.0	0.0360	120
16.09	12.03	1.1250	91.9700	100.024	0.3600	3.06	51.3	0.0031	120
16.12	12.14	1.4625	91.6440	98.922	0.2080	2.97	53.0	0.0210	180
16.15	12.24	1.8000	91.6940	99.132	0.1090	3.04	51.7	0.0410	300
16.18	12.35	2.1375	91.6730	100.160	0.0424	3.11	50.5	0.0240	420
16.19	12.38	2.2500	91.3870	97.592	0.0308	3.20	49.0	0.0830	420

Exp 73 — Flow Cell — 0.107 μm PSL — V.F. = 0.066% — θ = 112 deg

Front Tilt = 18.01 div. — Rear Translation = 12.23 div. — Flow Rate = 50%

Rear Tilt (div.)	Side Translation (div.)	Tilt Angle (mrad)	Intensity (kHz)		Y-Intercept	Decay Rate (1/ms)	Radius (nm)	Normalized Second Cumulant	Time (sec.)
			Ch 0	Ch 1					
16.00	11.70	0.0000	93.124	101.554	0.7710	3.43	45.9	0.08500	120
16.01	11.76	0.1125	91.844	100.323	0.7700	3.43	45.8	0.08200	120
16.02	11.79	0.2250	91.407	99.447	0.7310	3.41	46.1	0.07700	120
16.03	11.83	0.3375	91.130	99.162	0.6800	3.37	46.6	0.06300	120
16.04	11.87	0.4500	91.321	96.756	0.6660	3.32	47.4	0.06200	120
16.05	11.89	0.5625	91.089	99.185	0.5950	3.28	47.9	0.03900	120
16.06	11.92	0.6750	91.035	99.624	0.5580	3.23	48.7	0.04000	120
16.07	11.96	0.7875	91.265	100.647	0.4970	3.20	49.1	0.05000	120
16.08	12.00	0.9000	91.128	100.360	0.4340	3.13	50.3	0.01000	120
16.09	12.03	1.0125	91.129	101.234	0.3660	3.11	50.6	0.00590	120
16.10	12.08	1.1250	90.642	98.037	0.2960	3.09	50.8	0.00860	180
16.11	12.11	1.2375	90.999	98.877	0.2600	3.01	52.2	-0.02300	180
16.12	12.15	1.3500	90.879	100.588	0.2160	3.07	51.3	0.01500	300
16.13	12.18	1.4625	90.703	101.921	0.1710	3.07	51.1	0.02400	300
16.14	12.21	1.5750	90.706	99.225	0.1470	3.01	52.1	-0.01300	300
16.15	12.25	1.6875	90.892	100.228	0.1130	3.01	52.1	0.01100	300
16.16	12.28	1.8000	90.779	99.507	0.0927	2.95	53.2	-0.00083	420
16.17	12.32	1.9125	90.720	99.269	0.0652	3.00	52.3	-0.00280	420
16.18	12.35	2.0250	90.647	100.953	0.0492	3.20	49.2	0.01400	420
Exp 74		Repeat of Exp 73 at random points to verify repeatability							
16.03	11.82	0.3375	89.2920	97.468	0.7030	3.32	47.3	0.0700	120
16.08	12.01	0.9000	90.1530	98.759	0.4620	3.07	51.2	0.0130	120
16.12	12.16	1.3500	90.1000	97.756	0.2480	3.05	51.5	0.0130	240
16.15	12.25	1.6875	90.0900	100.291	0.1430	3.04	51.6	0.0300	300

Exp 75 — Flow Cell — 0.107 μm PSL — V.F. = 0.066% — θ = 112 deg

Front Tilt = 18.01 div. — Rear Translation = 12.23 div. — Flow Rate = 50%

Rear Tilt (div.)	Side Translation (div.)	Tilt Angle (mrad)	Intensity (kHz) Ch 0	Intensity (kHz) Ch 1	Y-Intercept	Decay Rate (1/ms)	Radius (nm)	Normalized Second Cumulant	Time (sec.)
16.00	11.70	0.0000	89.663	99.434	0.8020	3.68	42.7	0.1200	120
16.01	11.73	0.1125	88.699	103.900	0.7930	3.65	43.0	0.1100	120
16.02	11.73	0.2250	89.237	99.858	0.7860	3.61	43.6	0.0990	120
16.03	11.83	0.3375	92.450	100.135	0.6990	3.53	44.5	0.0860	120
16.04	11.87	0.4500	92.564	99.513	0.6500	3.47	45.3	0.0770	120
16.05	11.90	0.5625	91.827	97.968	0.6000	3.41	46.1	0.0680	120
16.06	11.94	0.6750	92.397	99.752	0.5450	3.34	47.0	0.0500	120
16.07	11.98	0.7875	92.118	98.654	0.4820	3.31	47.4	0.0530	120
16.08	12.01	0.9000	92.103	99.432	0.4240	3.27	48.0	0.0310	120
16.09	12.04	1.0125	92.176	99.682	0.3710	3.24	48.5	0.0330	120
16.10	12.08	1.1250	91.921	99.960	0.3250	3.17	49.6	0.0083	180
16.11	12.12	1.2375	91.632	98.774	0.2680	3.12	50.4	-0.0150	180
16.12	12.15	1.3500	91.316	99.962	0.2310	3.13	50.3	0.0180	180
16.13	12.18	1.4625	91.599	99.285	0.1900	3.12	50.4	0.0320	180
16.14	12.22	1.5750	91.067	100.822	0.1550	3.14	50.1	-0.0150	180
16.15	12.25	1.6875	91.298	100.465	0.1300	2.98	52.7	-0.0230	300
16.16	12.29	1.8000	91.189	99.810	0.0981	3.01	52.2	-0.0410	300
16.17	12.32	1.9125	91.025	100.110	0.0798	3.07	51.2	0.0350	300
16.18	12.36	2.0250	90.903	98.882	0.0588	3.12	50.3	0.0660	300
16.19	12.39	2.1375	90.701	100.552	0.0427	3.17	49.6	0.1300	420

Exp 76 — Repeat of Exp 75 at random points to verify repeatability

16.00	11.70	0.0000	88.5150	97.700	0.7990	3.61	43.5	0.1100	120
16.04	11.87	0.4500	88.3630	97.485	0.6520	3.42	45.9	0.0780	120
16.08	12.02	0.9000	87.9990	97.614	0.4290	3.25	48.3	0.0280	120
16.12	12.16	1.3500	88.3700	97.715	0.2300	3.17	49.6	0.0480	180
16.16	12.29	1.8000	88.3180	98.765	0.1030	3.06	51.4	0.0077	300

Exp 77 — Flow Cell — 0.107 μm PSL — V.F. = 0.198% — θ = 112 deg

Front Tilt = 18.02 div. — Rear Translation = 12.23 div. — Flow Rate = 0%

Rear Tilt (div.)	Side Translation (div.)	Tilt Angle (mrad)	Intensity (kHz) Ch 0	Intensity (kHz) Ch 1	Y-Intercept	Decay Rate (1/ms)	Radius (nm)	Normalized Second Cumulant	Time (sec.)
16.00	11.70	0.0000	93.279	101.081	0.7580	3.58	44.1	0.0990	120
16.01	11.77	0.1125	92.919	99.043	0.6900	3.53	44.5	0.0960	120
16.02	11.80	0.2250	92.588	99.955	0.6610	3.49	45.0	0.0900	120
16.03	11.84	0.3375	92.148	99.209	0.5970	3.45	45.5	0.0920	120
16.04	11.87	0.4500	93.21	100.120	0.5470	3.41	46.0	0.1000	120
16.05	11.91	0.5625	93.086	98.237	0.4820	3.33	47.1	0.0760	120
16.06	11.94	0.6750	93.046	99.058	0.4340	3.29	47.8	0.0660	120
16.07	11.98	0.7875	92.619	96.482	0.3700	3.20	49.1	0.0590	120
16.08	12.01	0.9000	93.179	98.033	0.3190	3.19	49.3	0.0670	120
16.09	12.04	1.0125	92.218	99.302	0.2770	3.17	49.6	0.0570	180
16.10	12.07	1.1250	91.785	102.089	0.2480	3.16	49.7	0.0570	180
16.11	12.12	1.2375	91.826	99.498	0.1930	3.12	50.4	0.0260	240
16.12	12.16	1.3500	91.736	98.252	0.1540	3.04	51.7	0.0019	240
16.13	12.19	1.4625	91.526	97.775	0.1280	2.95	53.3	0.0093	240
16.14	12.23	1.5750	91.594	97.802	0.1090	3.01	52.1	0.0340	300
16.15	12.26	1.6875	91.715	98.085	0.0897	3.03	51.9	0.0630	300
16.16	12.29	1.8000	91.644	98.426	0.0727	2.89	54.4	-0.0350	420
16.17	12.32	1.9125	91.608	99.210	0.0609	3.03	51.8	0.0650	420
16.18	12.36	2.0250	91.491	98.358	0.0460	3.08	51.0	0.0350	420
16.19	12.39	2.1375	91.792	98.753	0.0345	3.16	49.7	0.1400	420

Exp 78 — Repeat of Exp 77 at random points to verify repeatability

16.00	11.70	0.0000	93.902	102.306	0.7510	3.69	42.5	0.1100	120
16.04	11.88	0.4500	91.895	98.764	0.5210	3.42	45.9	0.0860	120
16.08	12.02	0.9000	91.828	98.367	0.2840	3.19	49.2	0.0400	120
16.12	12.17	1.3500	90.762	96.612	0.1280	2.98	52.7	0.0480	240
16.16	12.30	1.8000	92.806	97.575	0.0511	2.82	55.7	-0.0460	420

Exp 79 Flow Cell 0.107 μm PSL V.F. = 0.198% θ = 112 deg
Front Tilt = 18.02 div. Rear Translation = 12.23 div. Flow Rate = 25%

Rear Tilt (div.)	Side Translation (div.)	Tilt Angle (mrad)	Intensity (kHz) Ch 0	Ch 1	Y-Intercept	Decay Rate (1/ms)	Radius (nm)	Normalized Second Cumulant	Time (sec.)
16.00	11.70	0.0000	89.259	100.451	0.7230	4.08	38.5	0.0980	120
16.01	11.79	0.1125	88.263	97.518	0.6320	3.86	40.7	0.0780	120
16.02	11.83	0.2250	89.072	99.527	0.5860	3.86	40.7	0.0870	120
16.03	11.86	0.3375	89.169	100.247	0.5360	3.76	41.8	0.0770	120
16.04	11.89	0.4500	89.289	99.850	0.4790	3.67	42.8	0.0630	120
16.05	11.92	0.5625	89.264	99.619	0.4260	3.60	43.7	0.0640	120
16.06	11.96	0.6750	89.281	99.460	0.3730	3.45	45.5	0.0360	120
16.07	11.99	0.7875	89.213	99.458	0.3170	3.42	46.0	0.0480	120
16.08	12.03	0.9000	89.205	100.792	0.2650	3.29	47.8	0.0340	180
16.09	12.06	1.0125	89.825	101.524	0.2230	3.28	48.0	0.0480	180
16.10	12.09	1.1250	89.146	100.947	0.1820	3.26	48.2	0.0420	180
16.11	12.14	1.2375	89.100	99.267	0.1390	3.03	51.8	-0.0290	240
16.12	12.18	1.3500	88.766	99.083	0.1130	3.10	50.7	0.0440	240
16.13	12.21	1.4625	88.871	97.644	0.0884	2.98	52.6	0.0093	300
16.14	12.24	1.5750	88.754	99.489	0.0743	3.08	51.7	0.0043	300
16.15	12.28	1.6875	88.682	99.253	0.0500	2.88	54.5	0.0190	420
16.16	12.31	1.8000	88.742	99.879	0.0423	2.99	52.5	-0.0097	420
16.17	12.35	1.9125	88.538	98.904	0.0314	3.09	52.2	-0.0220	420
16.18	12.38	2.0250	88.695	98.120	0.0245	3.07	51.2	0.1500	420

Exp 80 Repeat of Exp 79 at random points to verify repeatability

16.00	11.70	0.0000	90.0330	100.214	0.7400	4.01	39.2	0.0920	120
16.04	11.89	0.4500	90.0360	99.939	0.4960	3.64	43.1	0.0760	180
16.08	12.03	0.9000	90.0860	100.169	0.2840	3.26	48.2	0.0290	300
16.12	12.17	1.3500	89.9820	99.566	0.1380	3.06	51.3	-0.0074	300
16.16	12.30	1.8000	89.8250	100.401	0.0584	3.01	52.2	-0.0140	420

Exp 81	Flow Cell		0.107 μm PSL		V.F. = 0.198%		θ = 112 deg		
	Front Tilt = 18.02 div.		Rear Translation = 12.23 div.				Flow Rate = 75%		
Rear Tilt (div.)	Side Translation (div.)	Tilt Angle (mrad)	Intensity (kHz) Ch 0	Intensity (kHz) Ch 1	Y-Intercept	Decay Rate (1/ms)	Radius (nm)	Normalized Second Cumulant	Time (sec.)
16.00	11.70	0.0000	90.254	100.828	0.7400	5.27	29.8	0.1800	120
16.01	11.80	0.1125	89.927	99.676	0.6500	4.91	32.0	0.1600	120
16.02	11.83	0.2250	89.950	100.234	0.6000	4.73	33.2	0.1500	120
16.03	11.86	0.3375	89.705	99.486	0.5490	4.60	34.1	0.1400	120
16.04	11.89	0.4500	89.842	100.372	0.5120	4.43	35.5	0.1400	120
16.05	11.92	0.5625	89.751	99.451	0.4500	4.29	36.7	0.1200	120
16.06	11.95	0.6750	89.593	100.052	0.4010	4.14	38.0	0.1100	120
16.07	11.99	0.7875	89.855	100.073	0.3490	3.97	39.6	0.0980	180
16.08	12.02	0.9000	89.768	101.210	0.2960	3.83	41.1	0.0970	180
16.09	12.07	1.0125	89.866	99.841	0.2390	3.62	43.4	0.0560	180
16.10	12.10	1.1250	89.613	100.061	0.2020	3.48	45.1	0.0390	180
16.11	12.13	1.2375	89.729	99.997	0.1660	3.44	45.6	0.0270	240
16.12	12.17	1.3500	89.635	100.618	0.1370	3.43	45.8	0.0530	240
16.13	12.20	1.4625	89.908	101.293	0.1150	3.20	49.0	-0.0015	240
16.14	12.24	1.5750	89.610	100.140	0.0865	3.18	49.4	-0.0043	300
16.15	12.27	1.6875	89.540	100.289	0.0711	3.17	49.5	0.0031	300
16.16	12.30	1.8000	89.644	100.708	0.0573	3.11	50.4	0.0042	360
16.17	12.34	1.9125	89.461	101.209	0.0420	2.89	54.3	-0.2000	360
16.18	12.37	2.0250	88.489	98.303	0.0332	2.88	54.6	-0.1200	420

Exp 82 — Repeat of Exp 81 at random points to verify repeatability

16.00	11.70	0.0000	87.8220	98.322	0.7380	5.37	29.3	0.1800	120
16.04	11.88	0.4500	88.0750	101.124	0.5170	4.42	35.6	0.1200	120
16.08	12.01	0.9000	87.9660	101.056	0.3030	3.80	41.4	0.0710	240
16.12	12.17	1.3500	87.9360	98.051	0.1310	3.41	46.1	0.0440	240
16.16	12.31	1.8000	87.6700	100.784	0.0548	3.07	51.2	-0.0083	420

Exp 83 Flow Cell 0.107 µm PSL V.F. = 0.198% θ = 112 deg

Front Tilt = 18.02 div. Rear Translation = 12.23 div. Flow Rate = 100%

Rear Tilt (div.)	Side Translation (div.)	Tilt Angle (mrad)	Intensity (kHz) Ch 0	Intensity (kHz) Ch 1	Y-Intercept	Decay Rate (1/ms)	Radius (nm)	Normalized Second Cumulant	Time (sec.)
16.00	11.70	0.0000	88.209	98.791	0.7350	6.50	24.2	0.2200	120
16.01	11.73	0.1125	88.213	100.974	0.7160	6.26	25.1	0.2200	120
16.02	11.75	0.2250	87.670	100.926	0.6910	6.11	25.7	0.2000	120
16.03	11.77	0.3375	88.009	101.683	0.6490	5.86	26.8	0.2000	120
16.04	11.88	0.4500	88.181	99.089	0.5120	5.30	29.7	0.1800	120
16.05	11.92	0.5625	87.859	99.409	0.4560	5.08	30.9	0.1800	180
16.06	11.96	0.6750	87.894	98.002	0.3950	4.74	33.1	0.1500	180
16.07	11.99	0.7875	87.973	98.076	0.3390	4.50	34.9	0.1400	180
16.08	12.03	0.9000	87.912	98.650	0.2910	4.37	36.0	0.1400	240
16.09	12.07	1.0125	87.934	97.922	0.2380	4.16	37.7	0.1300	240
16.10	12.10	1.1250	88.002	98.215	0.1970	3.98	39.4	0.1100	300
16.11	12.13	1.2375	87.938	99.646	0.1680	3.83	41.1	0.0760	300
16.12	12.17	1.3500	87.929	99.529	0.1390	3.72	42.2	0.0970	300
16.13	12.20	1.4625	88.026	98.887	0.1080	3.63	43.3	0.0670	420
16.14	12.24	1.5750	87.897	99.110	0.0880	3.54	44.4	0.0610	420
16.15	12.27	1.6875	88.245	99.329	0.0740	3.45	45.5	0.0780	840
16.16	12.31	1.8000	88.337	98.656	0.0555	3.27	48.1	0.0000	840
16.17	12.34	1.9125	88.324	100.398	0.0427	3.22	48.8	0.0069	840
16.18	12.37	2.0250	88.237	99.675	0.0309	3.16	49.7	-0.0400	840
16.19	12.41	2.1375	88.221	99.270	0.0225	3.04	51.6	-0.0440	600

Exp 84 Repeat of Exp 83 at random points to verify repeatability

16.00	11.70	0.0000	87.5940	98.642	0.7390	6.40	24.6	0.2200	120
16.04	11.89	0.4500	87.7010	99.272	0.4960	5.20	30.2	0.1800	120
16.08	12.03	0.9000	87.6290	99.547	0.2890	4.25	37.0	0.1300	240
16.12	12.17	1.3500	87.6970	100.147	0.1360	3.60	43.6	0.0880	300
16.16	12.31	1.8000	88.0050	99.835	0.0547	3.35	46.9	0.0720	480

Exp 86 — Flow Cell — 0.107 μm PSL — V.F. = 0.198% — θ = 112 deg

Front Tilt = 18.12 div. — Rear Translation = 12.27 div. — Flow Rate = 25% — **Maximize Intensity**

Rear Tilt (div.)	Side Translation (div.)	Tilt Angle (mrad)	Intensity (kHz) Ch 0	Intensity (kHz) Ch 1	Y-Intercept	Decay Rate (1/ms)	Radius (nm)	Normalized Second Cumulant	Time (sec.)
16.08	11.87	0.000	81.284	96.266	0.8330	3.52	44.7	0.092	120
16.09	11.93	0.113	83.322	98.066	0.7440	3.48	45.1	0.084	120
16.10	11.95	0.225	83.826	95.619	0.7360	3.45	45.6	0.081	120
16.11	12.02	0.338	82.570	98.248	0.6390	3.41	44.7	0.081	120
16.12	12.06	0.450	83.791	99.288	0.5700	3.39	45.0	0.060	120
16.13	12.10	0.563	84.677	98.219	0.5060	3.35	45.5	0.069	120
16.14	12.13	0.675	84.704	98.358	0.4580	3.25	46.8	0.044	120
16.15	12.15	0.788	83.815	98.852	0.4190	3.29	46.3	0.060	120
16.16	12.18	0.900	83.102	100.827	0.3610	3.19	47.7	0.032	120
16.17	12.21	1.013	82.335	101.650	0.3130	3.23	47.3	0.037	180
16.18	12.27	1.125	82.917	101.798	0.2570	3.19	47.7	0.056	180
16.19	12.32	1.238	84.435	99.543	0.2010	3.17	48.0	0.040	240
16.20	12.36	1.350	85.324	99.610	0.1630	3.12	48.8	0.035	240
16.21	12.38	1.463	84.268	101.233	0.1400	3.04	50.0	-0.025	300
16.22	12.40	1.575	82.914	99.888	0.1210	3.09	49.3	0.021	300
16.23	12.45	1.688	84.277	98.400	0.0901	2.98	51.1	-0.004	420
16.24	12.47	1.800	83.138	99.673	0.0773	3.12	48.8	0.055	420

Exp 87 — Flow Cell — 0.107 mm PSL — V.F. = 0.198% — θ = 112 deg

Front Tilt = 18.12 div. — Rear Translation = 12.27 div. — Flow Rate = 25% — **Maintain Intensity**

Rear Tilt (div.)	Side Translation (div.)	Tilt Angle (mrad)	Intensity (kHz) Ch 0	Intensity (kHz) Ch 1	Y-Intercept	Decay Rate (1/ms)	Radius (nm)	Normalized Second Cumulant	Time (sec.)
16.08	11.87	0.0000	84.346	98.108	0.8270	3.63	42.0	0.0930	120
16.09	11.96	0.1125	86.206	98.876	0.7450	3.53	43.1	0.0820	120
16.10	11.99	0.2250	86.327	98.217	0.6910	3.49	43.6	0.0790	120
16.11	12.04	0.3375	85.791	97.559	0.6200	3.45	44.2	0.0710	120
16.12	12.07	0.4500	85.605	98.050	0.5580	3.37	45.1	0.0610	120
16.13	12.12	0.5625	84.562	97.989	0.4830	3.30	46.2	0.0530	120
16.14	12.17	0.6750	84.058	97.882	0.4000	3.27	46.6	0.0520	120
16.15	12.21	0.7875	84.193	98.884	0.3480	3.20	47.6	0.0400	120
16.16	12.25	0.9000	84.053	98.338	0.2920	3.16	48.1	0.0370	180
16.17	12.28	1.0125	85.929	98.309	0.2530	3.17	48.1	0.0520	180
16.18	12.31	1.1250	86.708	98.658	0.2170	3.05	50.0	0.0240	240
16.19	12.35	1.2375	85.304	98.906	0.1710	3.16	49.6	0.0370	240
16.20	12.40	1.3500	84.428	98.315	0.1340	3.00	50.7	-0.0093	300
16.21	12.44	1.4625	84.036	98.630	0.1070	2.98	51.1	0.0460	300
16.22	12.48	1.5750	83.039	98.196	0.0837	3.03	50.2	0.0980	420
16.23	12.51	1.6875	83.198	98.425	0.0672	2.85	53.3	0.0009	420
16.24	12.54	1.8000	83.331	98.602	0.0546	2.98	51.1	0.0610	480
16.25	12.58	1.9125	83.405	98.876	0.0431	2.87	53.0	-0.0340	480

Exp 93 | Flow Cell | 0.107 μm PSL | V.F. = 0.198% | θ = 112 deg
Front Tilt = 18.12 div. | Rear Translation = 12.27 div. | Flow Rate = 0%

Rear Tilt (div.)	Side Translation (div.)	Tilt Angle (mrad)	Intensity (kHz) Ch 0	Intensity (kHz) Ch 1	Y-Intercept	Decay Rate (1/ms)	Radius (nm)	Normalized Second Cumulant	Time (sec.)
16.04	11.80	0.0000	114.759	146.581	0.9090	3.31	46.7	0.05500	120
16.05	11.83	0.1125	114.547	146.792	0.9030	3.31	46.7	0.05000	120
16.06	11.89	0.2250	114.407	143.958	0.8850	3.28	47.1	0.06100	120
16.08	11.96	0.4500	114.857	146.804	0.8530	3.21	48.2	0.04700	120
16.10	12.04	0.6750	114.702	145.092	0.7960	3.28	48.6	0.03900	120
16.12	12.12	0.9000	114.304	147.589	0.7480	3.16	49.0	0.04200	120
16.14	12.20	1.1250	113.113	150.027	0.7020	3.09	50.2	0.03400	120
16.16	12.27	1.3500	114.656	147.925	0.6700	3.03	51.0	0.00950	120
16.18	12.35	1.5750	115.055	146.796	0.6350	3.02	51.3	0.01700	120
16.20	12.43	1.8000	114.946	145.883	0.6000	2.99	51.7	0.00730	120
16.22	12.50	2.0250	114.599	146.715	0.5750	2.97	52.2	0.01000	120
16.24	12.58	2.2500	115.581	148.146	0.5500	2.98	51.9	0.00790	120
16.26	12.65	2.4750	114.713	144.648	0.5290	2.95	52.4	0.01700	120
16.28	12.73	2.7000	114.489	145.750	0.5000	2.98	52.0	0.02800	120
16.30	12.79	2.9250	115.295	143.078	0.4790	2.96	52.3	0.01200	120
16.32	12.87	3.1500	117.121	147.693	0.4570	2.94	52.6	0.00045	120
16.34	12.95	3.3750	115.383	142.492	0.4300	2.96	52.3	0.01800	120
16.36	13.02	3.6000	115.714	146.768	0.4110	2.96	52.3	0.02600	120
16.38	13.11	3.8250	115.067	143.877	0.3850	2.97	52.0	0.01700	120
16.40	13.17	4.0500	115.522	145.983	0.3700	2.95	52.5	0.01500	120
16.43	13.29	4.3875	116.021	145.791	0.3400	2.85	54.3	-0.01400	120
16.45	13.36	4.6125	115.724	145.424	0.3220	2.93	52.9	0.00290	120
16.47	13.43	4.8375	115.474	145.591	0.3090	2.94	52.7	-0.01000	120
16.49	13.50	5.0625	115.511	145.857	0.2910	2.90	53.4	-0.01400	120
16.51	13.58	5.2875	115.404	146.035	0.2760	2.92	53.0	0.00400	120
16.53	13.65	5.5125	115.569	144.355	0.2610	3.03	51.1	0.04000	120
16.55	13.72	5.7375	115.548	143.562	0.2490	2.98	52.0	0.02000	120
16.57	13.80	5.9625	115.792	142.496	0.2340	2.97	52.0	0.00830	120
16.59	13.87	6.1875	115.670	142.910	0.2240	2.89	53.3	-0.02100	120
16.61	13.93	6.4125	115.403	144.216	0.2110	2.99	51.8	-0.00045	120
16.63	14.01	6.6375	114.855	142.493	0.1960	2.91	52.2	0.02100	120
16.65	14.08	6.8625	114.614	141.048	0.1890	2.93	52.8	0.03300	120
16.67	14.14	7.0875	114.917	146.214	0.1790	2.84	54.5	0.02400	120
16.69	14.23	7.3125	119.281	138.562	0.1630	2.95	52.5	0.02300	180
16.71	14.30	7.5375	115.330	143.105	0.1560	2.91	53.2	0.00530	180
16.74	14.43	7.8750	114.748	144.387	0.1410	2.96	52.3	-0.00230	180
16.77	14.54	8.2125	115.129	144.895	0.1290	2.93	52.8	-0.04100	180
16.80	14.66	8.5500	115.475	145.015	0.1180	2.86	54.2	-0.03700	240
16.83	14.78	8.8875	115.424	144.625	0.1050	2.91	53.2	-0.01800	240
16.86	14.88	9.2250	115.398	145.536	0.0974	3.02	51.3	-0.02500	300
16.89	14.96	9.5625	115.926	142.215	0.0918	2.87	54.0	-0.06000	300

Exp 94 Flow Cell 0.107 μm PSL V.F. = 0.198% θ = 112 deg

Front Tilt = 18.12 div. Rear Translation = 12.27 div. Flow Rate = 50%

Rear Tilt (div.)	Side Translation (div.)	Tilt Angle (mrad)	Intensity (kHz)		Y-Intercept	Decay Rate (1/ms)	Radius (nm)	Normalized Second Cumulant	Time (sec.)
			Ch 0	Ch 1					
16.04	11.80	0.0000	118.276	146.859	0.9190	3.76	41.1	0.11000	120
16.05	11.85	0.1125	118.372	146.384	0.9140	3.76	41.1	0.10000	120
16.06	11.88	0.2250	118.288	146.323	0.9020	3.74	41.4	0.09800	120
16.08	11.96	0.4500	118.156	146.137	0.8640	3.65	42.4	0.08800	120
16.10	12.03	0.6750	118.231	146.293	0.8220	3.45	44.8	0.06500	120
16.12	12.12	0.9000	118.013	145.154	0.7560	3.34	46.3	0.05800	120
16.14	12.20	1.1250	118.288	144.817	0.7050	3.27	47.3	0.04900	120
16.16	12.27	1.3500	118.531	145.269	0.6670	3.12	49.6	0.02600	120
16.18	12.34	1.5750	118.846	146.896	0.6280	3.10	49.9	0.03200	120
16.20	12.42	1.8000	118.184	147.666	0.5930	3.08	50.2	0.03100	120
16.22	12.49	2.0250	118.282	147.242	0.5660	3.01	51.5	-0.00032	120
16.24	12.56	2.2500	118.108	147.175	0.5380	3.01	51.5	0.01500	120
16.26	12.64	2.4750	117.877	147.271	0.5050	2.99	51.7	0.00500	120
16.28	12.72	2.7000	117.969	146.829	0.4720	2.98	52.0	0.00480	120
16.30	12.80	2.9250	116.584	145.471	0.4400	3.00	51.6	0.00960	120
16.32	12.88	3.1500	117.875	147.171	0.4100	2.97	52.0	-0.00370	120
16.34	12.97	3.3750	122.194	147.622	0.3780	2.91	53.2	-0.03400	120
16.36	13.03	3.6000	111.456	145.233	0.3580	2.92	53.0	-0.01200	120
16.38	13.12	3.8250	118.218	147.386	0.3270	2.98	52.0	0.00210	120
16.40	13.19	4.0500	117.507	148.234	0.3070	2.97	52.1	-0.00270	120
16.42	13.27	4.2750	117.283	145.419	0.2810	2.95	52.5	-0.00340	120
16.44	13.35	4.5000	118.815	144.088	0.2590	3.01	51.4	0.00170	120
16.46	13.40	4.7250	117.515	147.537	0.2470	3.01	51.4	0.01600	120
16.48	13.47	4.9500	117.230	147.173	0.2270	2.91	53.2	-0.01900	120
16.50	13.56	5.1750	117.280	144.919	0.2090	2.03	51.1	0.02200	120
16.52	13.62	5.4000	117.511	145.890	0.1940	2.91	53.1	-0.01700	120
16.54	13.70	5.6250	118.785	138.490	0.1790	2.92	52.9	-0.02700	120
16.56	13.77	5.8500	117.440	145.850	0.1660	2.84	54.4	-0.01000	120
16.58	13.84	6.0750	117.355	145.516	0.1540	2.94	52.6	0.00580	120
16.60	13.90	6.3000	117.386	147.207	0.1440	2.87	53.9	-0.04500	120
16.62	13.98	6.5250	117.397	145.690	0.1310	2.96	52.3	-0.00540	180
16.64	14.06	6.7500	117.347	145.074	0.1170	3.02	51.2	0.04100	180
16.66	14.13	6.9750	117.529	142.435	0.1100	2.96	52.3	0.01800	180
16.70	14.27	7.4250	117.191	146.628	0.0936	2.87	53.9	-0.01800	180

Exp 95	Flow Cell		0.107 μm PSL		V.F. = 0.198%			θ = 112 deg	
	Front Tilt = 18.12 div.		Rear Translation = 12.27 div.					Flow Rate =100%	
Rear Tilt (div.)	Side Translation (div.)	Tilt Angle (mrad)	Intensity (kHz) Ch 0	Intensity (kHz) Ch 1	Y-Intercept	Decay Rate (1/ms)	Radius (nm)	Normalized Second Cumulant	Time (sec.)
16.04	11.80	0.000	117.281	142.977	0.9100	4.52	34.2	0.1900	120
16.06	11.88	0.225	116.510	144.543	0.8980	4.46	34.7	0.1900	120
16.08	11.95	0.450	116.650	143.331	0.8640	4.30	36.0	0.1800	120
16.10	12.03	0.675	116.766	141.372	0.8180	4.04	38.3	0.1600	120
16.12	12.11	0.900	117.078	142.159	0.7630	3.76	41.1	0.1200	120
16.14	12.19	1.125	117.276	139.888	0.7110	3.56	43.4	0.0920	120
16.16	12.26	1.350	117.809	143.627	0.6780	3.41	45.4	0.0710	120
16.18	12.34	1.575	119.677	144.017	0.6440	3.27	47.3	0.0440	120
16.20	12.41	1.800	118.019	141.195	0.6100	3.19	48.5	0.0330	120
16.22	12.48	2.025	118.653	141.415	0.5810	3.11	49.7	0.0200	120
16.24	12.55	2.250	118.481	143.786	0.5560	3.09	50.0	0.0067	120
16.26	12.63	2.475	118.880	142.615	0.5270	3.08	50.3	-0.0048	120
16.28	12.71	2.700	118.937	143.273	0.5010	3.03	51.0	0.0170	120
16.30	12.79	2.925	112.174	143.265	0.4700	3.02	51.2	0.0050	120
16.32	12.87	3.150	112.174	142.709	0.4350	3.02	51.2	0.0190	120
16.34	12.96	3.375	112.683	142.093	0.4070	3.01	51.5	0.0110	120
16.36	13.03	3.600	116.956	141.895	0.3890	3.01	51.4	0.0160	120
16.38	13.10	3.825	119.963.	145.791	0.3680	3.01	51.3	0.0430	120
16.40	13.17	4.050	116.862	143.643	0.3450	2.96	52.3	-0.0017	120
16.42	13.25	4.275	121.701	143.690	0.3190	3.00	51.6	-0.0085	120
16.44	13.33	4.500	116.509	142.787	0.3060	2.96	52.3	0.0180	120
16.46	13.40	4.725	116.272	141.820	0.2860	2.92	53.0	0.0019	120
16.48	13.47	4.950	116.242	141.507	0.2690	2.98	51.9	0.0088	120
16.50	13.54	5.175	116.175	142.155	0.2540	2.92	53.0	-0.0180	120
16.52	13.61	5.400	115.664	142.633	0.2360	2.99	51.7	-0.0048	120
16.54	13.68	5.625	115.568	143.095	0.2240	2.95	52.4	-0.0110	120
16.56	13.76	5.850	114.865	146.472	0.2110	2.86	54.1	-0.0350	120
16.58	13.84	6.075	115.400	141.599	0.1960	2.99	51.7	-0.0200	120
16.60	13.91	6.300	115.190	140.385	0.1830	2.95	52.4	0.0083	120
16.62	13.97	6.525	115.302	142.617	0.1720	2.88	53.7	-0.0700	120
16.64	14.05	6.750	115.138	141.599	0.1600	2.92	53.0	0.0120	120
16.66	14.12	6.975	110.402	142.851	0.1510	2.88	53.8	-0.0290	120
16.70	14.26	7.425	115.026	144.266	0.1330	2.83	54.7	-0.0350	180
16.74	14.42	7.875	114.915	142.421	0.1130	2.97	52.1	0.0400	240
16.78	14.59	8.325	115.453	142.348	0.0944	2.89	53.6	-0.0750	240
16.82	14.74	8.775	114.782	144.606	0.0823	2.83	54.8	0.0440	240

Exp 103 Flow Cell 0.098 μm PSL V.F. = 0.320% θ = 112 deg

Front Tilt = 18.09 div. Rear Translation = 12.29 div. Flow Rate = 0%

Rear Tilt (div.)	Side Translation (div.)	Tilt Angle (mrad)	Intensity (kHz) Ch 0	Intensity (kHz) Ch 1	Y-Intercept	Decay Rate (1/ms)	Radius (nm)	Normalized Second Cumulant	Time (sec.)
16.04	11.77	0.000	118.401	156.753	0.8930	3.64	43.2	0.0680	120
16.06	11.85	0.225	118.383	156.349	0.8510	3.60	43.6	0.0670	120
16.08	11.92	0.450	117.927	155.190	0.7990	3.51	44.7	0.0470	120
16.10	12.00	0.675	118.071	153.624	0.7460	3.45	45.6	0.0500	120
16.12	12.07	0.900	118.435	156.151	0.6960	3.38	46.5	0.0340	120
16.14	12.14	1.125	118.627	155.112	0.6490	3.36	46.8	0.0460	120
16.16	12.23	1.350	118.097	157.115	0.5990	3.31	47.5	0.0120	120
16.18	12.31	1.575	117.946	153.308	0.5560	3.28	47.9	0.0170	120
16.20	12.38	1.800	117.923	155.572	0.5240	3.26	48.1	0.0200	120
16.22	12.46	2.025	117.740	156.777	0.4890	3.21	49.0	0.0140	120
16.24	12.53	2.250	116.983	155.247	0.4600	3.22	48.7	0.0170	120
16.27	12.65	2.588	116.824	151.083	0.4070	3.20	49.2	-0.0016	120
16.30	12.76	2.925	116.781	153.858	0.3650	3.20	49.0	0.0260	120
16.33	12.89	3.263	116.949	156.675	0.3210	3.17	49.5	0.0230	120
16.36	12.99	3.600	118.126	156.177	0.2840	3.23	48.6	0.0420	120
16.39	13.10	3.938	117.121	158.184	0.2480	3.20	49.1	0.0270	180
16.42	13.22	4.275	116.644	152.989	0.2130	3.23	48.6	0.0320	240
16.45	13.32	4.613	116.662	153.841	0.1860	3.14	50.1	0.0110	240
16.48	13.41	4.950	117.515	154.081	0.1660	3.11	50.5	0.0220	240
16.51	13.52	5.288	118.482	152.235	0.1440	3.20	49.5	-0.0017	240
16.54	13.61	5.625	117.994	150.291	0.1280	3.21	48.9	0.0083	240
16.57	13.72	5.963	117.688	152.806	0.1120	3.16	49.8	0.0540	240
16.60	13.83	6.300	116.946	151.540	0.0961	3.20	49.1	0.0001	300
16.64	14.00	6.750	116.537	149.403	0.0762	3.16	49.7	0.0460	300
16.68	14.16	7.200	118.634	149.587	0.0616	3.22	48.8	0.0150	420
16.72	14.32	7.650	118.826	149.439	0.0509	3.34	47.1	0.0310	420

Exp 104 | Flow Cell | 0.098 μm PSL | V.F. = 0.320% | θ = 112 deg

Front Tilt = 18.09 div. | Rear Translation = 12.29 div. | Flow Rate = 100%

Rear Tilt (div.)	Side Translation (div.)	Tilt Angle (mrad)	Intensity (kHz) Ch 0	Intensity (kHz) Ch 1	Y-Intercept	Decay Rate (1/ms)	Radius (nm)	Normalized Second Cumulant	Time (sec.)
16.04	11.77	0.000	119.364	158.848	0.8980	4.72	33.3	0.1700	120
16.06	11.85	0.225	119.345	158.146	0.8610	4.49	35.0	0.1600	120
16.08	11.92	0.450	119.414	158.276	0.8080	4.27	36.8	0.1500	120
16.10	12.01	0.675	119.036	156.152	0.7330	4.03	39.0	0.1200	120
16.12	12.09	0.900	118.922	157.472	0.6780	3.77	41.7	0.0820	120
16.14	12.16	1.125	118.785	159.031	0.6290	3.62	43.4	0.0700	120
16.16	12.24	1.350	118.099	159.778	0.5820	3.43	45.7	0.0400	120
16.18	12.32	1.575	119.146	158.552	0.5460	3.37	46.6	0.0340	120
16.20	12.39	1.800	119.216	158.321	0.5070	3.35	46.9	0.0170	120
16.22	12.46	2.025	119.070	157.154	0.4750	3.32	47.3	0.0210	120
16.24	12.53	2.250	119.295	158.094	0.4450	3.27	48.0	0.0210	120
16.27	12.65	2.588	119.630	157.957	0.3950	3.22	48.8	0.0380	120
16.30	12.77	2.925	119.302	157.063	0.3400	3.21	49.0	0.0120	120
16.33	12.90	3.263	119.450	157.597	0.2930	3.22	48.8	0.0130	120
16.36	13.02	3.600	119.664	159.625	0.2560	3.26	48.2	0.0270	180
16.42	13.25	4.275	125.478	158.664	0.2120	3.11	50.6	0.0530	240
16.48	13.47	4.950	125.405	157.113	0.1530	3.02	52.0	0.0300	300
16.50	13.54	5.175	126.026	154.316	0.1400	3.14	50.1	0.0200	300
16.54	13.62	5.625	122.759	156.508	0.1240	3.16	49.7	0.0270	300
16.58	13.80	6.075	124.684	159.036	0.0983	3.14	50.0	0.0019	420

Exp 105	Flow Cell		0.098 μm PSL		V.F. = 0.860%			θ = 112 deg	
	Front Tilt = 18.09 div.		Rear Translation = 12.29 div.					Flow Rate = 0%	
Rear Tilt (div.)	Side Translation (div.)	Tilt Angle (mrad)	Intensity (kHz)		Y-Intercept	Decay Rate (1/ms)	Radius (nm)	Normalized Second Cumulant	Time (sec.)
			Ch 0	Ch 1					
16.04	11.77	0.000	139.072	184.903	0.8900	4.00	39.3	0.0950	120
16.06	11.84	0.225	139.630	185.198	0.8480	3.92	40.0	0.0960	120
16.08	11.92	0.450	141.678	182.834	0.7770	3.83	41.0	0.0810	120
16.10	12.00	0.675	139.999	184.336	0.7080	3.69	42.5	0.0620	120
16.12	12.08	0.900	140.559	185.916	0.6400	3.63	43.3	0.0740	120
16.14	12.17	1.125	140.595	185.113	0.5670	3.53	44.5	0.0660	120
16.16	12.24	1.350	140.492	184.097	0.5180	3.47	45.2	0.0560	120
16.18	12.32	1.575	141.202	185.131	0.4760	3.39	46.3	0.0370	120
16.20	12.40	1.800	141.167	184.500	0.4340	3.33	47.1	0.0170	120
16.22	12.47	2.025	141.377	184.714	0.4000	3.40	46.2	0.0330	120
16.24	12.54	2.250	141.730	186.144	0.3740	3.37	46.6	0.0390	120
16.26	12.62	2.475	142.055	182.742	0.3380	3.38	46.5	0.0480	120
16.28	12.69	2.700	142.279	186.109	0.3130	3.34	47.1	0.0380	180
16.30	12.78	2.925	143.151	184.721	0.2820	3.32	47.3	0.0190	180
16.33	12.89	3.262	142.853	185.888	0.2450	3.37	46.6	0.0380	180
16.36	13.01	3.600	143.350	185.861	0.2130	3.26	48.2	0.0067	240
16.39	13.13	3.938	143.212	184.384	0.1810	3.31	47.4	0.0130	240
16.42	13.24	4.275	143.471	184.890	0.1580	3.32	47.4	0.0110	240
16.45	13.34	4.613	143.698	184.999	0.1360	3.25	48.3	-0.0190	240
16.48	13.46	4.950	143.880	183.444	0.1150	3.33	47.2	0.0340	240
16.51	13.56	5.288	144.194	183.940	0.1020	3.28	47.9	0.0180	240
16.54	13.67	5.625	144.687	185.494	0.0872	3.12	49.4	-0.0290	240
16.57	13.78	5.963	145.198	185.027	0.0757	3.22	48.8	0.0250	300
16.60	13.89	6.300	144.593	185.923	0.0638	3.34	47.1	0.0380	300
16.64	14.04	6.750	144.644	182.030	0.0524	3.28	48.0	0.0170	300

<u>Exp 106</u>	Flow Cell		0.098 μm PSL		V.F. = 0.860%			θ = 112 deg	
	Front Tilt = 18.09 div.		Rear Translation = 12.29 div.					Flow Rate = 100%	
Rear Tilt (div.)	Side Translation (div.)	Tilt Angle (mrad)	Intensity (kHz)		Y-Intercept	Decay Rate (1/ms)	Radius (nm)	Normalized Second Cumulant	Time (sec.)
			Ch 0	Ch 1					
16.04	11.77	0.000	144.089	187.425	0.8990	5.01	31.4	0.1600	120
16.06	11.84	0.225	144.054	188.714	0.8540	4.76	33.0	0.1500	120
16.08	11.92	0.450	144.911	188.127	0.7790	4.49	35.0	0.1300	120
16.10	12.00	0.675	143.095	186.813	0.7030	4.25	37.0	0.1100	120
16.12	12.09	0.900	144.634	190.635	0.6280	4.01	39.2	0.0940	120
16.14	12.18	1.125	148.697	195.057	0.5630	3.74	42.0	0.0570	120
16.16	12.24	1.350	142.419	189.699	0.5190	3.68	42.7	0.0500	120
16.18	12.32	1.575	142.037	189.171	0.4680	3.55	44.3	0.0460	120
16.20	12.40	1.800	142.565	182.164	0.4310	3.49	45.1	0.0420	120
16.22	12.51	2.025	141.959	186.951	0.3770	3.45	45.6	0.0300	120
16.24	12.58	2.250	145.271	193.799	0.3500	3.32	47.3	0.0170	120
16.26	12.65	2.475	142.937	193.405	0.3140	3.37	46.7	0.0190	120
16.28	12.68	2.700	142.535	186.617	0.3020	3.35	46.9	0.0270	120
16.30	12.77	2.925	141.983	187.093	0.2710	3.30	47.5	0.0230	120
16.33	12.90	3.262	142.598	184.138	0.2330	3.31	47.4	0.0260	120
16.36	13.02	3.600	142.318	186.151	0.2000	3.17	49.5	-0.0095	120
16.39	13.13	3.938	142.205	186.407	0.1690	3.25	48.4	0.0140	120
16.42	13.25	4.275	144.341	178.609	0.1430	3.20	49.1	-0.0086	180
16.45	13.36	4.613	142.165	185.701	0.1230	3.24	48.5	0.0390	180
16.48	13.45	4.950	142.244	188.625	0.1070	3.25	48.3	0.0087	240
16.51	13.56	5.288	142.177	186.865	0.0916	3.19	49.3	-0.0430	240
16.54	13.67	5.625	142.667	184.853	0.0771	3.24	48.5	0.0300	300
16.57	13.77	5.963	142.577	185.137	0.0658	3.14	50.1	-0.0380	300
16.60	13.88	6.300	142.615	185.132	0.0579	3.10	50.6	0.0430	300
16.64	14.00	6.750	142.905	185.970	0.0495	3.30	47.7	0.0710	300

Exp 111	Flow Cell		0.203 μm PSL		V.F. = 0.20%			θ = 112 deg	
	Front Tilt = 18.10 div.		Rear Translation = 12.31 div.					Flow Rate = 0%	
Rear Tilt (div.)	Side Translation (div.)	Tilt Angle (mrad)	Intensity (kHz) Ch 0	Intensity (kHz) Ch 1	Y-Intercept	Decay Rate (1/ms)	Radius (nm)	Normalized Second Cumulant	Time (sec.)
16.03	11.71	0.000	99.520	150.610	0.8990	1.68	93.8	0.0720	120
16.05	11.78	0.225	99.450	151.261	0.8600	1.67	93.9	0.0610	120
16.07	11.86	0.450	99.765	150.594	0.8020	1.63	96.6	0.0590	120
16.09	11.93	0.675	94.898	148.120	0.7350	1.61	97.7	0.0490	120
16.11	12.00	0.900	99.518	150.435	0.6490	1.58	99.7	0.0450	120
16.13	12.09	1.125	99.545	152.204	0.5870	1.56	101	0.0380	120
16.15	12.18	1.350	100.047	149.361	0.5230	1.56	101	0.0400	120
16.17	12.25	1.575	99.651	150.768	0.4880	1.52	103	0.0470	120
16.19	12.32	1.800	99.400	150.485	0.4450	1.52	104	0.0360	120
16.21	12.40	2.025	99.636	150.346	0.3980	1.52	103	0.0260	180
16.23	12.47	2.250	100.341	150.654	0.3670	1.52	104	0.0480	180
16.25	12.55	2.475	96.922	149.996	0.3300	1.52	103	0.0550	180
16.27	12.63	2.700	101.073	151.431	0.3010	1.48	106	0.0110	240
16.29	12.71	2.925	99.788	152.083	0.2680	1.51	104	0.0270	240
16.31	12.80	3.150	90.568	153.792	0.2370	1.51	104	-0.0170	120
16.33	12.89	3.375	99.076	141.698	0.2140	1.51	104	0.0320	120
16.35	12.96	3.600	98.911	148.326	0.1960	1.52	103	0.0360	240
16.37	13.02	3.825	99.285	150.411	0.1800	1.55	101	0.0740	120
16.39	13.11	4.050	98.588	148.786	0.1580	1.56	101	0.0190	240
16.41	13.19	4.275	98.953	149.803	0.1420	1.53	102	0.0520	120
16.43	13.26	4.500	99.229	148.234	0.1320	1.47	107	0.0520	240
16.45	13.32	4.725	98.608	148.459	0.1160	1.59	98.6	0.0820	180
16.47	13.39	4.950	98.446	147.094	0.1020	1.51	104	0.0400	300
16.49	13.46	5.175	98.500	148.067	0.0933	1.45	108	-0.0270	300

Exp 112 Flow Cell 0.203 μm PSL V.F. = 0.20% θ = 112 deg

Front Tilt = 18.10 div. Rear Translation = 12.31 div. Flow Rate = 100%

Rear Tilt (div.)	Side Translation (div.)	Tilt Angle (mrad)	Intensity (kHz) Ch 0	Intensity (kHz) Ch 1	Y-Intercept	Decay Rate (1/ms)	Radius (nm)	Normalized Second Cumulant	Time (sec.)
16.03	11.72	0.000	96.776	146.167	0.8830	2.34	67.0	0.2000	120
16.05	11.81	0.225	98.672	144.693	0.8320	2.26	69.6	0.1900	120
16.07	11.89	0.450	99.143	146.527	0.7620	2.08	75.6	0.1600	120
16.09	11.97	0.675	98.867	147.319	0.6900	1.95	80.8	0.1400	120
16.11	12.05	0.900	98.522	145.951	0.6130	1.80	87.2	0.0890	120
16.13	12.13	1.125	98.351	146.407	0.5500	1.71	92.1	0.0650	120
16.15	12.20	1.350	101.118	147.986	0.4960	1.62	96.7	0.0330	120
16.17	12.28	1.575	98.508	145.524	0.4520	1.58	99.6	0.0380	120
16.19	12.35	1.800	93.937	142.503	0.4200	1.54	102	0.0140	120
16.21	12.42	2.025	98.620	148.365	0.3860	1.53	103	0.0015	120
16.23	12.49	2.250	98.761	147.941	0.3530	1.51	104	-0.0052	120
16.25	12.58	2.475	98.954	146.634	0.3160	1.49	105	0.0270	180
16.27	12.67	2.700	98.551	145.583	0.2790	1.47	107	-0.0150	120
16.29	12.74	2.925	98.332	146.225	0.2540	1.48	106	-0.0012	240
16.31	12.81	3.150	98.014	148.159	0.2300	1.50	105	0.0099	240
16.33	12.87	3.375	95.551	154.264	0.2120	1.52	103	0.0480	120
16.35	12.96	3.600	98.223	149.720	0.1920	1.50	104	0.0230	240
16.37	13.04	3.825	98.316	149.800	0.1710	1.47	107	0.0180	240
16.39	13.11	4.050	98.002	147.499	0.1590	1.48	106	0.0400	120
16.41	13.20	4.275	98.118	147.093	0.1380	1.47	107	-0.0051	240
16.44	13.32	4.613	97.756	144.985	0.1170	1.55	102	-0.0035	180
16.48	13.44	5.062	97.910	148.611	0.0982	1.49	105	0.0085	180

Appendix IV

Flow Profile Discussion

The purpose of a dynamic light scattering experiment is to determine the diffusion constant associated with the Brownian motion of the particles within a test sample. Section 3.3 showed how the diffusion constant was then used to calculate particle size. When conducting experiments in a flowing fluid, factors other than Brownian motion can influence the motion of the particles, and therefore influence the data used to determine particle size. These factors are a product of the flow profile as it passes through the detection area. As mentioned in Section 5.2, fully developed laminar flow is necessary to conduct dynamic light scattering experiments in flowing samples. The calculations given in Section 5.2 prove that the flow associated with the experiments described in this thesis was laminar. Those calculations also prove that the possibility of entrance effects influencing the flow in the detection area was minimal due to the length of the test cell. Although the flow used in the experiments covered by this thesis were laminar, several questions remained about the flow profile. Therefore, this appendix will concentrate on the fully developed flow profile found in the detection area. The following equations were used to determine the flow profile [White (1991)]:

$$v_x(y,z) = \left(\frac{16c^2}{\mu\pi^3}\right)\left(\frac{-d\hat{p}}{dx}\right)\sum_{j=1,3,5,\ldots}^{\infty}(-1)^{\frac{(j-1)}{2}}\left[1-\frac{\cosh\left[j\pi\, z/(2c)\right]}{\cosh\left[j\pi\, b/(2c)\right]}\right]\left[\frac{\cos\left[i\pi\, y/(2c)\right]}{j^3}\right] \quad \text{(A-IV-1)}$$

where $v_x(y,z)$ is the x-direction velocity as a function of position in the y-z plane, 2c is the width of the test cell, 2b is the height of the test cell, μ is the viscosity of the sample, and $\frac{-d\hat{p}}{dx}$ is the pressure gradient of the system. For the flow system associated with this thesis, the only unknown of Eq. (A-IV-1) is the pressure gradient, and it was solved for with the following equation [White (1991)]:

$$\frac{-d\hat{p}}{dx} = \frac{Q}{\left(\frac{4bc^3}{3\mu}\right)\left[1 - \frac{192c}{b\pi^5}\sum_{j=1,3,5,\ldots}^{\infty}\frac{\tanh\left[\frac{j\pi c}{(2a)}\right]}{j^5}\right]} \qquad \text{(A-IV-2)}$$

where Q is the overall flow rate (see Table 2 in Section 5.2). These equations were used to determine the flow profile of the system. Mathcad 7.0, a commercial mathematical software package, was used to plot the profile as follows.

Once the flow profile is determined, the next step was to use the information from the time constants associated with the flow system. The first time constant calculated was the diffusion time constant. This time constant relates the time it takes a particle to move under Brownian motion through a unit length scale determined by the scattered wave vector. The single scattering time constant is defined by [Nobbmann (1997)]

$$\tau_{\text{diffusion}} = \frac{1}{D_o k^2} \qquad \text{(A-IV-3)}$$

where D_o is the diffusion constant, and k is the scattering wave vector. The second time constant to be calculated was the transit time constant. This time constant relates the time it takes a particle to travel through the focused incident laser beam and is defined by

$$\tau_{transit} = \frac{L}{v} \qquad \text{(A-IV-4)}$$

where $L = \frac{b}{\cos(\alpha_L)}$ and is the length the particle travels through the focused laser beam, and v is the centerline velocity of the flow. The centerline velocity was calculated using Eq. (A-IV-1). The final time constant calculated was the Doppler time constant. The Doppler time constant measured how misalignments affected the calculation of particle diameter. The Doppler time constant was defined by

$$\tau_{Doppler} = \frac{1}{k\cos(90-\delta)v} \qquad \text{(A-IV-5)}$$

where $\delta = 5°$ and is the cell rotation angle (see Fig. 13 in Section 5.2).

Knowledge about these three time constants are valuable in determining the likelihood of success in collecting data using DLS techniques. To make DLS measurements, a particle must diffuse while in the detection area. If the time it takes a particle to diffuse (i.e., the diffusion time constant) is larger than the transit time constant; no usable data will be collected.

The following pages contain the calculation of the flow profile and the time constants describe above. The first two pages of calculations describe the flow profile determined by the conditions associated with the flow setup used in this research. From the profile, it can be seen that the flow is fully developed and the maximum velocity associated with the setup is 0.0162 m/sec at the centerline. The collection of data was conducted at an estimated depth of 1 mm and the velocity calculated there was found to be 0.00926 m/sec.

The second set of calculations presented is for the three time constants. The diffusion time constant was calculated for 0.107 μm PSL particles and was found to be 0.0019 seconds. The transit time constant associated with a centerline velocity was found to be 0.0022 seconds. From these calculations $\tau_{diffusion} < \tau_{transit}$; and therefore Brownian motion diffusion occurs in the detection area. The Doppler time constant for a misalignment of $\delta = 5°$ was calculated to be 0.045 msec. The effects of this misalignment were discussed in Section 6.5.1.

The same calculations were performed using the velocity at 1 mm from the wall and similar results were found. The difference between the diffusion time constant ($\tau_{diffusion} = 0.0019$ sec) and the transit time constant ($\tau_{transit} = 0.0038$ sec) increased by a factor of two. This was due to the lower velocities seen near the wall.

Time constants were then calculated for 0.204 μm PSL particles at a distance of 1 mm from the wall. For the 0.204 μm particles, the diffusion time constant ($\tau_{diffusion} = 0.0036$ sec) was found to be nearly twice that for 0.107 μm particles. However, the diffusion time constant was still less than the transit time constant ($\tau_{transit} = 0.0038$ sec) seen at 1 mm from the wall.

A final set of calculations was performed using a flow rate that was 10 times the value seen in the actual experiments. The flow profile was calculated first. From this calculation, it was determined that the velocity was proportional to the flow rate and therefore, increased as well by a factor of 10. From the time constants associated with this higher flow rate, it was determined that $\tau_{diffusion}$ (0.0019 sec)> $\tau_{transit}$ (0.00038 sec); and therefore no usable data could be collected. The calculations were performed using the velocity 1 mm from the wall. Table 8 gives a summary of all of the calculations performed on the flow profile and time constants.

Table 8: Summary of results from flow profile and time constant calculations

Flow Rate Q (ml/min)	Measurement Location (mm)	Particle Diameter (nm)	Velocity (mm/sec)	$\tau_{Diffusion}$ (sec)	$\tau_{Transit}$ (sec)	$\tau_{Doppler}$ (sec)
22.40	3	0.107	16.2	0.0019	0.0022	0.000045
22.40	1	0.107	9.26	0.0019	0.0038	0.000079
22.40	1	0.204	9.26	0.0036	0.0038	0.000079
224.03	1	0.107	92.6	0.0019	0.00038	0.000008

Flow profile calculations for the conditions and test cell used during experiments.

$c := 0.003\ \text{m}$ $\quad b := 0.004\ \text{m}$ $\quad Q1 := 22.4025\ \frac{\text{mL}}{\text{min}}$ $\quad \mu := 947.95 \cdot 10^{-6}\ \text{Pa} \cdot \text{sec}$

$\text{convertq} := \frac{0.000001}{60}$ $\quad Q := Q1 \cdot \text{convertq}$ $\quad Q = 3.734 \cdot 10^{-7}\ \frac{\text{m}^3}{\text{sec}}$

$j := 1, 3 .. 11$

$$\text{dpdx} := \frac{-Q}{\frac{4 \cdot b \cdot c^3}{3 \cdot \mu} \cdot \left[1 - \frac{192 \cdot c}{\pi^5 \cdot b} \sum_j \frac{\tanh\left(\frac{j \cdot \pi \cdot b}{2 \cdot c}\right)}{j^5}\right]}$$

$\text{dpdx} = -4.5402\ \frac{\text{Pa}}{\text{m}}$

$$v(y, z) := \left(\frac{16 \cdot c^2}{\mu \cdot \pi^3}\right) \cdot (-\text{dpdx}) \cdot \left[\sum_j (-1)^{\frac{j-1}{2}} \cdot \left[1 - \frac{\cosh\left(\frac{j \cdot \pi \cdot z}{2 \cdot c}\right)}{\cosh\left(\frac{j \cdot \pi \cdot b}{2 \cdot c}\right)}\right] \cdot \left(\frac{\cos\left(\frac{j \cdot \pi \cdot y}{2 \cdot c}\right)}{j^3}\right)\right]$$

$ny := 10$ $\quad j := 0 .. ny$ $\quad nz := 10$ $\quad k := 0 .. nz$

$y_j := -c + 2 \cdot c \cdot \frac{j}{ny}$ $\quad z_k := -b + 2 \cdot b \cdot \frac{k}{nz}$ $\quad V_{j,k} := v(y_j, z_k)$

Velocity at wall

$v(0.003, 0) = 0\ \frac{\text{m}}{\text{sec}}$

Velocity at 1 mm from wall

$v(0.002, 0) = 9.2618 \cdot 10^{-3}\ \frac{\text{m}}{\text{sec}}$

Centerline velocity

$v(0, 0) = 0.0162\ \frac{\text{m}}{\text{sec}}$

The values given below depict the position in the y- and z-directions at which the velocity calculations were performed to create the following velocity table and flow profile graph. Integer designation was used on the graph, rather than the actual locations in meters.

$y^T =$

-0.003	-0.002	-0.002	-0.001	-0.001	0	0.001	0.001	0.002	0.002	0.003

m

$z^T =$

-0.004	-0.003	-0.002	-0.002	-0.001	0	0.001	0.002	0.002	0.003	0.004

m

Velocities (m/sec) associated with the positions given by y and z

$V^T =$

0	0	0	0	0	0	0	0	0	0	0
0	0.003	0.0048	0.006	0.0066	0.0068	0.0066	0.006	0.0048	0.003	0
0	0.0046	0.0077	0.0098	0.011	0.0114	0.011	0.0098	0.0077	0.0046	0
0	0.0055	0.0094	0.0121	0.0137	0.0142	0.0137	0.0121	0.0094	0.0055	0
0	0.006	0.0103	0.0133	0.0151	0.0157	0.0151	0.0133	0.0103	0.006	0
0	0.0061	0.0106	0.0137	0.0156	0.0162	0.0156	0.0137	0.0106	0.0061	0
0	0.006	0.0103	0.0133	0.0151	0.0157	0.0151	0.0133	0.0103	0.006	0
0	0.0055	0.0094	0.0121	0.0137	0.0142	0.0137	0.0121	0.0094	0.0055	0
0	0.0046	0.0077	0.0098	0.011	0.0114	0.011	0.0098	0.0077	0.0046	0
0	0.003	0.0048	0.006	0.0066	0.0068	0.0066	0.006	0.0048	0.003	0
0	0	0	0	0	0	0	0	0	0	0

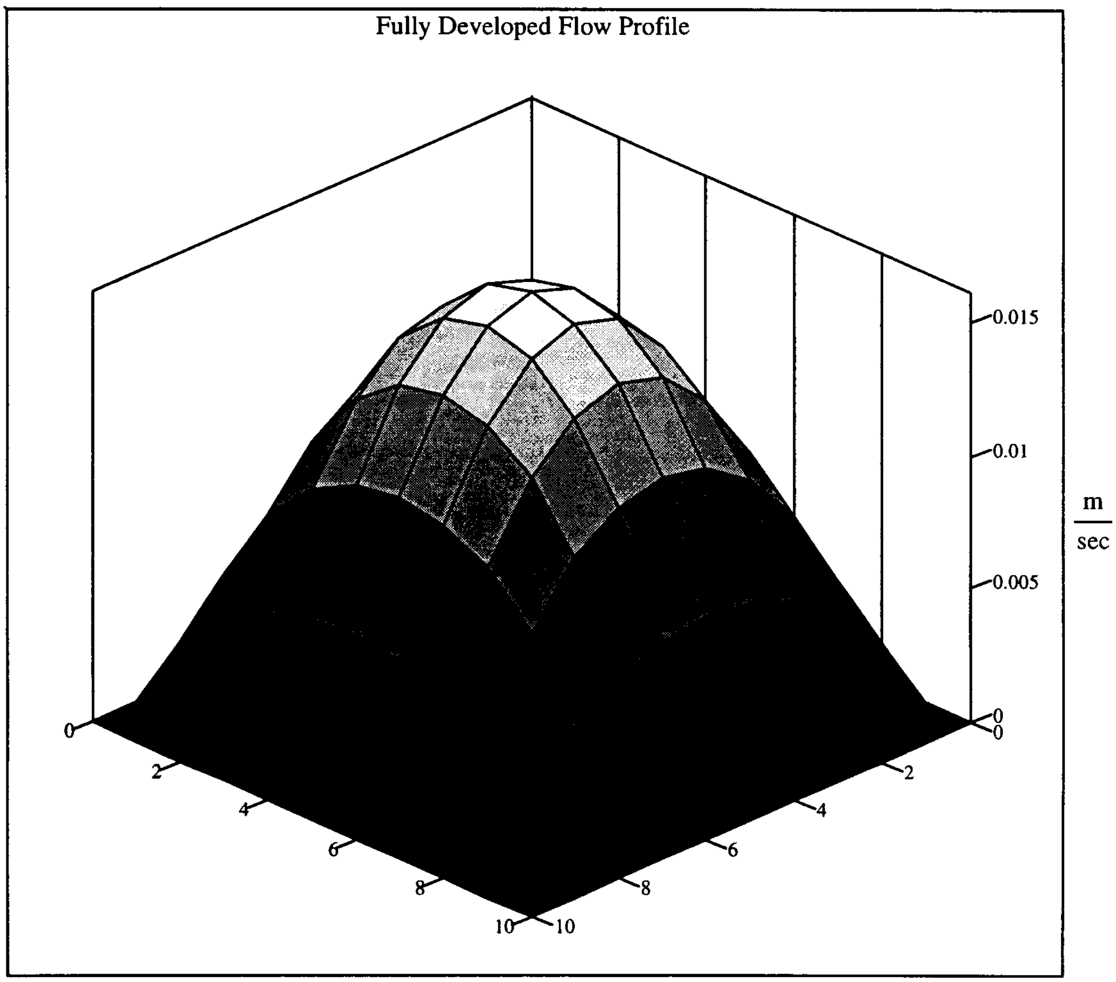

V

Time constants of 0.107 μm PSL particles

Time constants associated with the Brownian motion of 0.107 μm particles

$a := 0.107 \cdot 10^{-6}\,m$ $\quad Kb := 1.380658 \cdot 10^{-23}\,\frac{J}{K}$ $\quad \eta := 947.95 \cdot 10^{-6}\,Pa \cdot sec$

$T := 296\,K$ $\quad n := 1.33$ $\quad \lambda := 532.5 \cdot 10^{-9}\,m$

$$Do := \frac{Kb \cdot T}{6 \cdot \pi \cdot \eta \cdot a} \qquad Do = 2.138 \cdot 10^{-12}\ \frac{m^2}{s} \qquad k := \frac{2 \cdot \pi \cdot n}{\lambda} \qquad k = 1.569 \cdot 10^{7}\ m^{-1}$$

$$\tau diffusion := \frac{1}{Do \cdot k^2} \qquad \tau diffusion = 0.0019\ sec$$

Time constant associated with the travel of the particle through the focused laser beam.

Focused beam diameter in sample = b and is defined in Sundaresan (1999). The velocity used is the center line velocity found by the profile Eqs. (A-IV-1) and (A-IV-2).

$$b := \frac{1}{\sqrt{18 \cdot 10^8}} \qquad b = 2.357 \cdot 10^{-5}\ m \qquad \alpha L := .837758040957\,rad \qquad v := .0162\ \frac{m}{s}$$

Length traveled in the laser beam by particle = L

$$L := \frac{b}{\cos(\alpha L)} \qquad L = 3.523 \cdot 10^{-5}\ m$$

$$\tau transit := \frac{L}{v} \qquad \tau transit = 0.002174\ sec$$

Time constant associated with Doppler beating if the bisector between the angles created by the laser arm and the detector arm is not perpendicular to the flow vector. For this calculation, it is assumed that the cell rotation is 5 degrees from perpendicular (85 degrees).

$$\tau doppler := \frac{1}{k \cdot \cos(1.4835298642) \cdot v} \qquad \tau doppler = 0.000045\ sec$$

Time constants of 0.107 μm PSL particles

Time constant associated with Brownian motion of the particles

$a := 0.107 \cdot 10^{-6}\, m$ $\quad Kb := 1.380658 \cdot 10^{-23}\, \frac{J}{K}$ $\quad \eta := 947.95 \cdot 10^{-6}\, Pa \cdot sec$

$T := 296\, K$ $\quad n := 1.33$ $\quad \lambda := 532.5 \cdot 10^{-9}\, m$

$$Do := \frac{Kb \cdot T}{6 \cdot \pi \cdot \eta \cdot a} \qquad Do = 2.138 \cdot 10^{-12}\ \frac{m^2}{s} \qquad k := \frac{2 \cdot \pi \cdot n}{\lambda} \qquad k = 1.569 \cdot 10^{7}\ m^{-1}$$

$$\tau diffusion := \frac{1}{Do \cdot k^2} \qquad \tau diffusion = 0.0019\ sec$$

Time constant associated with the travel of the particle through the focused laser beam.

Focused beam diameter in sample = b and is defined in Sundaresan (1999). The velocity used is the value found by the flow profile Eqs. (A-IV-1) and (A-IV-2) at 1 mm from the wall.

$$b := \frac{1}{\sqrt{18 \cdot 10^8}} \qquad b = 2.357 \cdot 10^{-5}\ m \qquad \alpha L := .837758040957 rad \qquad v := 9.2618 \cdot 10^{-3}\, \frac{m}{s}$$

Length traveled in the laser beam by particle = L

$$L := \frac{b}{\cos(\alpha L)} \qquad L = 3.523 \cdot 10^{-5}\ m$$

$$\tau transit := \frac{L}{v} \qquad \tau transit = 0.003803\ sec$$

Time constant associated with Doppler beating if the bisector between the angles created by the laser arm and the detector arm is not perpendicular to the flow vector. For this calculation, it is assumed that the cell rotation is 5 degrees from perpendicular (85 degrees).

$$\tau doppler := \frac{1}{k \cdot \cos(1.4835298642) \cdot v} \qquad \tau doppler = 0.000079\ sec$$

Time constants associated 0.204 μm PSL particles

Time constant for Brownian motion

$a := 0.204 \cdot 10^{-6}\,\text{m}$ $\quad Kb := 1.380658 \cdot 10^{-23}\,\frac{J}{K}$ $\quad \eta := 947.95 \cdot 10^{-6}\,\text{Pa} \cdot \text{sec}$

$T := 296\,K$ $\quad n := 1.33$ $\quad \lambda := 532.5 \cdot 10^{-9}\,\text{m}$

$$Do := \frac{Kb \cdot T}{6 \cdot \pi \cdot \eta \cdot a} \qquad Do = 1.121 \cdot 10^{-12}\,\frac{m^2}{s} \qquad k := \frac{2 \cdot \pi \cdot n}{\lambda} \qquad k = 1.569 \cdot 10^{7}\,m^{-1}$$

$$\tau diffusion := \frac{1}{Do \cdot k^2} \qquad \tau diffusion = 0.003622\ \text{sec}$$

Time constant associated with the travel of the particle through the focused laser beam.

Focused beam diameter in sample = b and is defined in Sundaresan (1999). The velocity used is the value found by the flow profile Eqs. (A-IV-1) and (A-IV-2) at 1 mm from the wall.

$$b := \frac{1}{\sqrt{18 \cdot 10^{8}}} \qquad b = 2.357 \cdot 10^{-5}\,\text{m} \qquad \alpha L := .837758040957\,\text{rad} \qquad v := 9.2618 \cdot 10^{-3}\,\frac{m}{s}$$

Length traveled in the laser beam by particle = L

$$L := \frac{b}{\cos(\alpha L)} \qquad L = 3.523 \cdot 10^{-5}\,\text{m}$$

$$\tau transit := \frac{L}{v} \qquad \tau transit = 0.003803\ \text{sec}$$

Time constant associated with Doppler beating if the bisector between the angles created by the laser arm and the detector arm is not perpendicular to the flow vector. For this calculation, it is assumed that the cell rotation is 5 degrees from perpendicular (85 degrees).

$$\tau doppler := \frac{1}{k \cdot \cos(1.4835298642) \cdot v} \qquad \tau doppler = 0.000079\ \text{sec}$$

Flow profile calculations for flow 10 times the value found in the actual test cell during experiments.

$c := 0.003 \text{ m}$ $\quad b := 0.004 \text{ m}$ $\quad Q1 := 224.025 \dfrac{\text{mL}}{\text{min}}$ $\quad \mu := 947.95 \cdot 10^{-6} \text{ Pa}\cdot\text{sec}$

$\text{convertq} := \dfrac{0.000001}{60}$ $\quad Q := Q1 \cdot \text{convertq}$ $\quad Q = 3.734 \cdot 10^{-6} \dfrac{\text{m}^3}{\text{sec}}$

$j := 1, 3 .. 11$

$$\text{dpdx} := \frac{-Q}{\dfrac{4 \cdot b \cdot c^3}{3 \cdot \mu} \cdot \left[1 - \dfrac{192 \cdot c}{\pi^5 \cdot b} \displaystyle\sum_j \frac{\tanh\left(\dfrac{j \cdot \pi \cdot b}{2 \cdot c}\right)}{j^5} \right]} \qquad \text{dpdx} = -45.4015 \frac{\text{Pa}}{\text{m}}$$

$$v(y, z) := \left(\frac{16 \cdot c^2}{\mu \cdot \pi^3}\right) \cdot (-\text{dpdx}) \cdot \left[\sum_j (-1)^{\frac{j-1}{2}} \cdot \left[1 - \frac{\cosh\left(\dfrac{j \cdot \pi \cdot z}{2 \cdot c}\right)}{\cosh\left(\dfrac{j \cdot \pi \cdot b}{2 \cdot c}\right)} \right] \cdot \left(\frac{\cos\left(\dfrac{j \cdot \pi \cdot y}{2 \cdot c}\right)}{j^3} \right) \right]$$

$ny := 10$ $\quad j := 0 .. ny$ $\quad nz := 10$ $\quad k := 0 .. nz$

$y_j := -c + 2 \cdot c \cdot \dfrac{j}{ny}$ $\quad z_k := -b + 2 \cdot b \cdot \dfrac{k}{nz}$ $\quad V_{j,k} := v(y_j, z_k)$

Velocity at wall	Velocity at 1 mm from wall	Centerline velocity
$v(0.003, 0) = 0 \dfrac{\text{m}}{\text{sec}}$	$v(0.002, 0) = 0.0926 \dfrac{\text{m}}{\text{sec}}$	$v(0, 0) = 0.1615 \dfrac{\text{m}}{\text{sec}}$

The values given below depict the position in the y- and z-directions at which the velocity calculations were performed to create the following velocity table and flow profile graph. Integer designation was used on the graph, rather than actual locations in meters.

$y^T =$

-0.003	-0.002	-0.002	-0.001	-0.001	0	0.001	0.001	0.002	0.002	0.003

m

$z^T =$

-0.004	-0.003	-0.002	-0.002	-0.001	0	0.001	0.002	0.002	0.003	0.004

m

Velocities (m/sec) associated with the positions given by y and z

$V^T =$

0	0	0	0	0	0	0	0	0	0	0
0	0.0295	0.048	0.0598	0.0664	0.0684	0.0664	0.0598	0.048	0.0295	0
0	0.0455	0.077	0.0979	0.1099	0.1136	0.1099	0.0979	0.077	0.0455	0
0	0.0547	0.0942	0.1211	0.1367	0.1416	0.1367	0.1211	0.0942	0.0547	0
0	0.0595	0.1033	0.1335	0.1511	0.1568	0.1511	0.1335	0.1033	0.0595	0
0	0.061	0.1061	0.1374	0.1556	0.1615	0.1556	0.1374	0.1061	0.061	0
0	0.0595	0.1033	0.1335	0.1511	0.1568	0.1511	0.1335	0.1033	0.0595	0
0	0.0547	0.0942	0.1211	0.1367	0.1416	0.1367	0.1211	0.0942	0.0547	0
0	0.0455	0.077	0.0979	0.1099	0.1136	0.1099	0.0979	0.077	0.0455	0
0	0.0295	0.048	0.0598	0.0664	0.0684	0.0664	0.0598	0.048	0.0295	0
0	0	0	0	0	0	0	0	0	0	0

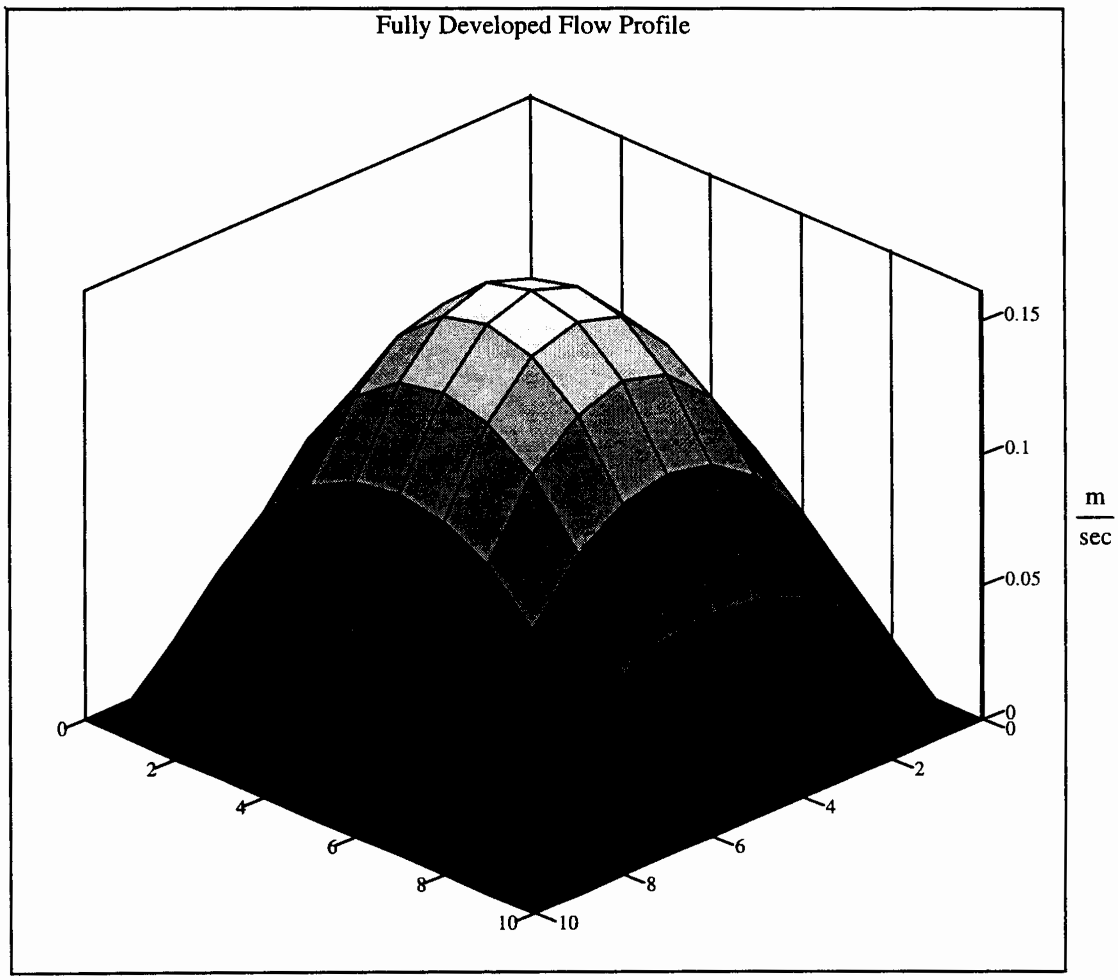

V

Time constants of 0.107 μm PSL particles for 10 times the actual flow rate

Time constant associated with Brownian motion of the particles

$a := 0.107 \cdot 10^{-6}\,\text{m}$ $Kb := 1.380658 \cdot 10^{-23}\,\frac{J}{K}$ $\eta := 947.95 \cdot 10^{-6}\,\text{Pa} \cdot \text{sec}$

$T := 296\,\text{K}$ $n := 1.33$ $\lambda := 532.5 \cdot 10^{-9}\,\text{m}$

$Do := \frac{Kb \cdot T}{6 \cdot \pi \cdot \eta \cdot a}$ $Do = 2.138 \bullet 10^{-12}\,\frac{m^2}{s}$ $k := \frac{2 \cdot \pi \cdot n}{\lambda}$ $k = 1.569 \bullet 10^{7}\,m^{-1}$

$\tau diffusion := \frac{1}{Do \cdot k^2}$ $\tau diffusion = 0.0019\,\text{sec}$

Time constant associated with the travel of the particle through the focused laser beam.

Focused beam diameter in sample = b and is defined in Sundaresan (1999). The velocity used is the value found by the flow profile Eqs. (A-IV-1) and (A-IV-2) at 1 mm from the wall.

$b := \frac{1}{\sqrt{18 \cdot 10^8}}$ $b = 2.357 \bullet 10^{-5}\,\text{m}$ $\alpha L := .837758040957\,\text{rad}$ $v := 9.2618 \cdot 10^{-2}\,\frac{m}{s}$

Length traveled in the laser beam by particle = L

$L := \frac{b}{\cos(\alpha L)}$ $L = 3.523 \bullet 10^{-5}\,\text{m}$

$\tau transit := \frac{L}{v}$ $\tau transit = 0.00038\,\text{sec}$

Time constant associated with Doppler beating if the bisector between the angles created by the laser arm and the detector arm is not perpendicular to the flow vector. For this calculation, it is assumed that the cell rotation is 5 degrees from perpendicular (85 degrees).

$\tau doppler := \frac{1}{k \cdot \cos(1.4835298642) \cdot v}$ $\tau doppler = 0.000008\,\text{sec}$

VITA

Ryan Matthew Cambern

Candidate for the Degree of

Master of Science

Thesis: MULTIPLE SCATTERING SUPPRESSION CROSS-CORRELATION OF A FLOWING FLUID TO DETERMINE PARTICLE SIZE

Major Field: Mechanical Engineering

Biographical:

Personal Data: Born in Beaver, Oklahoma, January 10, 1974. The son of Charles Cambern and Joe and Lou Ann Perkins.

Education: Graduated from Union High School, Tulsa Oklahoma in May 1992; received Bachelor of Science degree in Mechanical Engineering from Oklahoma State University, Stillwater, Oklahoma in May 1997. Completed the requirements for the Master of Science Degree at Oklahoma State University in July 1999.